



University of  
Stavanger

**Faculty of Science and Technology**

## **MASTER'S THESIS**

Study program/ Specialization:  Environmental Technology/ Water Science	Spring semester, 2013  Open
Writer: Diba Haddadi	..... (Writer's signature)
Faculty supervisor:  Meret Vadla Madland	
Title of thesis:  <b>“An investigation of permeability and porosity evolution of Kansas chalk under in-situ conditions”</b>	
Credits (ECTS): 30	
Key words:  Permeability evolution, Porosity, Kansas Chalk, Compaction, Chemical alterations	Pages: .....71.....  + Appendix: .....8.....  Stavanger, June 16 <sup>th</sup> , 2013

## Table of Contents

<i>Acknowledgments</i> .....	IV
<i>Abstract</i> .....	V
1. Introduction.....	1
2. Theory and Backgrounds .....	4
2.1 Carbonate Rocks .....	4
2.1.2 Chalk .....	4
2.1.3 Chalk as Reservoir Rock .....	4
2.1.4 Kansas Chalk.....	5
2.2 Mechanical Properties of Chalk .....	5
2.2.1 Stress .....	5
Axial Stress .....	5
Effective Stress.....	6
2.2.2 Strain .....	6
Axial strain .....	7
Radial strain.....	7
Volumetric strain.....	8
2.2.3 Stress-Strain Relationship .....	8
2.2.4 Creep .....	9
2.2.5 Porosity.....	9
2.2.6 Estimating the Time-dependent Porosity Evolution .....	10
2.2.7 Permeability .....	11
2.2.8 Permeability and Porosity Relationship .....	12
Carman-Kozeny Model .....	12
3. Material and Methods of Experiment.....	13
3.1 Test Material .....	13
3.1.1 Chalk .....	13
3.1.2 Brines .....	13
3.1.3 Confining Oil.....	14
3.2. Test Equipment .....	14
3.2.1 Equipment for saturating the core/ vacuum vessel.....	14
3.2.2 Triaxial Cell.....	15
3.2.3 Heating System .....	16
3.2.4 Pumps .....	16
3.2.5 Flooding Cell.....	17
3.2.6 LVDT (Linear Variable Displacement Transducer) .....	18
3.2.7 Chemical Testing (IC) .....	18
3.2.8 pH Meter .....	19
3.2.9 Pycnometer.....	19
3.2.10 Friction/auto sampler.....	20
3.3 Preparation .....	20
3.3.1 Chalk Cores .....	20
Drilling .....	20

Shaping.....	21
Cutting.....	22
3.3.2 Saturating the Chalk to Determine the Porosity.....	23
3.3.3 Mixing the Brine.....	23
Formation Water (FW).....	23
Synthetic Sea Water (SSW).....	23
3.4 Procedure of the Test.....	24
3.5 Core analyzing after the test.....	25
3.5.1 Drying and weighing the core.....	25
3.5.2 Measuring the Volume of the Core.....	26
Bulk Volume Measurement.....	26
Solid Volume Measurement by Pycnometer.....	27
3.6 Chemical Analysis.....	28
3.6.1 Ionic Chromatography (IC).....	28
4. Results.....	29
4.1 Core Measurements before Testing.....	29
4.2 Flooding Test Results.....	29
4.2.1 Stress-Strain.....	29
4.2.2 Permeability-Strain.....	32
4.2.3 Creep Strain vs. Creep Time; and Permeability vs. Time.....	33
4.2.4 Porosity vs. Time.....	38
4.2.5 Permeability vs. Axial Creep Strain.....	38
4.2.6 Permeability vs. Porosity.....	40
4.2.7 Permeability Evolution ( $K(t)/K_0$ ) vs. Time.....	41
4.2.8 Permeability Evolution ( $K(t)/K_0$ ) vs. Volumetric Strain ( $\epsilon_v$ ).....	41
4.3 Core Analyzing after Test.....	43
4.3.1 Bulk Volume Measurement.....	43
4.3.2 Solid Volume Measurement by Pycnometer.....	45
4.4 Chemical Analysis.....	50
4.4.1 Ionic Chromatography (IC).....	50
5. Discussion.....	57
5.1 Flooding Test.....	57
5.1.1 Stress-Strain.....	57
5.1.2 Permeability-Strain.....	57
5.1.3 Creep Strain vs. Creep Time.....	57
5.1.4 Permeability vs. Time.....	58
5.1.5 Volumetric Strain vs. Time.....	59
5.1.6 Porosity vs. Time.....	59
5.1.7 Permeability vs. Axial Creep Strain.....	61
5.1.8 Permeability Evolution ( $K(t)/K_0$ ) vs. Time.....	61
5.1.9 Permeability Evolution ( $K(t)/K_0$ ) vs. Volumetric Strain ( $\epsilon_v$ ).....	63
5.2. Core analyzing after test.....	65
5.2.1. Solid Volume Measurement by Pycnometer.....	65
5.3. Chemical Analysis.....	65
5.3.1. Ionic Chromatography (IC).....	65
6. Conclusion.....	67

References .....	68
Appendix .....	72

## *Acknowledgments*

Hereby, I would like to express my gratitude towards faculty supervisor *Associate Professor Merete Vadla Madland* for her valuable supervision and also for giving me this opportunity to work as her student, even though I was not a student in the Petroleum Department. Her kindness gave me the chance to learn a lot and to know nice people. I cannot express how grateful I am for that.

I would like to thank *Dr. Reidar I. Korsnes* as my co-supervisor for his excellent guidance and assistance throughout all stages of writing my thesis. He was helping me in every stage of my experimental work and I would say that everything in the lab was “Reidar-dependent”. I appreciate his extensive knowledge and skills in the laboratory.

My special thanks are addressed to *Dr. Anders Neramoen* as my co-supervisor for his patience, support, encouragements and all inspirations he gave me in this work. He is so intelligent and passionate to his work which had a huge impact on my effort. I would never be able to do this without his supervision.

I would like also to thank *Tania Hildebrand Habel* and *Mona Minde* for SEM imaging.

I would like to thank my family, friends and fellow students for supporting me and motivating me; specially *my parents* whom whatever I have in my life is because of them.

Finally, I owe my deepest gratitude to my husband *Alireza* in particular. He had always been beside me when I was occupied with my master education during the last two years. I would never be able to do this without his patience, sympathy and support. Thanks for being my love and my best friend.

*Diba Haddadi*  
*June 2013, Stavanger*

## *Abstract*

Injections of brine into the chalk can lead to compaction. The chemical impacts of water injection on the mechanical strength of chalk have been investigated for several years. Also, porosity and permeability evolution resulting from compaction is a debate among scientists for many years. In this study we investigate the link between the observed compaction and the permeability evolution. The link between compaction and permeability evolution is studied both via theoretical modeling in combination with experimental work in laboratory. We have also studied the impact of different fluids (NaCl solution 1.833 M, synthetic sea water and distilled water) on the mechanical strength of Kansas chalk under high pressure (20 MPa) and high temperature (130 °C). We observed that flooding SSW did not have a significant impact on the mechanical strength of chalk. However, injecting DW contributed to an increase in the creep strain of the Kansas core. In addition, chemical analysis is conducted employing Ionic Chromatography (IC) method. The IC results enlighten that Magnesium-bearing minerals are precipitating inside the core and calcium-bearing minerals produced in the effluent. However, we have not observed a noteworthy change in concentration of sulfate ions. We have also suggested the volumetric strain as 2.5 order of magnitude of the axial strain. In addition, permeability and porosity evolution is concluded to be affected by the chemical alterations. Accordingly, mechanical factors are not the only issues responsible for permeability and porosity evolution.

*KEY WORDS: Permeability evolution, Porosity, Chalk, Compaction, Chemical alteration*

## 1. Introduction

Carbonate rocks are important rocks in oil and gas industry. In 1985, an investigation was done on hundreds of the largest hydrocarbon field whole over the world. The result was that more than 60 % of all recoverable oil was held in carbonate reservoirs (Roehl et al. 1985). Another survey done more recently by Schlumberger supports this result and in addition claims that approximately 40 % of the world's gas reserves are also held in carbonate reservoirs (Schlumberger, 2013).

Chalk is a soft, porous and very fine-grained limestone type of carbonate rock in the sedimentary rock's category. Chalk has maintained its biogenic origin, and thus, mainly consists of the mineral calcite ( $\text{CaCO}_3$ ), (Roehl et al. 1985).

In 1984, the seabed subsidence was observed at the Ekofisk field for the first time with the average rate of approximately 33 cm/year as a result of compaction. The Ekofisk Field is an over-pressured, naturally fractured chalk reservoir, with 130 °C temperature in the Norwegian sector of the North Sea which began the production in 1971 and the water injection was started in this field in 1987 (Sylte et al. 1999). It was considered that the reduction in reservoir pressure was the main driving force for reservoir compaction at that time (Sulak et al. 1991). Therefore, the water injection was increased gradually to maintain the pressure and enhance recovery, and as a result stop the subsidence. However, it was observed that it had minor preventing effect on the subsidence rate. Finally, a so-called "*water weakening*" phenomenon was pointed out as the key mechanism for compaction in the field (Sylte et al. 1999).

Since water weakening could lead to enormous costs for specifically oil companies due to subsidence of the platform and the loss of reservoir equipment, there is a growing interest to discover the causes of this effect to reduce the degree of negative consequences. Thus, research activities have been widely carried out on chalk behavior and its mechanical properties.

In the last 3 decades, several mechanisms were suggested by different scientists for water weakening process of chalk including physical effects, physico-chemical effects and chemical effects (Omdal et al. under review, Newman 1983, Rhett 1990, Risnes et al. 1999, Baud et al. 2000, Heggheim et al. 2005, Madland 2005, Risnes et al. 2005, Korsnes et al. 2006a, Korsnes et al. 2006c, Madland et al. 2006, Fjær et al. 2008, Korsnes et al. 2008, Madland et al. 2008, K. et al. 2011, Madland et al. 2011, Royne et al. 2011, Zangiabadi et al. 2009, Zangiabadi et al. 2011, Zangiabadi et al. 2013). In 1985 scientists argued that the strength of the chalk was only controlled by the porosity and silica content and no chemical effect affecting the water weakening process (DaSilva et al., 1985). However, Risnes (2001) claimed in his study on high porosity outcrop chalk, that the chalk mechanical properties are highly dependent on the composition of the pore fluids. Meaning that the chalk saturated with water is significantly weaker than the dry one or the oil saturated chalk and this is exactly the phenomenon referred as "*water weakening effect*". He mentions the possibilities of interactions between chalk and fluids through capillary forces and through surface physical/chemical reactions. The capillary forces take place when two immiscible fluids are in the pore space of the rock. However, other indications came out with the possibility of the forces generated by dipole-dipole interactions in the very narrow grain contact areas. Nevertheless, in a later experimental work a number of tests have been conducted with glycol and high concentration brines as saturating fluids. Glycol is miscible with water. However, it is very similar to oil in many features. It

turned out that both glycol and oil had the same effect on the chalk compared to dry chalk, but this weakening effect is considerably less than with water. According to this outcome, it was concluded that capillary effects play a minor role, if any, in chalk–fluid interactions and water activity is a key factor in the water weakening effect. A mechanism was proposed involving an additional pressure exerted on the grains by attraction of water molecules to the chalk surface which leads to an increase in pore pressure and thus, decreasing the cohesion of the chalk. Consequently pressure solution and adsorption pressure was suggested as two main contributing issues possible (Risnes et al. 2003, Risnes et al. 2005). Several other studies have been conducted to investigate the physical and the physico-chemical effects on the water weakening of rock (Rhett 1990, Andersen 1995, Risnes et al. 1999, Fjær et al. 2008)

Finding out that the physical and physico-chemical effects have negligible impact on water weakening process, chemical effects received more attention during the last years (Newman 1983, Madland et al. 2006, Zangiabadi et al. 2009, Andersen 2010, Fabricius 2010, Øvstebø 2011, Veen 2012).

Korsnes (2006a, 2006c, 2007) came up with a new proposal in which substitution was defined as a possible solution. In this experimental work, the temperature-dependent chemical interactions between chalk and the injected seawater-like brines were studied. Analyzing the effluent chemistry showed an increase in the total  $\text{Ca}^{2+}$  ions produced, while other ions (i.e.  $\text{Mg}^{2+}$ ) was reduced during flooding. Thus, a substitution mechanism was suggested. In addition, the impact of presence of  $\text{SO}_4^{2-}$  was examined and based on the results; presence of  $\text{SO}_4^{2-}$  was indicated vital for the process. However, a later study carried out by Madland et al. (2009) confirmed that  $\text{SO}_4^{2-}$  is not a compulsory component for considerable chemical deformation. On the other hand, the total amount of calcium produced, was reported in an excess amount than that could be explained by substitution phenomenon only. In light of these new results, it was concluded that proposed substitution mechanism could not explain the water weakening of chalk exclusively. As an alternative, they suggest a Dissolution/precipitation mechanism for minerals in the chalk core (Madland et al. 2009)

Wide investigations have been executed to study the dissolution/precipitation mechanism more clearly. Several studies were performed which present a chemical model of both aqueous chemistry and surface chemistry of a calcium carbonate rock. According to the results, no evidence was found to clarify these experiments could be due to changes in surface potential or charge. However, a dissolution process inside the core could explain both wettability change and water weakening of chalk (Hiorth et al. 2008, Hiorth et al. 2010). Flooding brine with different composition from rock fluid in equilibrium with grains mineral, causes a disturbance in the equilibrium due to the common ions existence. Hence, it leads to dissolution of some minerals (i.e. calcite,  $\text{CaCO}_3$ ) and precipitation of others (i.e. anhydrite,  $\text{CaSO}_4$ ) to reestablish the state of the equilibrium (Heggheim et al. 2005, Madland et al. 2011). The effect of sulfate on mechanical strength of chalk has been examined extensively (Megawati et al. 2012).

Following the compaction resulted from the water weakening; an evolution in permeability of the rock can take place. Newman (1983) claimed that injecting sea water into the chalk leads to a significant reduction in permeability due to the large amount of compaction. In an experimental study conducted by David et al. (1994), it was tried to explain how the compaction mechanism does influence the relation among permeability, porosity and effective pressure. Laboratory data show that the porosity sensitivity is relatively high when the permeability is reduced by a coupled mechanical and chemical compaction process in porous



rock. There have been several studies done in terms of porosity-permeability relation and the permeability and porosity evolution in rocks i.e. (Nelson 1994, Shouxiang Ma et al. 1996, O.Saar 1998, Bernabé et al. 2003, Ghabezloo et al. 2009).

There are still numerous of studies that should be conducted to obtain a more clear vision of the water weakening process and its possible contributory factors.

Water weakening enhances compaction of the rock; indicating that the fluid interacts with the rock that carries the subjected load. The question is then, which mechanisms are at play in this system and how does the observed compaction affect other measurable quantities important to the oil and gas industry (such as the permeability).

In this thesis we investigate the link between the observed compaction and the permeability evolution. The link between compaction and permeability evolution is studied both via theoretical modeling in combination with core tests. We also examine the impact of different fluids (NaCl solution, synthetic sea water and distilled water) on the mechanical strength of Kansas chalk under high pressure (20 MPa) and high temperature (130 °C).

## 2. Theory and Backgrounds

### 2.1 Carbonate Rocks

Carbonate rock is a type of sedimentary rocks. In general, Sedimentary rocks form at/near the earth surface. Carbonate rocks are placed in the two categories, *limestone* and *dolostone*, and make up 10-15 % of this surface layer (Blatt et al. 1996).

#### 2.1.2 Chalk

Chalks are granular materials, made of calcite skeletons produced by planktonic algae mainly with wholes and fractured parts in the structure. The chalk structure consists of coccolith rings which are built of calcite tablets and platelets of 1  $\mu\text{m}$  in average. The coccolith ring diameters are normally around 10  $\mu\text{m}$ . A mixture of the intact coccolith rings with different fragment size makes a porous structure with porosity up to 40 %. However, small grains make the porous throats narrow which leads to a low permeability. In Fig. 2.1 a typical image of a high porosity chalk is shown.

In such high porosity chalk the nature of bonding elements is still a matter of debate. Cement bond between the grains is not easily seen in the scanning electron microscope (SEM) pictures like what is shown Fig. 2.1. However, it doesn't mean that there are not such bonds within the chalk materials (Risnes 2001).

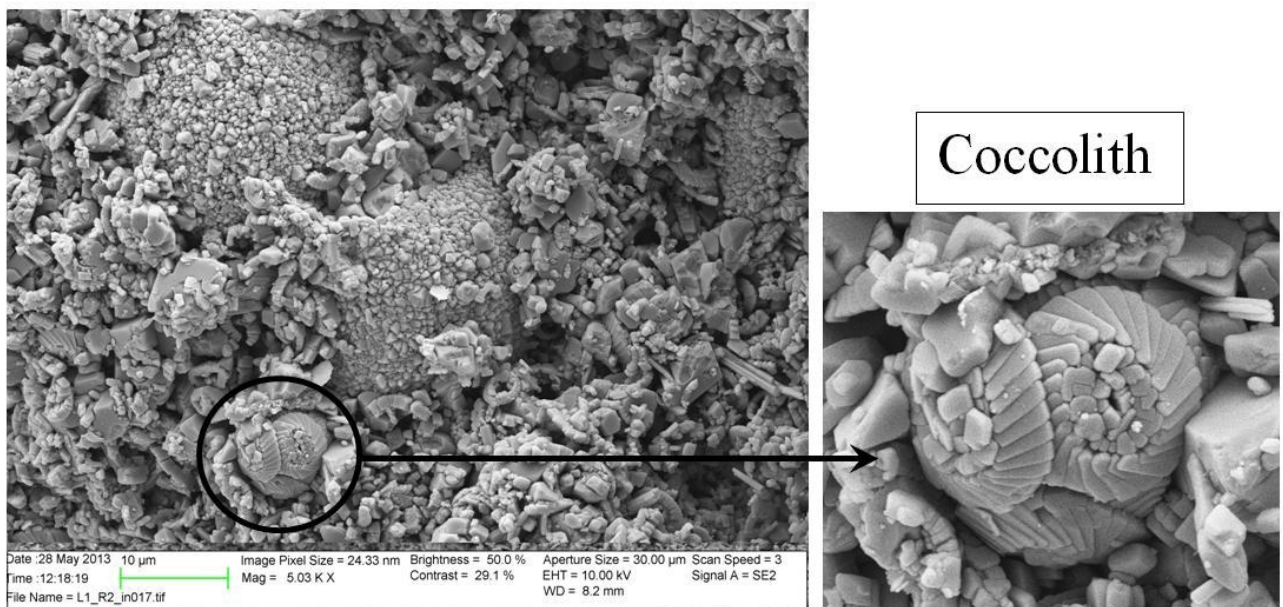


Fig. 2.1. SEM image of Kansas chalk

#### 2.1.3 Chalk as Reservoir Rock

High porosity, low permeability and soft matrix are three characteristics that interact to differentiate chalk's behavior from most reservoir rocks. These properties could lead to

problematic challenges in different area of reservoir development such as; drilling, stimulation and production. Due to these challenges a need is indicated for basic information on the mechanical behavior of chalks (Blanton 1981).

### 2.1.4 Kansas Chalk

“In Kansas, the Greenhorn Limestone, the Fairport Chalk Member of the Carlile Shale, and the Smoky Hill Chalk Member of the Niobrara Chalk are composed predominantly of impure, weakly cemented, more or less laminated, micritic carbonate rock that is best described as shaly chalk” (Hattin 1975). Analysis of Kansas samples showed 99 % calcite and 1 % quartz which is similar to that of “clean” North Sea chalks lacking clay and chert minerals. The porosity of the Kansas outcrop chalk is approximately 30-40 % and the permeability of that is 2-5 mD (Pooladi-Darvish et al. 2000, Tang et al. 2001)

## 2.2 Mechanical Properties of Chalk

### 2.2.1 Stress

*Stress* is generally defined as average force acting over an area. Thus it is independent of the size and shape of the body and is defined as:

$$\sigma = \frac{F}{A} \quad (\text{Eq. 2.1})$$

Where  $\sigma$  is the stress,  $F$  is the force [N] and  $A$  is the area of the cross section [ $\text{m}^2$ ].

The SI unit for stress is Pa (Pascal) which is equal to  $\text{N}/\text{m}^2$ . The other units which are mostly used in engineering calculations are bar, atmosphere, psi (= lb/sq.inch.) or dynes/ $\text{cm}^2$ . (Fjær et al. 2008) During our experimental tests,  $A$  is not corrected for distortions during deformation for practical reasons.

### Axial Stress

Considering a cylinder (Fig. 2.2), forces can be exerted in either axial or radial direction.

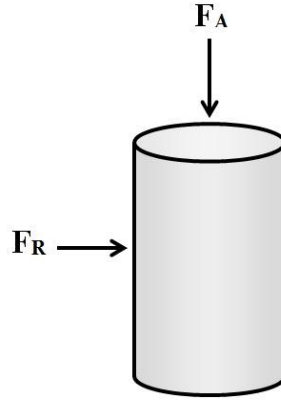


Fig. 2.2. Axial and radial forces exerted on the surface of a cylinder

The *axial stress*,  $\sigma_A$ , generally is defined as:

$$\sigma_A = \frac{F_A}{\pi r^2} \quad (\text{Eq. 2.2})$$

Where  $F_A$  is the axial forces exerted to the cylinder with a radius  $r$ .

### Effective Stress

The average stress taken by the rock grains is known as *effective stress*, which is defined as the total stress exerted to the grains minus fluid pressure inside the pores of the rock (pore pressure) and can be shown as:

$$\sigma' = \sigma - P_p \quad (\text{Eq. 2.3})$$

Where  $\sigma$  is the total stress,  $\sigma'$  is the effective stress and  $P_p$  is the pore pressure (The fluid pressure inside the pores of the rock.)

For more details we refer to (Fjær et al. 2008, Aadnøy et al. 2011).

In our study, we have calculated the effective axial stress as following:

$$\sigma'_A = (P_{Confining} - P_{Pore}) + [(P_{Piston} - P_{Friction})]\alpha \quad (\text{Eq. 2.4})$$

Where  $\sigma'_A$  is the effective axial stress,  $P_{confining}$  is the confining pressure,  $P_{pore}$  is the pore pressure,  $P_{piston}$  is the piston pressure and  $P_{friction}$  is the friction pressure caused by a friction force between the O-rings on the piston and the cell wall.  $(P_{piston} - P_{friction})$  is assumed as constant and equal to 0.3 MPa in our study. And  $\alpha$  is an area constant set as 1.365 in our study.

### 2.2.2 Strain

The deformation of a body which caused by a stress would be defined as *Strain*. Strain is a dimensionless parameter. There are two types of strain. The first type is *Elastic*, whereas the body can return to the original shape. While, *Plastic* is when the deformation would be irreversible.

## Axial strain

The axial strain is expressed by:

$$\varepsilon_A(t) = \frac{\Delta L}{L_0} = \frac{L(t) - L_0}{L_0} \quad (\text{Eq. 2.5})$$

Where,  $L_0$  is the initial dimension of the material [m],  $L(t)$  is the dimension of the material at time(t) [m] and  $\Delta L$  is the difference between the  $L_0$  and  $L(t)$  [m].

Eq. 2.5 can be written as:

$$L(t) = L_0 (\varepsilon_A + 1) \quad (\text{Eq. 2.6})$$

Axial forces can lead to deformation of the rock as shown in Fig. 2.3.

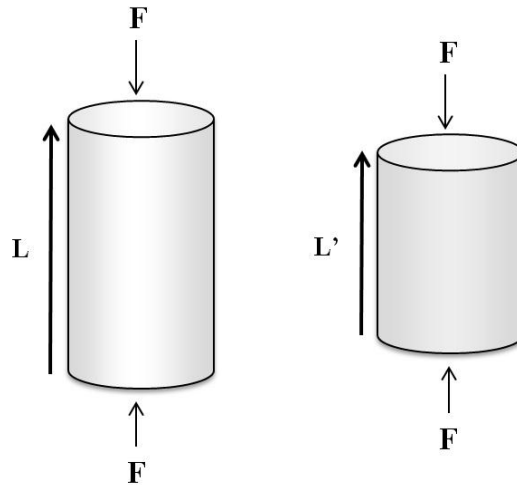


Fig. 2.3. Axial stress deformation due to axial force  $F$

## Radial strain

Just same as axial strain, the radial strain is expressed by:

$$\varepsilon_R(t) = \frac{\Delta R}{R} = \frac{\Delta D}{D_0} = \frac{D(t) - D_0}{D_0} \quad (\text{Eq. 2.7})$$

Where  $D_0$  is the initial diameter of the material [m],  $D(t)$  is the diameter of the material at time(t) [m] and  $\Delta D$  is the difference between  $D_0$  and  $D(t)$  [m],

Eq. 2.7 can be written as:

$$D(t) = D_0 (\varepsilon_R + 1) \quad (\text{Eq. 2.8})$$

## Volumetric strain

The *volumetric strain* referred to in this study is defined by the following equation:

$$\varepsilon_v = \frac{\Delta V}{V} = \frac{V(t) - V_0}{V_0} \quad (\text{Eq. 2.9})$$

Where  $V_0$  is the initial volume of the specimen and  $V(t)$  is the deformed volume.

From the Eq. 2.9 can be written as:

$$\varepsilon_v = \frac{(D(t)^2 L(t)) - (D_0^2 L_0)}{D_0 L_0} \quad (\text{Eq. 2.10})$$

Inserting Eq. 2.6 and Eq. 2.8 into Eq. 2.10; and assuming  $\varepsilon_A \varepsilon_R \rightarrow 0$  and  $\varepsilon_A \varepsilon_R^2 \rightarrow 0$  give us:

$$\varepsilon_v = 2\varepsilon_R + \varepsilon_A \quad (\text{Eq. 2.11})$$

### 2.2.3 Stress-Strain Relationship

The Stress-strain relations for elastic materials are linear since a constant relationship would be seen between the applied stress and the strain resulted. The slope of the strain vs. stress curve is said to be the *elastic modulus* in low stresses (Fig. 2.4). However, when the stress is sufficiently large, the rock may enter a new phase in which the deformation will be permanent, while, the material is still loading resistible. At this point the material is called *ductile (plastic)* and the point of transition from elastic to ductile is known as the *yield point* (Fjær et al. 2008).

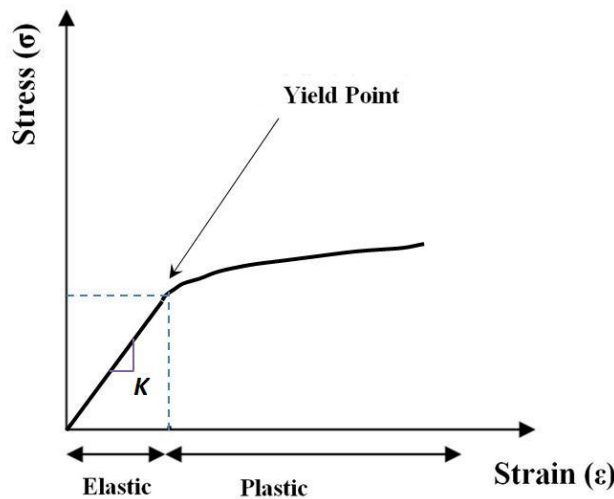


Fig. 2.4. Stress – Strain relation. After the material has reached yield point, it would not return to the original condition.

An elastic coefficient known as bulk modulus  $K$ , shows the relationship between stress and the volumetric strain under the hydrostatic condition.  $K$  shows how much the material resists hydrostatic compression and defined as:

$$K = \frac{\sigma_P}{\varepsilon_V} \quad (\text{Eq. 2.12})$$

Where  $\sigma_P$  is the hydrostatic stress and  $\varepsilon_V$  is the volumetric strain. While the inverse of  $K$ -modulus,  $1/K$  is defined as compressibility with unit [1/Pa].

It should be noted that under the hydrostatic condition,  $\sigma_P = \sigma_x = \sigma_y = \sigma_z$ . We can assume that the material is isotropic under the hydrostatic stress. Thus:

$$\varepsilon_V = 3\varepsilon_A \quad (\text{Eq. 2.13})$$

Where  $\varepsilon_A$  is the axial strain (Fjær et al. 2008).

However, some experimental works suggest the volumetric strain as other factor of the axial strain rather than 3. It can be basically because the normal chalk cores used in experiments are not isotropic. We have compared both ideas in our results and discussed about it in our discussion section.

### 2.2.4 Creep

A time-dependent deformation that may occur in materials under constant stress is defined as Creep which may occur in both dry and saturated rocks. A material under a constant stress will normally follow two stages of creep during the time (Fig. 2.5). *Transient* (or *primary*) creep is the first stage where the time-dependent deformation rate decreases with time. The second region is called *steady state* (or *secondary*) creep in which the deformation rate is constant. This stage involves a permanent deformation of the material (Fjær et al. 2008).

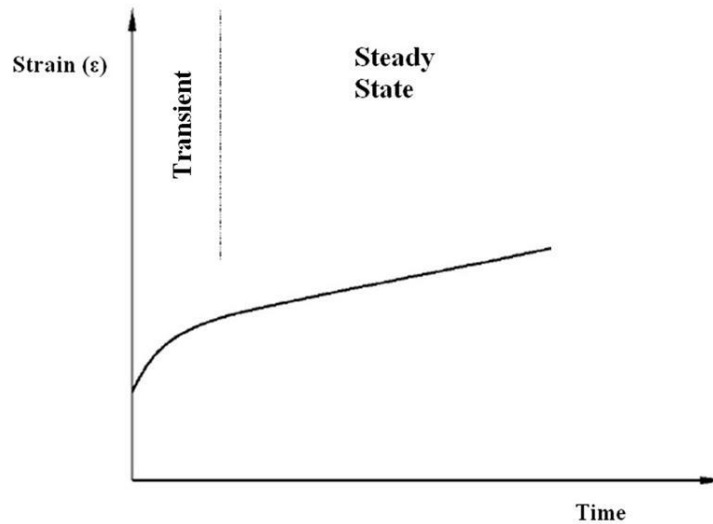


Fig. 2.5. Strain-time diagram for a creeping material and 2 creep stages.

### 2.2.5 Porosity

The solid grains and other cementing materials, make up the rock. However, they are just a part of rock structure. The space between the solid parts makes the rock a porous medium. Soil and rock are often heterogeneous and anisotropic (Aadnøy et al. 2011).

Considering the total volume (bulk volume) of an object is called  $V_B$ , the volume of solid material (matrix volume) is called  $V_S$  and the volume of void space (pore volume) is called  $V_P$ , the bulk volume can be defined as:

$$V_B = V_S + V_P \quad (\text{Eq. 2.14})$$

Porosity is defined as:

$$\phi = \frac{V_P}{V_B} \quad (\text{Eq.2.15})$$

The bulk densities given are based on the dimensions and weights of the cores tested. Two methods of measuring porosity implemented in our study: one based on bulk density as compared with matrix density and the other based on helium invasion of the plugs. We have saturated the chalk cores with distilled water. Implementing the first method, the density is defined as:

$$\rho = \frac{W_D}{V_B} \quad (\text{Eq. 2.16})$$

Where  $W_D$  is the dry weight of the plug measured on the scale and  $V_B$  is the bulk volume of the plug calculated by measuring the length and the diameter of the chalk core and defined as:

$$V_B = L \pi \left(\frac{D}{2}\right)^2 \quad (\text{Eq. 2.17})$$

Where  $V_P$  is the pore volume and defined as:

$$V_P = \frac{(W_w - W_D)}{\rho_{DW}} \quad (\text{Eq. 2.18})$$

And  $\rho_{DW} = 1 \text{ gr/ml}$  (Density of Distilled Water)

Implementing the second method, the density is defined as:

$$\rho = \frac{W_D}{V_S} \quad (\text{Eq. 2.19})$$

Where  $V_S$  is the solid volume of the core measured by the Pycnometer. In other word we can consider that as:

$$\phi = \frac{V_P}{V_B} = \frac{(V_B - V_S)}{V_B} = 1 - \frac{V_S}{V_B} \quad (\text{Eq. 2.20})$$

## 2.2.6 Estimating the Time-dependent Porosity Evolution

There would be a third option to calculate the porosity.

Porosity in time (t) is defined as:

$$\phi(t) = \frac{V_P(t)}{V_B(t)} \quad (\text{Eq. 2.21})$$



This equation may be written with respect to changes as:

$$\phi(t) = \frac{V_{P0} + \Delta V_P(t)}{V_{B0} + \Delta V_B(t)} \quad (\text{Eq. 2.22})$$

Assuming all volumetric strain accumulated in the collapse of the pore volume due to re-organization of the grains, we can assume that the volumetric strain of the bulk equals the reduction of pore volume.

$$\Delta V_B(t) = \Delta V_P(t) \quad (\text{Eq. 2.23})$$

and inserting the Eq. 2.9 and Eq. 2.20 into the Eq.2.22, then:

$$\phi(t) = \frac{\phi_0 + \varepsilon_V(t)}{1 + \varepsilon_V(t)} \quad (\text{Eq. 2.24})$$

However, during the flooding of non-equilibrium fluids, chemical fluid-rock interactions may occur. The effluent analysis that we perform in our test may enlighten the total effect of dissolution and/or precipitation process (see section 5.2). This fact can affect the solid volume so that  $V_S$  would not be constant anymore and as a result:

$$\Delta V_B = \Delta V_P + \Delta V_S \quad (\text{Eq. 2.25})$$

And then the porosity could be written as:

$$\phi(t) = \frac{V_{P0} + \Delta V_B(t) - \Delta V_S(t)}{V_{B0} + \Delta V_B(t)} \quad (\text{Eq. 2.26})$$

Employing eq. 2.9 and Eq. 2.20, then:

$$\phi(t) = \frac{\phi_0 + \varepsilon_V(t) - \frac{\Delta V_S(t)}{V_{B0}}}{1 + \varepsilon_V(t)} \quad (\text{Eq. 2.27})$$

which can be written also as:

$$\phi(t) = \frac{\phi_0 + \varepsilon_V(t) - \frac{\Delta M_S(t)}{\rho_S V_B}}{1 + \varepsilon_V(t)} \quad (\text{Eq. 2.28})$$

## 2.2.7 Permeability

Permeability is the rate at which a fluid flows through a permeable material per unit area and is governed by *Darcy's Law*:

$$K = -\mu \frac{\dot{u}}{\Delta P} \quad (\text{Eq. 2.29})$$

Where  $K$  is the permeability ( $\mu\text{m}^2 \cong \text{darcy}$ ),  $\mu$  is the fluid dynamic viscosity (Pa.s),  $\dot{u}$  is the fluid velocity in one direction (m/s) and  $\Delta P$  is the pressure gradient in the same direction ( $\text{N/m}^3$ ) (Fjær et al. 2008, Aadnøy et al. 2011).

We can also define the permeability using Darcys Law as (Korsnes et al. 2006b):

$$K = \frac{-q \mu (\Delta L)}{A (\Delta P)} \quad (\text{Eq. 2.30})$$

Where  $q$  is the fluid-pump flow rate (ml/s),  $\mu$  is the fluid dynamic viscosity (Centipoise/CP),  $A$  is the cross section area of the core ( $\text{Cm}^2$ ) and  $\Delta P/\Delta L$  is the pressure gradient over the length  $L$ . We have used the equation above in our study.

It should be noted that the fluids with the different compositions have the different viscosity. Accordingly, to calculate the permeability for various fluids, an online calculator so-called “CREWES Fluid Properties Calculator” has been used (Crewes 2007).

## 2.2.8 Permeability and Porosity Relationship

To estimate the permeability and its relationship with the porosity we can apply several models. *Katz and Thompson* model, *Johnson* model and *Kozeny-Carman* model are some examples among them (O.Saar 1998). *Carman-Kozeny Model* is one of the most famous and successful models and we will use it in our study.

### Carman-Kozeny Model

It is a model that can estimate the permeability for a porous material when the microstructural information is available (Dullien 1979). Based on this model, the permeability is obtained from following equation:

$$K = \left(\frac{D^2}{9t}\right) \left(\frac{\phi^3}{(1-\phi)^2}\right) \quad (\text{Eq. 2.31})$$

Where  $D$  is the grain diameter of minerals and  $t$  is the tortuosity factor.

According to this model and with the assumption that  $D$  and  $t$  would be constant in our experiments, we can write the evolution of permeability as:

$$\frac{K(t)}{K_0} = \frac{\phi^3 (1 - \phi_0)^2}{(1 - \phi)^2 \phi_0^3} \quad (\text{Eq. 2.32})$$

Inserting the equation Eq. 2.24 into the equation Eq. 2.32 gives us:

$$\frac{K(t)}{K_0} = \frac{(\phi_0 + \varepsilon_v)^3}{(1 + \varepsilon_v) \phi_0^3} \quad (\text{Eq. 2.33})$$

For more details we refer to (Carman 1956, Carman 1997)

### 3. Material and Methods of Experiment

The presented tests are performed at hydrostatic stress conditions where the axial and radial stresses are the same. The axial and radial stresses are increased simultaneously until a pre-defined level with the same rate. We performed three tests in our experiment. However, one of them failed in a very early stage. Thus we consider only the two others in our analysis.

#### 3.1 Test Material

##### 3.1.1 Chalk

High porosity outcrop chalk, Kansas from Niobrara, Kansas quarry, US was used. Two of the drilled cores were used for the two tests that we performed, KD2-LOWER and KD2-UPPER for test 1 and test 2 respectively. KD stands for Kansas/ Diba. The number 2 stands for the number of core-bit drilled out from the chalk outcrop. LOWER and UPPER stands for the lower piece and upper piece of the core bit drilled out from the chalk outcrop, since each core bit that we drilled was a basis of two cores proper for triaxial. The properties of the cores were measured and calculated and the results are shown in Section 4.

##### 3.1.2 Brines

We have used two different brine compositions during our test including: *Formation Water (FW)* and *Synthetic Sea Water (SSW)*. The tables below (Table 3.1 and Table 3.2) show the detail of each brine composition and concentration of each ion contained.

Salt	FW (g/L)	FW (mole/L)	SSW (g/L)	SSW (mole/L)
NaCl	107.1	1.833	23.38	0.400
KCl			0.75	0.010
MgCl <sub>2</sub> .6H <sub>2</sub> O			9.05	0.045
CaCl <sub>2</sub> .2H <sub>2</sub> O			1.91	0.013
Na <sub>2</sub> SO <sub>4</sub>			3.41	0.024
NaHCO <sub>3</sub>			0.17	0.002

Table 3.1. The concentration of salts contained in the FW brine and SSW brine

SSW Ions	g/L	mole/L
HCO <sub>3</sub> <sup>-</sup>	0.12	0.0020
Cl <sup>-</sup>	18.62	0.5251
SO <sub>4</sub> <sup>2-</sup>	2.31	0.0240
Mg <sup>2+</sup>	1.08	0.0445
Ca <sup>2+</sup>	0.52	0.0130
Na <sup>+</sup>	10.35	0.4500
K <sup>+</sup>	0.39	0.0100
Ionic Strength		0.6567

Table 3.2. The concentration of ions contained in SSW

### 3.1.3 Confining Oil

During our experiments *Marcol Oil* (Fig. 3.1) was used as the confining oil inside the triaxial cell. However, in the first test (Test-0) which was failed in the very first days after beginning, the *Tellus Oil* was used. Both of the oil is regarded as safe and not toxic.

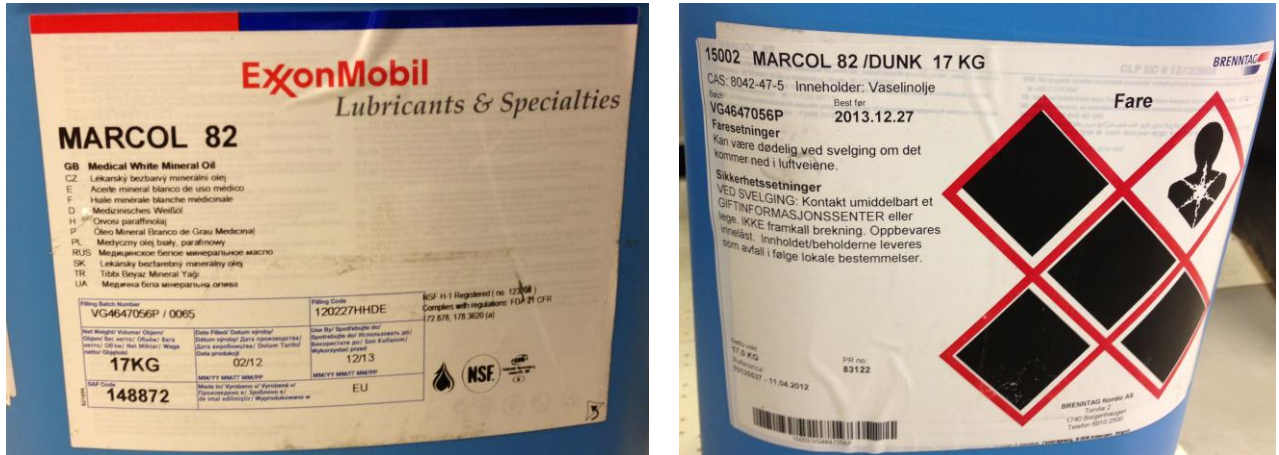


Fig. 3.1. Marcol Oil, used as the confining oil in the triaxial cell

## 3.2. Test Equipment

### 3.2.1 Equipment for saturating the core/ vacuum vessel

In purpose to saturate the cores we have used a vacuum vessel. The vacuum system contains a glass container with a heavy lid on top, and a rubber ring between them assures that the chamber is perfectly sealed. Through the lid, there are 2 connections to the container. One connected to the vacuum pump (Edwards RV5) and the other one, piped to fluid container (Distilled Water in our tests). Both pipes can be controlled by connected valves. A pressure gauge indicates the pressure inside the glass container. Fig. 3.2 shows the vacuum system set-up.

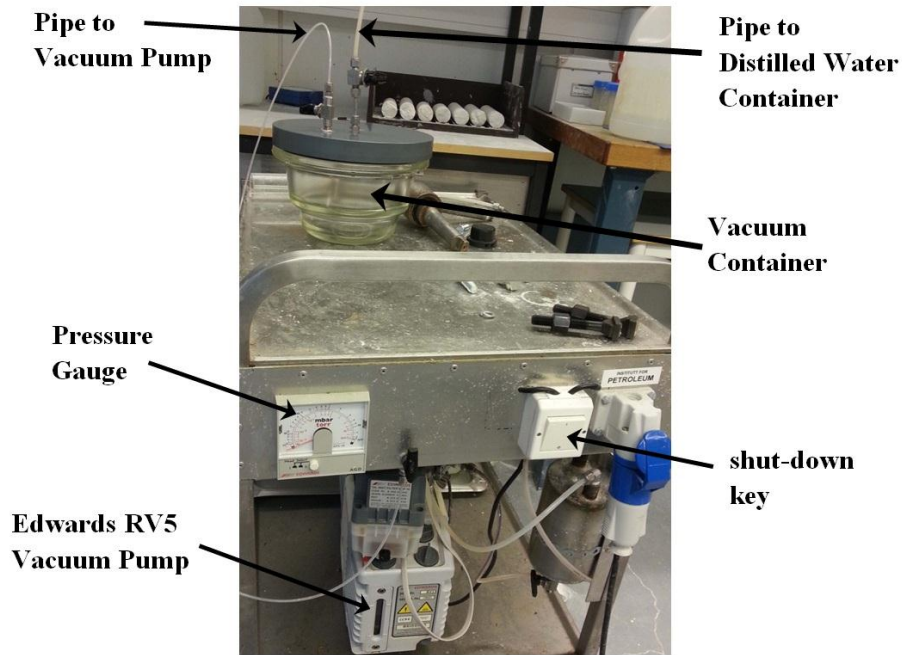


Fig. 3.2. The Vacuum System Set-up

### 3.2.2 Triaxial Cell

During our experimental work, we have used a triaxial cell. Fig. 3.3 shows the external view of the cell and Fig. 3.4 shows a cross section image of that. 6 steel bolts was installed around the cell for the safety reasons to keep the cell consolidate during the test. For more detail on Triaxial cell we refer to (Fjær et al. 2008).

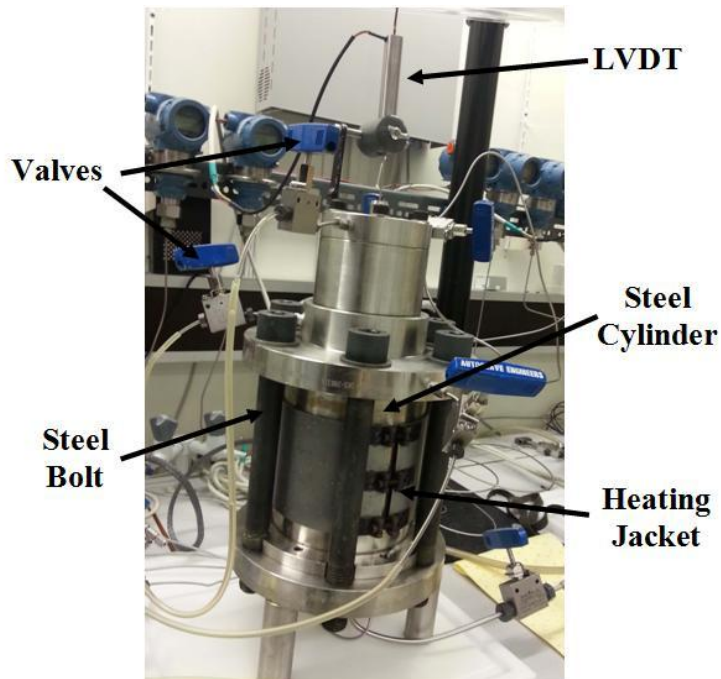


Fig. 3.3. An external view of the Triaxial cell

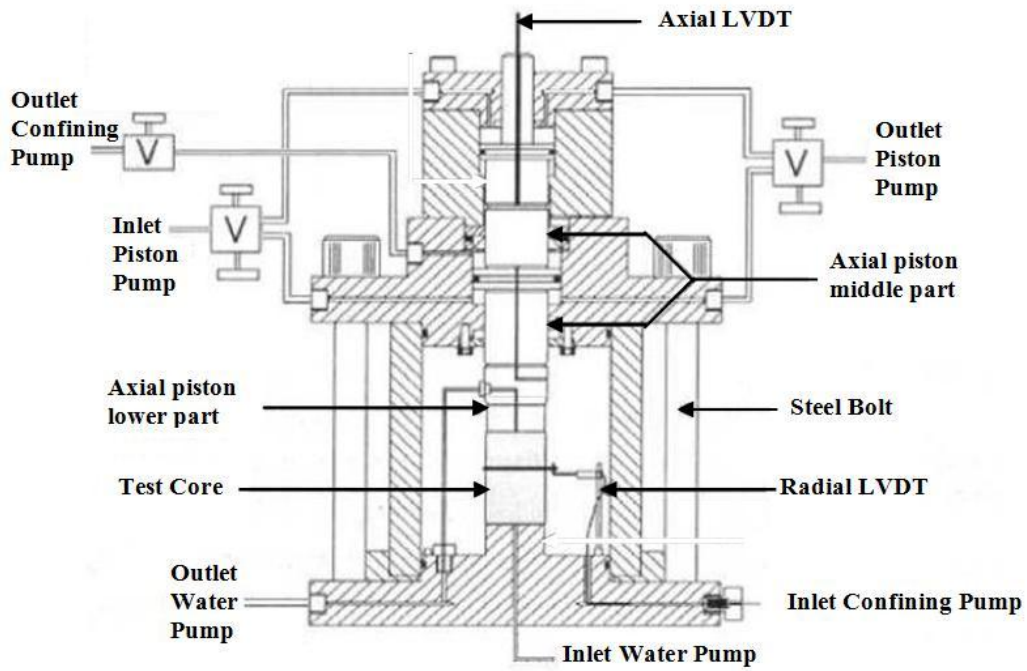


Fig. 3.4. A cross-section view of the Triaxial cell

### 3.2.3 Heating System

A *Backer 1500W heating jacket* was mounted around the steel cylinder of the triaxial cell to raise the temperature to the desired level (130 °C in our tests) and keep it constant during the experiment (Fig. 3.3).

### 3.2.4 Pumps

Three high pressure pumps are connected to the triaxial cell to control the piston pressure, confining pressure and the fluid circulation. In Fig. 3.5, the high pressure *Gilson Pump, Model 307 HPLC*, is shown.

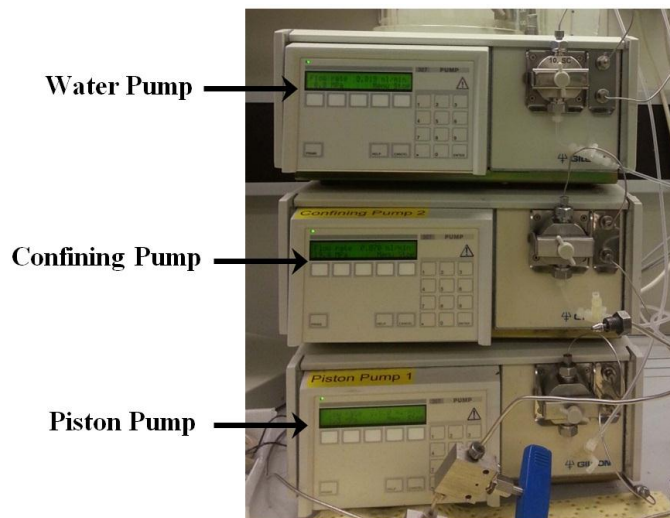


Fig. 3.5. The high pressure *Gilson Pump, Model 307 HPLC*

### 3.2.5 Flooding Cell

In purpose to circulate the brine in the triaxial system and through the chalk core a flooding cell was used. The flooding cell includes two chambers which are separated from each other by a piston in between. The upper chamber is connected to the water pump and the lower one to the triaxial cell. Distilled water pumped to the chamber make the piston press the brine in the lower chamber and the fluid is flooded to the chalk core in this way. The flooding rate can easily be controlled by the pump. Fig. 3.6 and Fig. 3.7 illustrate the flooding cell used in our tests.

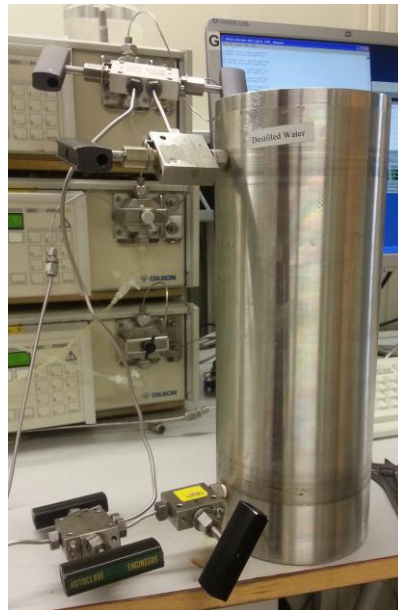


Fig. 3.6. The flooding cell

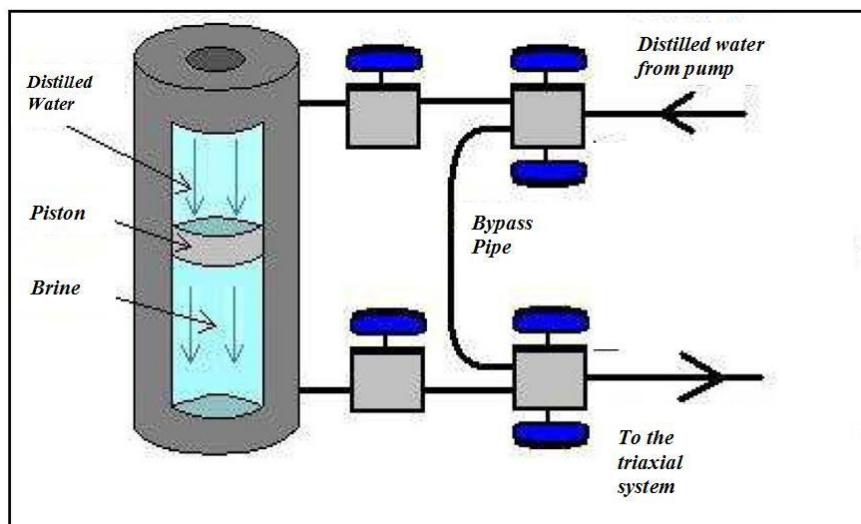


Fig. 3.7. Principle sketch of the flooding piston cell, and how it is connected to the rest of the flooding system

### 3.2.6 LVDT (Linear Variable Displacement Transducer)

To measure the axial deformation of the chalk core an external LVDT was installed in the cell (see Fig. 3.3). An external pressure on the piston was implemented by the piston pump to keep the LVDT on the top of the core at any time to assure that it measures the actual deformation. The radial strain was not measured in the presented tests.

### 3.2.7 Chemical Testing (IC)

The chemical constituents of the downstream fluids that had been flushed through the plug were measured by Ion Chromatography (IC). A Dionex ICS-3000 ion chromatograph was used in this matter (Fig. 3.9). It should be noted that, before doing the IC test all the samples should be diluted with distilled water (500 times) using a Gilson Gx-271 diluter (Fig. 3.8). In addition, after dilution, each sample was filtered manually using a syringe filter (Fig. 3.10) and poured in to the proper glasses for being used in the IC machine.

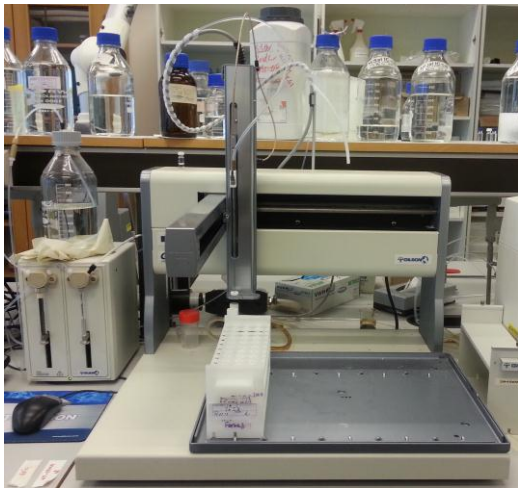


Fig. 3.8. Gilson Gx-271 diluter



Fig. 3.9. A Dionex ICS-3000 Ion Chromatograph



Fig. 3.10. A syringe filter



### 3.2.8 pH Meter

To measure the brine's pH, a SevenEasy METTLER TOLEDO pH meter was used (Fig. 3.11).

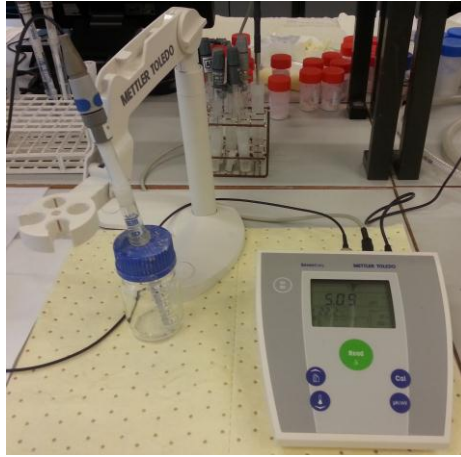


Fig. 3.11. The SevenEasy METTLER TOLEDO pH meter

### 3.2.9 Pycnometer

To calculate the density of the solid constituents of the core, we need to measure both the weight and the solid volume of the chalk. In this matter we cut the core to several smaller pieces to be able to place them in to the pycnometer pot. A *Micromeritics Gas Pycnometer model AccuPyc II 1340* was used to measure the actual solid volume of each piece of chalk after the test. The pycnometer is equipped with a gas capsule of Helium gas. Fig. 3.12 shows a complete pycnometer system used in our experiments.



Fig. 3.12. Pycnometer

### 3.2.10 Friction/auto sampler

In our tests, after flooding formation water (FW) through the core, we have changed the brine to synthetic sea water (SSW). In the first two days of flooding SSW, effluent samples were taken in more frequent time order than the normal sampling was done during the whole test. It was done to be able to see the dramatic changes in the very first stages of interaction between SSW and the core minerals, if any, and to follow the chemical change trend easier. For this purpose, two Gilson, Liquid Handler fraction sampler model 222 XL (Fig. 3.13) and model GX-271 (Fig. 3.14) were used in the Test-1 and Test-2 respectively.



Fig. 3.13. Friction/auto Sampler Gilson 222 XL



Fig. 3.14. Friction/auto Sampler Gilson GX-271

## 3.3 Preparation

### 3.3.1 Chalk Cores

A chalk outcrop from the Kansas quarry was used to prepare the tested cores. Since the outcrop is likely non-homogen, we drilled all the sample cores from the same outcrop to be able to compare our results based on the same standard. In addition, the top and the bottom side of the drilled core was marked to make sure that the flooding direction will be the same for all the sample cores during the tests (vertically upward in our cases). For the test in the triaxial cell, chalk cores were cut in a cylindrical shape with the length of approximately 70 mm (maximum 72 mm) and somehow the exact diameter of 37 mm. We also tried to make a smooth and uniform surface on the cores and avoid breaking of the edges.

### Drilling

A number of cylindrical core with an approximate length of 200 mm were drilled out from an outcrop of Kansas chalk with an oversize diameter. During the drilling the chalk block was fasten in a basket to prevent moving and water was used as a cooling liquid. The picture below (Fig. 3.15) shows the drilling machine (Koenisto Norge) that we have used.



Fig. 3.15. The drilling machine

After drilling we put the cores into the oven (Fig. 3.16) to dry out in 118 °C for one day to be ready for the next steps which are shaping and cutting.



Fig. 3.16. The Termaks LABOGLASS oven/heating-cabinet

## Shaping

To achieve the required diameter (37 mm) in a smooth and even form we took the advantage of using a turning lathe machine STANKOIMPORT - Moscow USSR (Fig. 3.17). This process performed in 2 steps. First, we scraped the core in a roughly 38 mm diameter with a

fast speed. In the second step, the cores were shaved in an exact diameter of 37 mm with a lower speed to get a uniform surface.



Fig. 3.17. The STANKOIMPORT Moscow USSR turning lathe machine

## Cutting

Each of the core bits forms a basis for two test cores (we also keep the top and the bottom and the middle piece as a reference). In this matter we cut the cores in an approximate length of 70 mm by using the Struers Discotom-5 Cutting Machine (Fig. 3.18). To avoid any damage to the core ends and breaking of the edges, we made the cores wet and it perfectly worked.



Fig. 3.18. The Struers Discotom-5 Cutting Machine

Finishing shaping the cores, we put all of them in the oven/heating cabinet again (118 °C) for 2 more days to be completely dry and get ready for calculating the effective porosity.

### 3.3.2 Saturating the Chalk to Determine the Porosity

We have weighed each dried core ( $W_D$ ) and also measured the exact lengths ( $L$ ) and diameters ( $D$ ) by using a sliding caliper. Thereafter, all the cores were saturated with distilled water in the vacuum vessel (Fig. 3.2) and again weighed individually on the scale to measure the wet weight ( $W_w$ ).

To saturate a core we put it in a small plastic container to use less distilled water during the procedure. Then the plastic container was placed in to the glass chamber with the lid on the top. The pump was started vacuuming with three different levels, each for 10 minutes; Level 0, level 1 and level 2 respectively. When the pressure gauge indicates the pressure of  $4 \times 10^{-4}$  bar, the system is ready to start flooding distilled water. After flooding DW we let the chalk to be in the water for some times to assure that it is saturated properly.

The porosity ( $\phi$ ) was calculated by applying equations as defined in Section 2.2.5. Calculating the effective porosity for each individual core, gives us the possibility of choosing the best core for the test among existing ones which has the porosity close to the average. The core's properties for the chalk cores used in our triaxial tests are listed in Table 4.1. We stored all of the cores in the heating cabinet in 118 °C to be dry and ready for the test at any time (Fig. 3.16).

### 3.3.3 Mixing the Brine

During our tests we have used same brine for both tests. Formation Water (FW) and Synthetic Sea Water (SSW) were flooded through the chalk cores respectively. The exact properties of the brines are shown in Tables 3.1 and Table 3.2. The procedure for preparing and mixing the brines is expressed as following:

#### Formation Water (FW)

- 1- Mix 107.1 gr NaCl into 1 Lit of distilled water. Let the solution to be properly dissolved for an hour.
- 2- Filter the solution with a filter of 0.65  $\mu\text{m}$  pore size.
- 3- Measure the pH of the solution at the ambient temperature.
- 4- Pour the filtered solution to a 1 Lit container and store it in the refrigerator for the next step which is flooding the core in a triaxial cell.

#### Synthetic Sea Water (SSW)

- 1- Mix the required salts into 1 Lit of distilled water. Let the solution to be properly dissolved for an hour or more. Mixing the salts should be in the following order: First, mix the chloride ions ( $\text{Cl}^-$ ); 23.38 gr NaCl, 0.75 gr KCl, 9.05 gr  $\text{MgCl}_2 \cdot 6\text{H}_2\text{O}$ , 1.91 gr  $\text{CaCl}_2 \cdot 2\text{H}_2\text{O}$ . Then, mix 3.41 gr  $\text{Na}_2\text{SO}_4$  very gently and slowly.

Finally, mix 0.17 gr  $\text{NaHCO}_3$ . Consider that it should be first diluted in some distilled water for a better dissolution.

- 2- Filter the solution with a filter of 0.65  $\mu\text{m}$  pore size.
- 3- Measure the pH of the solution at the ambient temperature.
- 4- Pour the filtered solution to a 1 Lit container and store it in the refrigerator for the next step which is flooding the core in a triaxial cell.

### 3.4 Procedure of the Test

Three similar tests were performed in the laboratory. The first test (*so-called "Test-0"*) was failed in the very beginning steps (after 5 days). The reason is not very clear. Thus, we ignore the results from the test mentioned above since it was flooded for very short period.

All the tests performed have exactly the same procedure, so that we can be able to compare the results properly. We defined our tests as "*KD2-LOWER-FW-SSW-DW-130°C*" or (KD2-L) and "*KD2-UPPER-FW-SSW-DW-130°C*" or (KD2-U) for the *Test-1* and the *Test-2* respectively. Each test consists of two phases. In the first phase, *Hydrostatic Loading*, the confining pressure (radial and axial stress) increased gradually to reach a pre-set level (20 MPa in our tests). When the pressure reached 20 MPa the second phase, *so-called "Creep Phase"* will be started. The stress level will be constant from then on. During the test in both phases the brine is flooded with the rate of 1 pore volume per day (PV/day). The chalk core was sealed with a shrinking sleeve and an industrial heater was used to deform the sleeve layer and cover the core so that no leakage between the confining oil and the pore fluid could occur during flooding (Fig. 3.19). After placing the sealed core inside the cell, the steel cylinder was installed on the triaxial cell base. Then the confining oil (Marcol oil) was poured into it, so that it covered around the core. The triaxial cell was secured by installing 6 huge steel bolts around it (Fig. 3.3). Finally, the LVDT was mounted on the top of the cell. The confining pressure was built up to 0.5 MPa and the pore pressure (water pump) to maximum 0.2 MPa. Note that the pore pressure should always be lower than the confining pressure to avoid any leakage through the sleeve. Distilled water was flooded through the core with the rate of 3 pore volume per day and the next day, flooding of the Formation Water was started.

To start flooding of FW we used a pressure regulator. When it gets to 0.4 MPa, the bypass was opened and the pore pressure was building up. The FW flooding rate (water pump) was set to 2 ml/min. There should always be 0.5 MPa gap between the pore pressure and the confining pressure to assure no leakage will occur. When the pore pressure reaches 0.4 MPa the gas pressure regulator was increase to 0.7 MPa and the water droplets come out. At this stage the water flooding rate was decreased to 0.1 ml/min. When the pore pressure gets to 0.7 MPa, the bypass was closed and the flooding rate decreased again to 0.05 ml/min. The heater turned on at this stage to reach the pre-set temperature level (130 °C) and the confining pressure was adjusted between 1.2 to 1.3 MPa. It is very important to open the piston valve during increasing of temperature. Thus the expanded oil gets out and avoids the pressure built up. Finally, when the temperature reaches 130 °C, the piston was started to move down gently to hit the core. The system was left until the next day that the hydrostatic flooding was started.

To start the hydrostatic flooding, we set the rate of 0.07 ml/min and the maximum pressure of 20 MPa for the confining pump. The confining pressure increased and reached the maximum level of 20 MPa and the creep phase started at this point. Afterward, the pressure is kept constant and the water was flooded with the rate of 1 PV/day during the whole test.

Flooding of formation water was continued for 3 weeks. Meanwhile, the effluent samples were collected almost every day for chemical testing later on. After 3 weeks, the brine was switched from FW to *Synthetic Sea Water (SSW)*. During shifting FW to SSW, we flooded distilled water through the bypass the core. A fraction/auto sampler machine was used to take 8 effluent samples in the first two days of flooding SSW (Fig. 3.13 and Fig. 3.14). Subsequently, the effluent samples were taken manually almost every day.

To end up the test, we stopped flooding SSW and started flooding of distilled water for 2 or 3 days. Flooding distilled water was done in porous to clean up the core and to avoid crystallization of the salts inside the core. In the end, the heating system was turned off and the test was completed.



Fig. 3.19. Installing the core inside the triaxial cell

### 3.5 Core analyzing after the test

When a test was finished and cooled down to ambient temperature, the cell was dismantled and the chalk core tested was carefully taken out. To ensure that the weight will be measuring is the actual weight of the tested core; we should try not to lose any small part of the chalk core. The shrinking sleeve was carefully cut off and separated from the core.

#### 3.5.1 Drying and weighing the core

To measure the dry weight of the tested core both the core and shrinking sleeve was placed in the oven for 1 day on 120 °C. The day after both the dried core and the dried shrinking sleeve was weighed on the scale. Then the shrinking sleeve was washed and weighed again in order to calculate the amount of chalk mass attaching to the sleeve. This way, we could calculate the total mass of dried chalk core after the test. The pictures below (Fig. 3.20 and Fig. 3.21) show the core so called “KD2-LOWER” after the test.

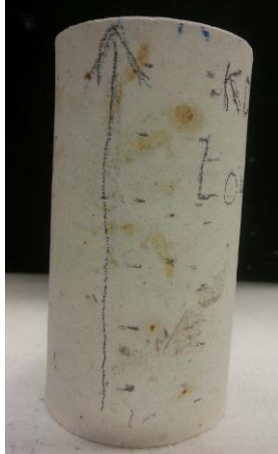


Fig. 3.20. Chalk core “KD2-LOWER” after the test, (the side view). Fig. 3.21. Chalk core “KD2-LOWER” after the test (the top view)

### 3.5.2 Measuring the Volume of the Core

To calculate the porosity and the density of a tested core we needed to measure both the bulk volume and the solid volume of the tested core.

#### Bulk Volume Measurement

To calculate the bulk volume of the tested core we needed to measure the length and the diameter of the core. To have a more precise measurement, the core was marked in three different directions, for length measurements. In addition, the core was marked in the length to be divided into smaller pieces and the diameter of each piece was measured. Implementing this method, it was considered that one whole chalk core consist of several pieces which have truncated cone (conical frustum) shape and then the volume of each piece was calculated and summed up to find out the total bulk volume of the core. Fig. 3.21 shows the core end, marked in three directions for length measurement. And Fig 3.22 shows the core marked for the diameter measurements.

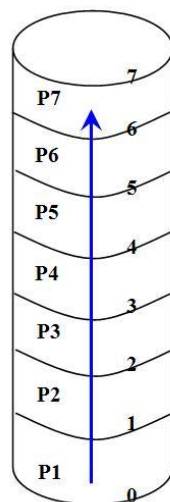


Fig. 3.22. The cylindrical core marked to be divided into several pieces



Fig 3.23 shows a truncated cone with the radials of  $R_1$  and  $R_2$  and the height of  $H$ .

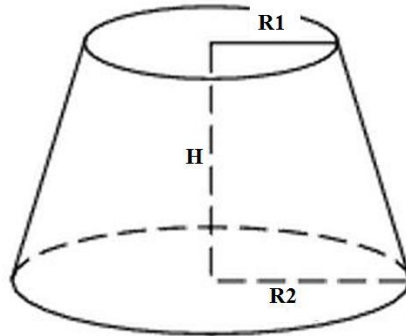


Fig. 3.23. A truncated cone (conical frustum) shape

The volume of a truncated cone is calculated by following equation:

$$V = \frac{(R_1^2 + R_2^2 + R_1R_2) \pi H}{3} \quad (\text{Eq. 3.1})$$

The results of measurements are given in the result section.

### Solid Volume Measurement by Pycnometer

To measure the solid volume of the tested core by the Pycnometer, the core was cut to the smaller pieces first, to be able to place them inside the machine (Fig. 3.24).



Fig. 3.24. The core which is cut in to the smaller pieces

All the pieces were placed in to the oven in 120 °C. We weighed each piece on the scale in the first step. Measuring the solid volume was done twice for each piece, once when it was just taken out of the oven which was very hot, and the next time, when it was cooled down.

The second step is working with the pycnometer. To start, we opened the Helium gas valve. Then we took off the cap of the machine container. After that, the chalk piece was gently placed inside the container and the container was fully pushed down. We put on the cap again and closed the machine. To start measuring, we pressed the “Alt”, “4” and “Enter” buttons

respectively. It took between 20 to 30 minutes to finish each measurement. When finishing the process, the machine beeps and the blue light for “Active” sign will be off. To read the result, we press the “choice” key. The result will be shown on the monitor. We can read an “Average Volume amount” and the “Standard Deviation” as a result. To finish the test we pressed the “Clear” button and opened the machine to take out the core sample. The test was repeated with the same procedure and the density was calculated for each test. The average density of all measured pieces can be calculated as:

$$\langle \rho \rangle = \frac{\sum_{i=1}^7 V_{s_i} \rho_i}{V_{s_{Tot}}} \quad (\text{Eq. 3.2})$$

## 3.6 Chemical Analysis

### 3.6.1 Ionic Chromatography (IC)

Before starting the chemical analysis using the IC machine, the samples should be diluted. To be able to start diluting process, we need to prime the machine/system so that we take out the air stocked inside the tubes. We programmed the machine to dilute our samples 500 times. After dilution of each sample is done, a cap should be put on the original sample to avoid any evaporation or dust getting into our effluent samples. From each diluted sample we prepare one sample proper to be placed in the IC machine (in a small IC-glass) with the following procedure:

1. Clean the syringe with ~ 1 ml DW.
2. Wet the syringe with diluted brine (~ 1 ml)
3. Pull out remaining diluted brine with syringe.
4. Put on the filter and wash until there is approx. 1.5 ml brine left in the syringe.
5. Fill up IC-glass with that 1.5 ml remaining brine through the filter, put the cap on and write the ID number on that.

Making the IC samples ready, the IC machine should be programmed to do the test. The “Flow Rate (Q)” for both the anions and cathions was set as 1 ml/min. The “Suppressor Current” was set as 45.0 mA and 50.0 mA, and finally the “Concentration” was set as 18 mM and 17 mM for Anions and cathions respectively. All the samples were placed in the IC basket in a specific order including placing the “Standard FW and SSW” in between and “DW” in the end. Finally we started the program and came the next day to take the results.

## 4. Results

In this experiment we conducted two similar tests under hydrostatic conditions in a triaxial cell. Both of the cores which had been tested were drilled from the same block of outcrop Kansas chalk to ensure homogeneity. We flooded formation water (FW), synthetic sea water (SSW) and distilled water (DW) through the core respectively. The temperature was constantly 130 °C during the tests.

We have performed two tests in our experimental work. In the test KD2-L, we flooded FW, SSW and DW for 18, 35 and 3 days respectively. Similarly, in the test KD2-U, FW, SSW and DW were flooded for 22, 18 and 4 days respectively through the core. The maximum confining pressure was set to 20 MPa for both of the tests.

The main objective of this work is to study the permeability evolution, the effect of different brine composition flooded through the core on the porosity and compaction of the Kansas chalk under in-situ condition.

### 4.1 Core Measurements before Testing

Prior to starting a test, the length ( $L$ ) and diameter ( $D$ ) of each core was measured. Using the results, the bulk volume ( $V_B$ ) has been calculated (see Eq. 2.17). In addition, the dry weight of the core ( $W_D$ ) before saturating with distilled water, and the wet weight of the core ( $W_W$ ) after saturating the core with DW were measured. Finally, the pore volume ( $V_P$ ) and the effective porosity ( $\phi$ ) were calculated (see Eq. 2.18 and Eq. 2.15 respectively). The table below (Table 4.1) shows the results.

Sample name	Length $L$ [mm]	Diameter $D$ [mm]	Bulk Volume $V_B$ [mL]	Dry Weight $W_D$ [gr]	Wet Weight $W_W$ [gr]	Pore Volume $V_P$ [mL]	Effective Porosity $\Phi$ [%]	Density $\rho$ [gr/ml]
KD2- LOWER	69.64	36.96	74.68	128.97	155.85	26.88	35.99	2.70
KD2- UPPER	70.71	36.98	75.91	129.44	157.43	27.99	36.87	2.70

Table 4.1. Core properties before flooding any fluid

### 4.2 Flooding Test Results

#### 4.2.1 Stress-Strain

In the first phase of our hydrostatic tests, the confining pressure was built up to a pre-set maximum level of 20 MPa. While the stress level was increasing, the axial strain in the core was logged on the LabView Software. The results are shown in Fig. 4.1 and Fig. 4.2 for the tests KD2-L and KD2-U respectively. The images illustrate the stress-strain relationship. For both test, we can see a linear trend in the beginning of the curve. However, after a while, a deviation is visible which clarify the yield point. To be able to see the deviation more clearly, we have also plotted the so-called “Residue” which demonstrates the difference between the values on the stress-strain curve and the linear line. The term “Residue” is calculated as following:

$$R = \sqrt{(a - b)^2} \quad (\text{Eq. 4.1})$$

Where **R** is residue, **a** is the stress value in one strain level and **b** is the linear line value in the same strain level. In the area that stress-strain curve almost matches the linear line; the residue is close to zero. Deviating from the line trend, the residue starts to increase.

As Fig. 4.1 and Fig. 4.2 display, the yield is equal to 13.5 MPa and 15 MPa; and the bulk modulus (*K*) is equal to 2.94 GPa and 2.79 GPa for the test KD2-L and KD2-U correspondingly. *K* has been calculated employing Eq. 2.12. Axial stress reaching to 20 MPa, the core had been compacted and shown 1.14 % and 0.87 % axial strain in test KD2-L and KD2-U respectively. These results are summarized in Table 4.2.

Test Name	Mechanical Properties		
	Yield Point [MPa]	K-modulus [GPa]	Axial Strain [%]
KD2-L	13.5	2.94	1.14
KD2-U	15.0	2.79	0.87

Table 4.2. Mechanical properties of the cores

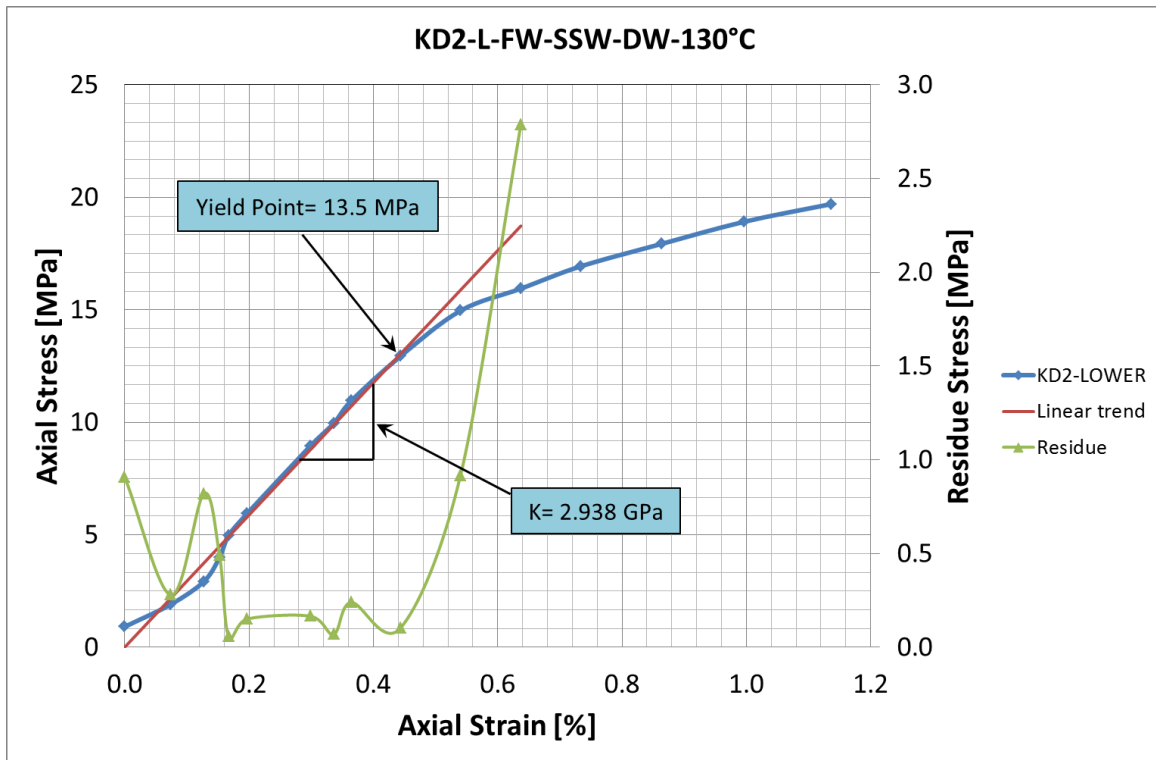


Fig. 4.1. The Stress-Strain Relation for the test KD2-L, The yield is 13.5 MPa and the bulk modulus ( $K$ ) is 2.94 GPa.

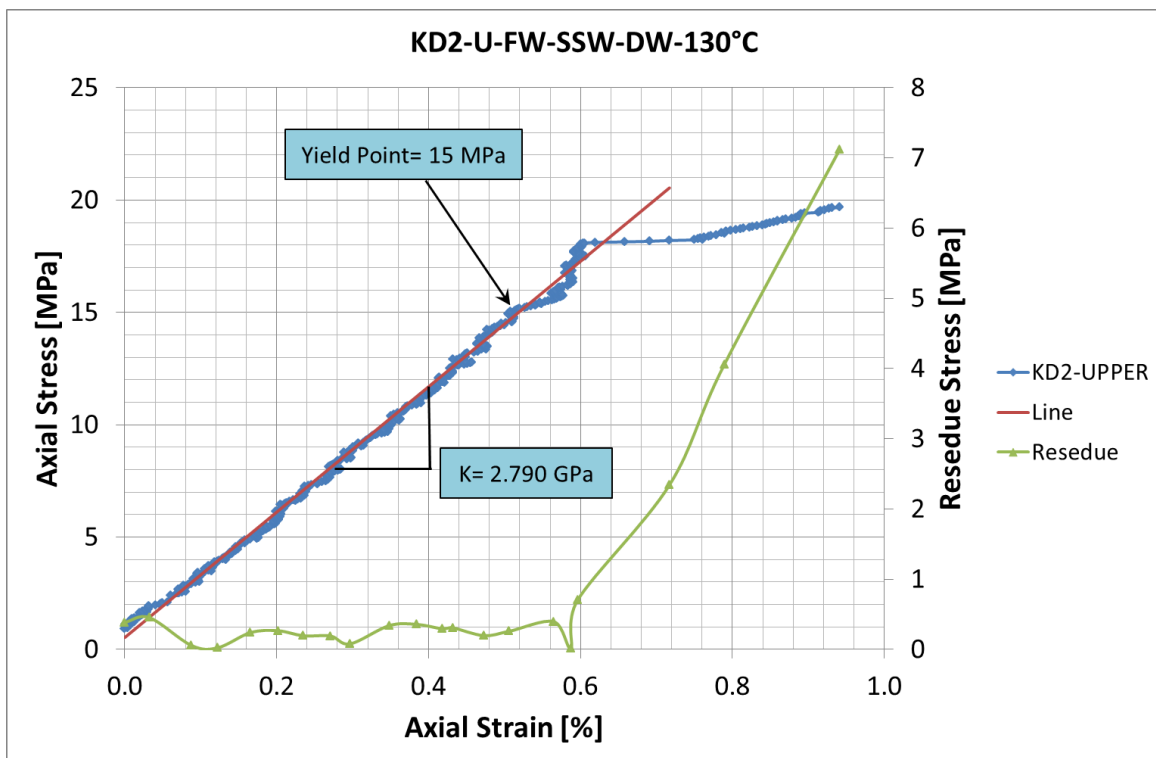


Fig. 4.2. The Stress-Strain Relation for the test KD2-U, The yield is 15 MPa and the bulk modulus ( $K$ ) is 2.79 GPa.

### 4.2.2 Permeability-Strain

We have also plotted the permeability progress while the stress was increasing employing Eq. 2.30. It is presented in Fig. 4.3 and Fig. 4.4 for the test KD2-L and KD2-U respectively. In the both tests, we can see a declining trend for permeability when the axial stress and consequently axial strain increase. Permeability has been decreased from approx. 2 to 1.3 milliDarcy (mD) similarly in the both tests.

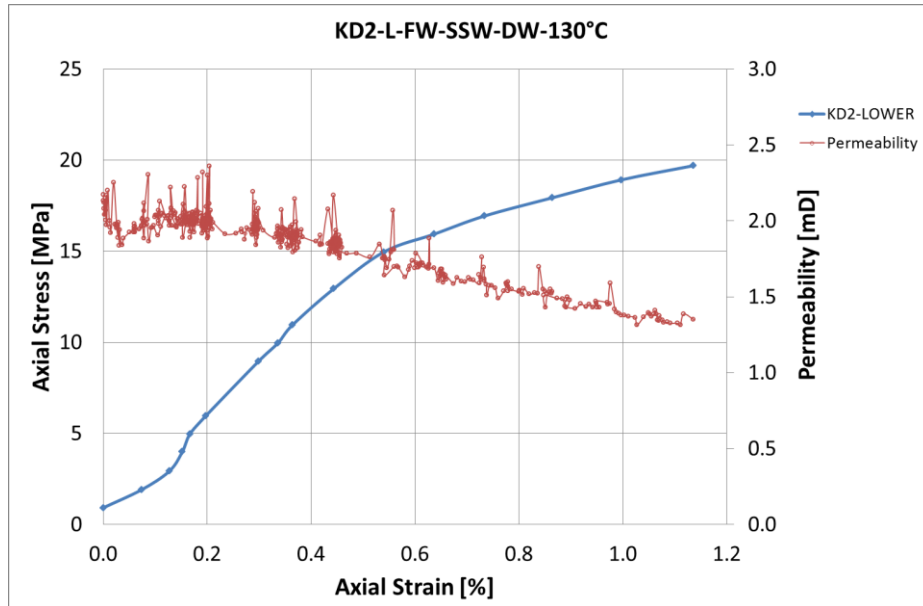


Fig. 4.3. The Stress-Strain Relation and the Permeability-Strain Relation for the test KD2-L

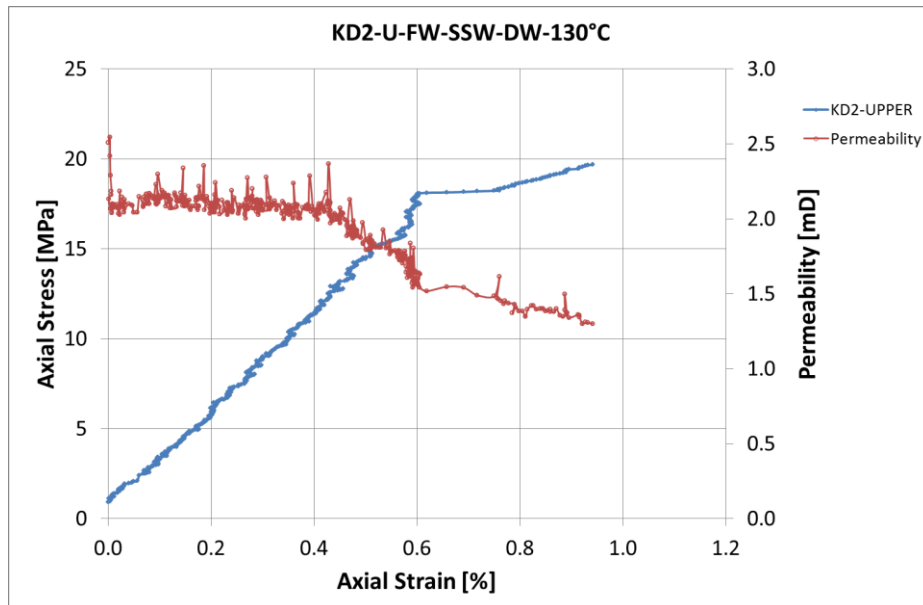


Fig. 4.4. The Stress-Strain Relation and the Permeability-Strain Relation for the test KD2-U

### 4.2.3 Creep Strain vs. Creep Time; and Permeability vs. Time

The second phase of the test (creep phase) starts when the stress level reaches its maximum level (20 MPa) and would stay constant for rest of the test interval. During the creep phase, the core compacts over time. However, the rate of compaction is much higher in the beginning and can vary based on the situation (i.e. Changes in temperature or composition of flooding brine, strength of the chalk, etc.). We have flooded FW through the core in the beginning and following that, SSW and DW were flooded. Fig. 4.5 and Fig. 4.6 illustrate the creep strain development during the creep time in our experiments KD2-L and KD2-U respectively. The axial creep strain of the core in the end of flooding each fluid has been given in Table 4.3 for both tests which have been measured by LVDT. The axial creep strain in the end of flooding each fluid varies between 2.0 % to 2.7 % for both tests.

Test name	Axial Creep Strain ( $\epsilon_A$ ) [%]		
	FW	SSW	DW
KD2-L	2.07	2.59	2.64
KD2-U	2.17	2.46	2.53

Table 4.3. The axial creep strain [%] in the end of flooding each fluid for tests KD2-L and KD2-U

Furthermore, Table 4.4 presents the Total Axial Strain [%] during the whole tests KD2-L and KD2-U which is equal to 3.78 % and 3.40 % respectively. Total axial strain is the axial strain in the beginning phase plus the axial strain in the creep phase. This is also measured by LVDT during the test.

Test Name	Total Axial Strain ( $\epsilon_A$ ) [%]
KD2-L	3.78
KD2-U	3.40

Table 4.4. The total axial strain [%] during the tests KD2-L and KD2-U

Fig. 4.5 and Fig. 4.6 illuminate that changing the brine from FW to SSW has not affected the strain dramatically. However, shifting the brine from SSW to DW shows an increase in the strain trend. Permeability of the core has been calculated using Eq. 2.30 and plotted during the test period and shown in these images too. The same trend can be observed here as could be in Fig. 4.3 and Fig. 4.4. It means that increasing the creep strain has the inverse effect on the permeability and the permeability drops as the compaction grows. The initial permeability is approx. equal to 1.45 mD. The permeability volumes in the end of flooding each fluid have been given in Table 4.5 for both tests which vary between 0.3 mD to 0.7 mD.

Test name	Permeability (K), [mD]		
	FW	SSW	DW
KD2-L	0.7	0.5	0.4
KD2-U	0.6	0.4	0.3

Table 4.5. The permeability [mD] in the end of flooding each fluid for tests KD2-L and KD2-U

It should be noted that a correction on the permeability had been done due to the brine shift. Meaning that due to the change in the brine composition, the viscosity of the brine also changes. Using a fluid properties calculator (Crewes 2007), the viscosity ( $\mu$ ) has been calculated for all of our flooding fluids. Table 4.6 shows the results.

Flooding Fluid	Viscosity $\mu$ [cP]
FW	0.3290
SSW	0.2560
DW	0.1997

Table 4.6. The viscosity of flooding fluids [cP] used in the experiments



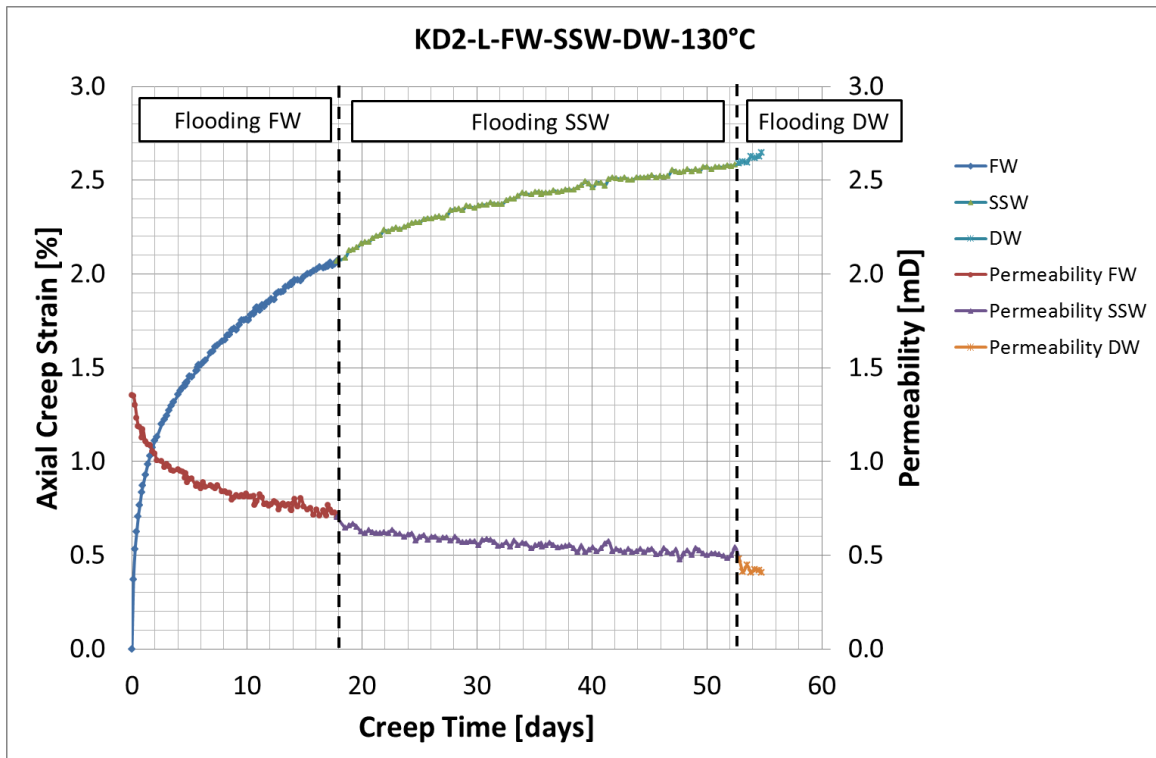


Fig. 4.5. Creep strain vs. Creep time for the test KD2-L

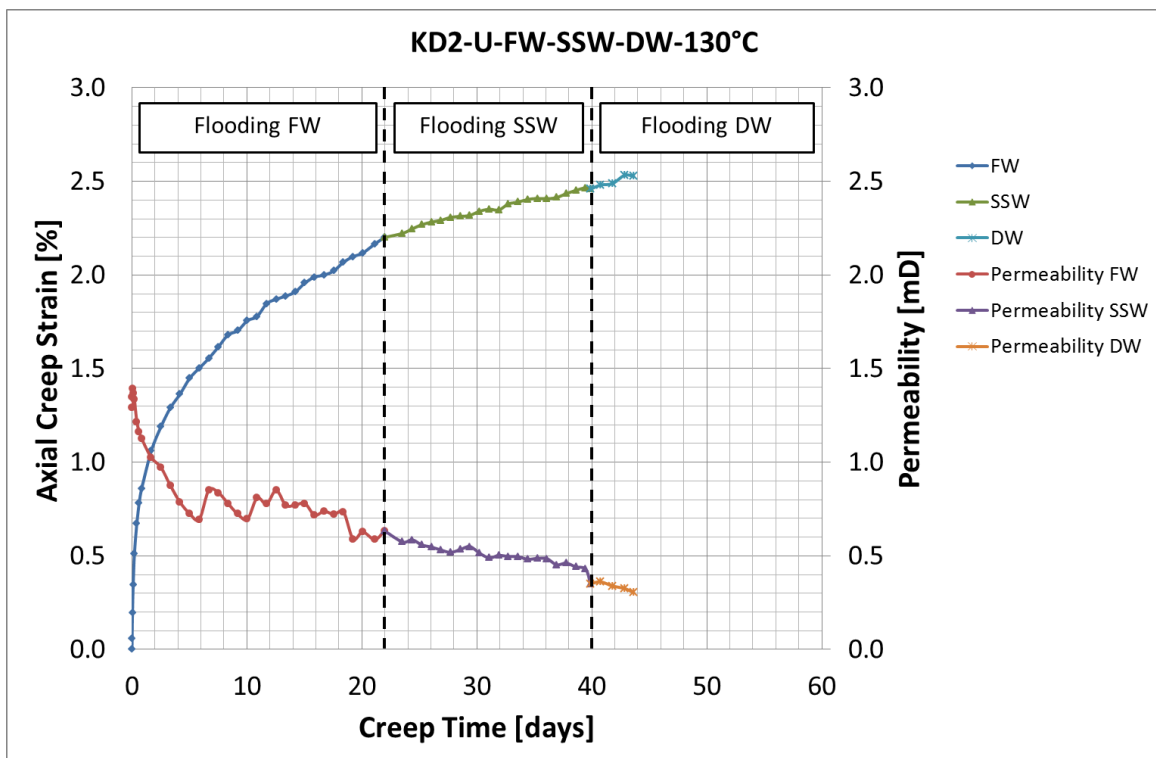


Fig. 4.6. Creep strain vs. Creep time for the test KD2-U

We have also plotted the  $\text{Log}(d\varepsilon/dt)$  vs.  $\text{Log}(\text{Time})$  curve in Fig 4.7 and Fig. 4.8 for the tests KD2-L and KD2-U respectively. This shows that the strain rate is reduced as the time is increased throughout the test. Meaning that, the strain rate is quite higher in the beginning of the test and decreases over time. The pictures illustrate that the strain rate is decreasing more when injecting SSW and increasing significantly while DW is injected. A trend line is sketched for each part of the test and the equation of these trend-lines is listed in Table 4.7.

<b>Log(<math>d\varepsilon/dt</math>) vs. Log(<math>\text{Time}</math>)</b>		
<b>Test Name</b>	<b>Trend-line Equations</b>	
KD2-L	FW	$y = -0.7259x - 0.5636$
		$R^2 = 0.9695$
	SSW	$y = -1.4085x + 0.2686$
		$R^2 = 0.7436$
	DW	$y = 11.068x - 20.87$
		$R^2 = 0.9748$
KD2-U	FW	$y = -0.439x - 0.8905$
		$R^2 = 0.9538$
	SSW	$y = -0.7599x - 0.6802$
		$R^2 = 0.4488$
	DW	$y = 1.6832x - 4.4827$
		$R^2 = 0.646$

Table 4.7. The equations for trend-lines in the  $\text{Log}(d\varepsilon/dt)$  vs.  $\text{Log}(\text{Time})$  curve.

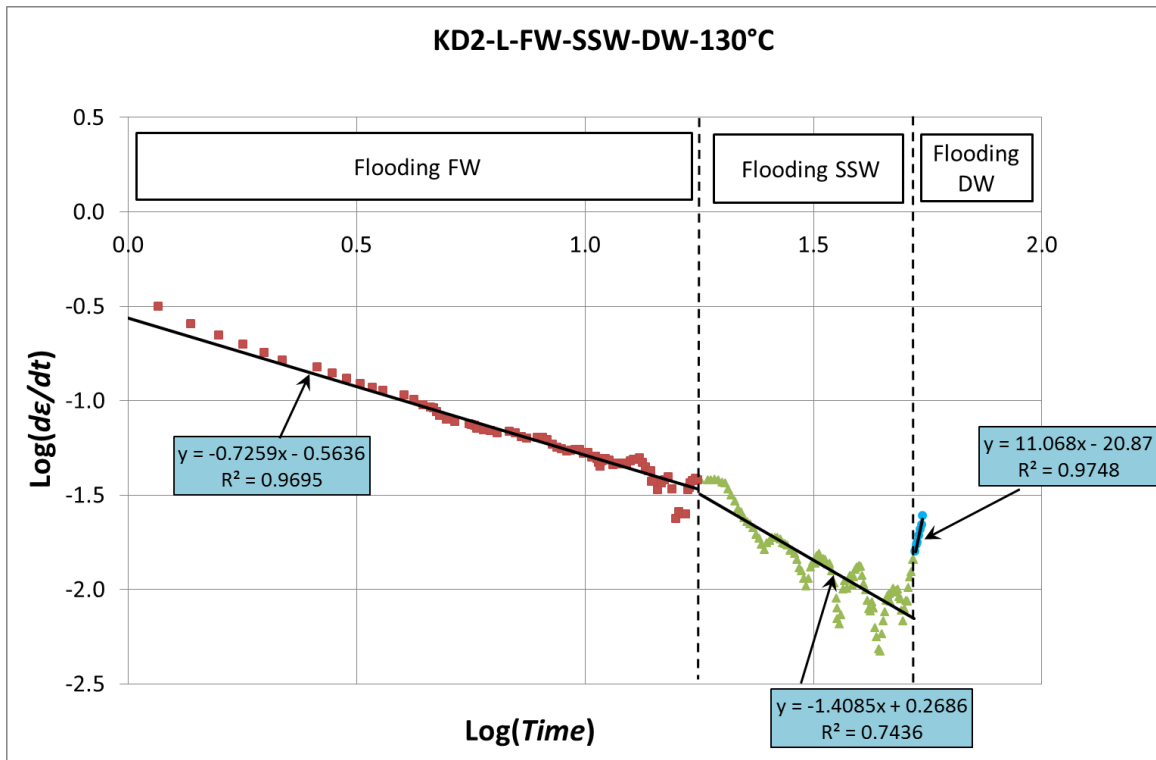


Fig. 4.7.  $\text{Log}(d\epsilon/dt)$  vs.  $\text{Log}(Time)$  for KD2-L test

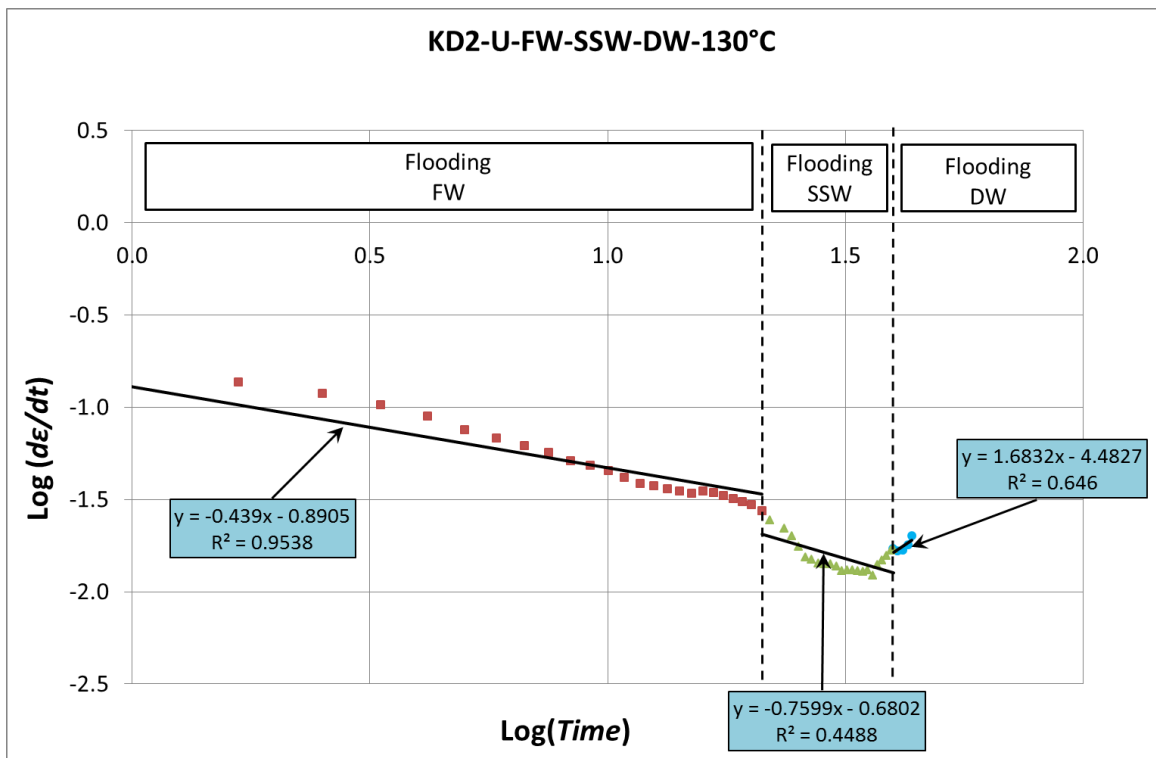


Fig. 4.8.  $\text{Log}(d\epsilon/dt)$  vs.  $\text{Log}(Time)$  for KD2-U test

#### 4.2.4 Porosity vs. Time

Porosity evolution has been plotted in Fig. 4.9 employing Eq. 2.24 and Eq. 2.13 for both tests KD2-L and KD2-U. We can see declining trends in the curves. The decreasing rate of porosity is higher in the beginning. The figure illustrates that the initial porosity varies between 36 to 37 % and the final porosity varies between 30 to 32 %.

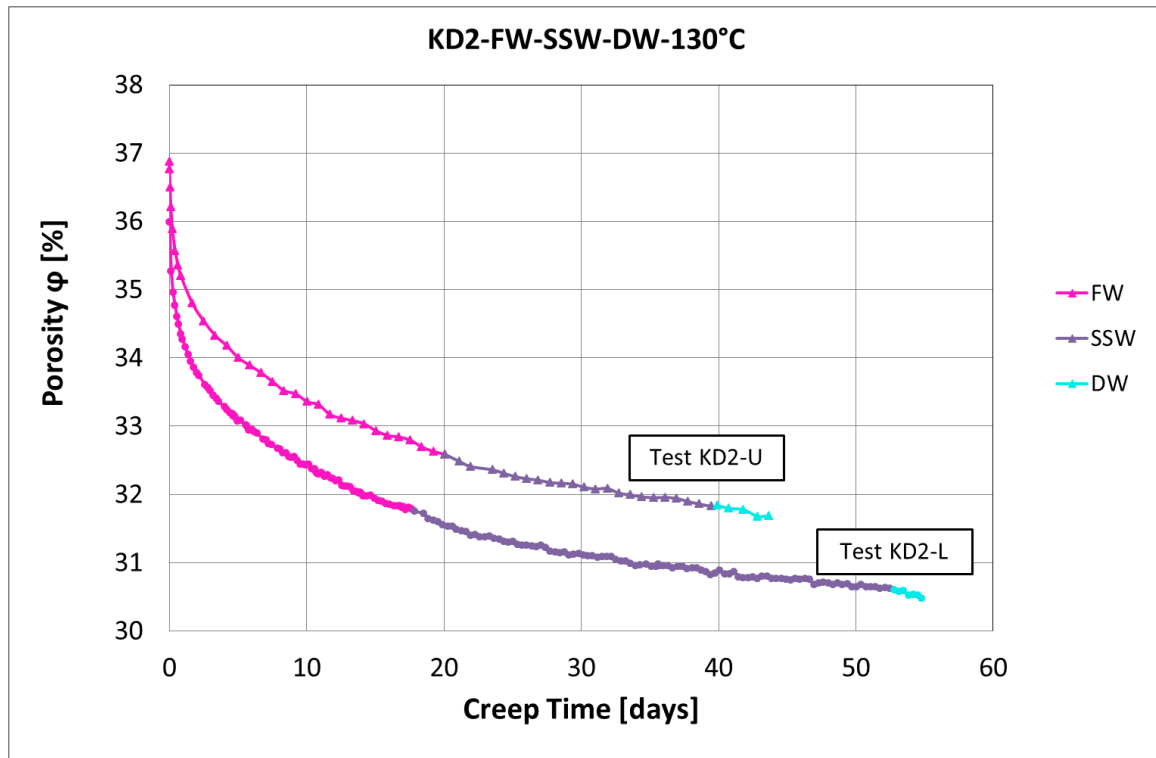


Fig. 4.9. Porosity ( $\phi$ ) versus Time For the tests KD2-L and KD2-U

#### 4.2.5 Permeability vs. Axial Creep Strain

Fig. 4.10 and Fig. 4.11 determine the relation between permeability and the axial creep strain. The interception of the trend line is equal to 1.46 and 1.45; and the slope of that is equal to -0.37 and -0.40 for the test KD2-L and KD2-U in turn. We can see an inverse, linear-relation between permeability and axial creep strain.

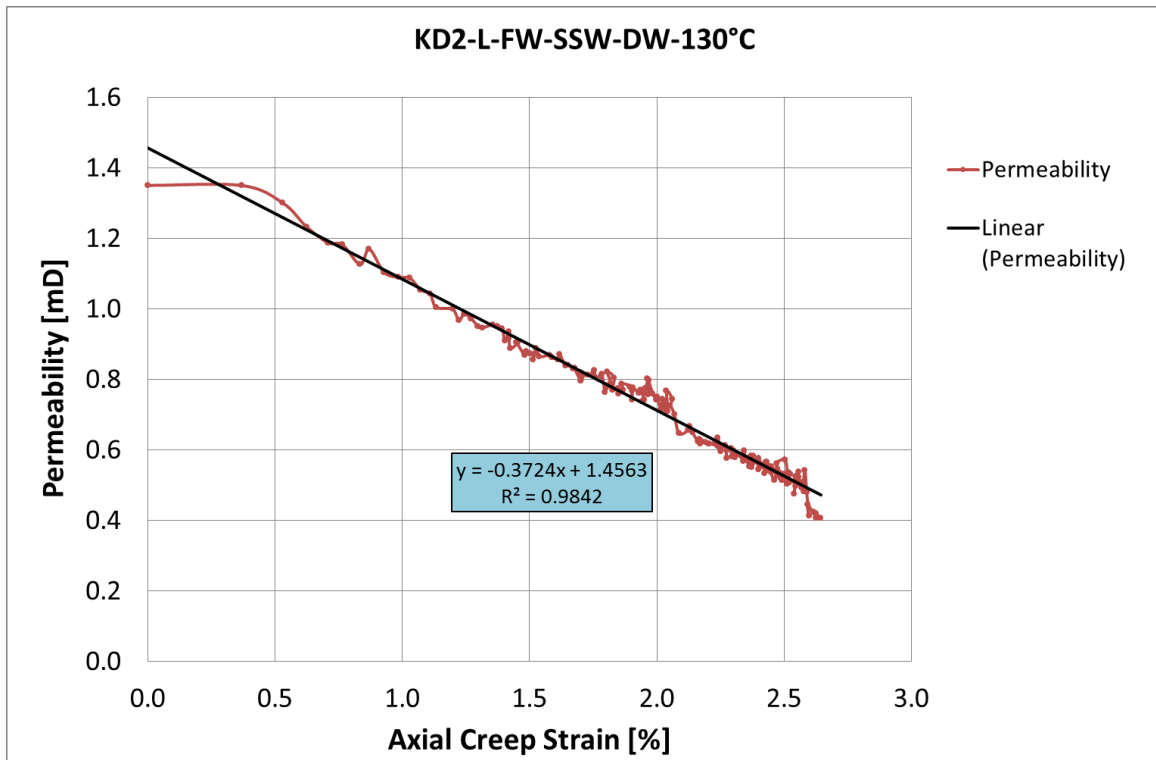


Fig. 4.10. Permeability vs. Axial creep Strain for the test KD2-L

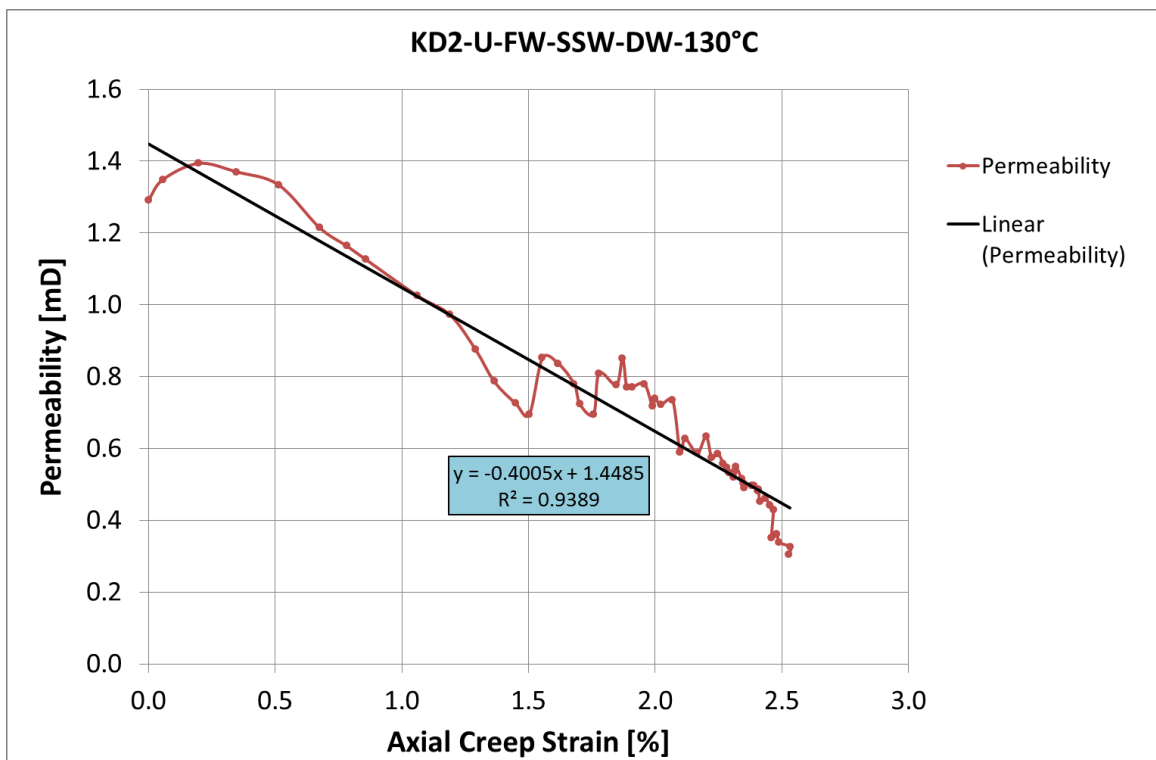


Fig. 4.11. Permeability vs. Axial creep Strain for the test KD2-U

### 4.2.6 Permeability vs. Porosity

The graphs in Fig. 4.12 and Fig. 4.13 indicate the permeability-porosity relation in our study. A linear direct relation can be observed in both tests. The higher is the porosity, the higher is the permeability.

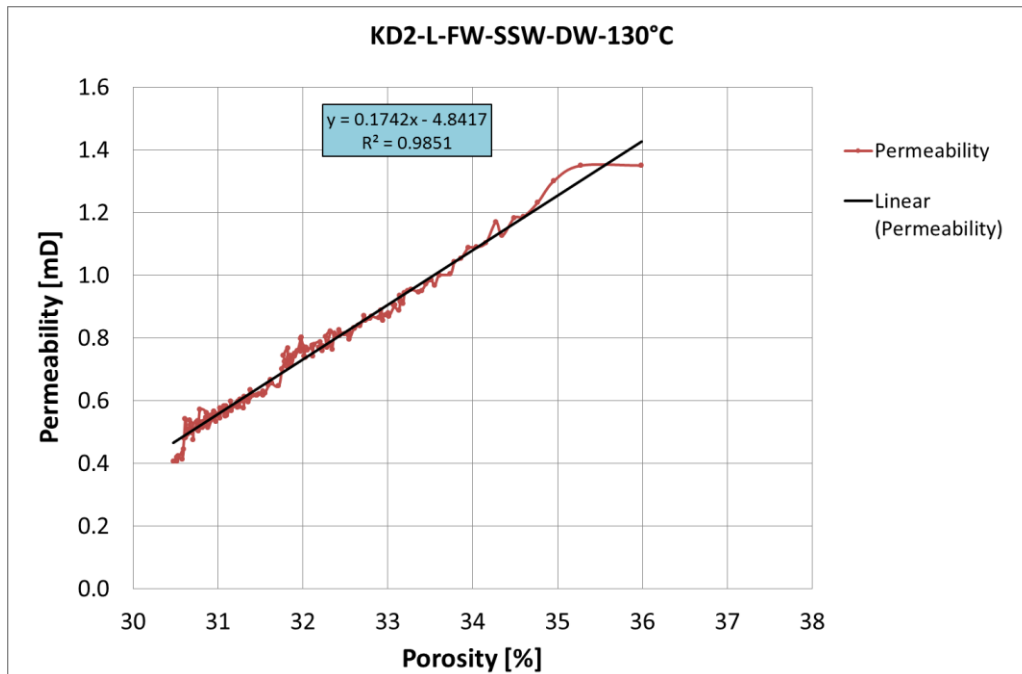


Fig. 4.12. Permeability versus Porosity for the test KD2-L

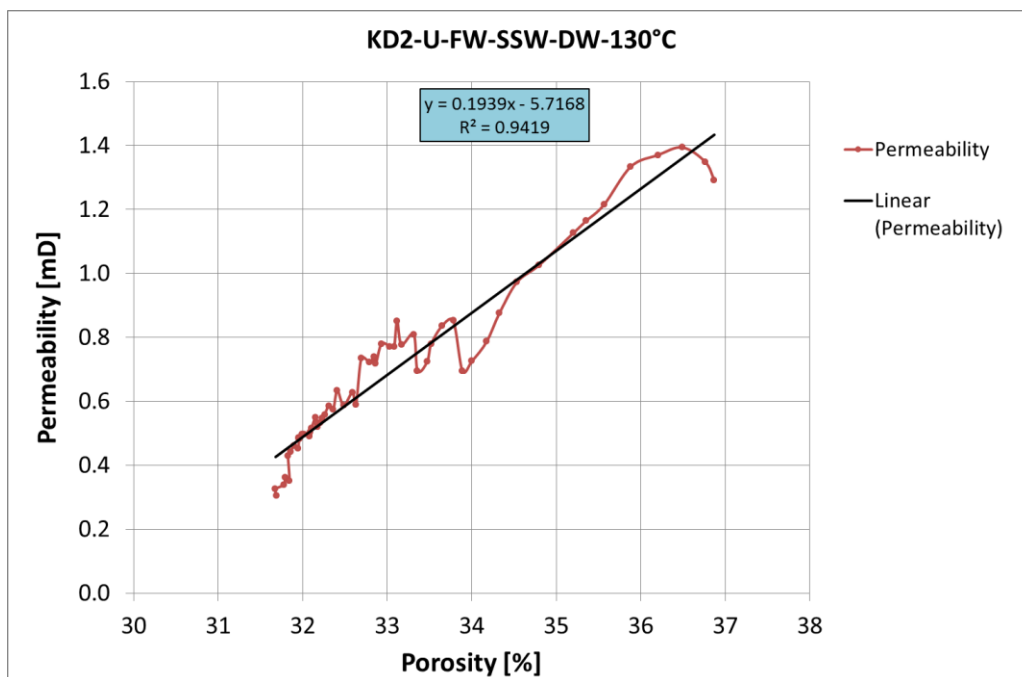


Fig. 4.13. Permeability versus Porosity for the test KD2-U

### 4.2.7 Permeability Evolution ( $K(t)/K_0$ ) vs. Time

Permeability evolution has been plotted for both tests over time using Eq. 2.13 and Eq. 2.33 which is shown in the Fig. 4.14. A declining trend can be observed in both tests. The rate of reduction is expressively higher in the beginning. Obviously, the graph starts from 1 for both cases and it ends up to 0.3 for test KD2-L and to 0.25 for test KD2-U in the end of the tests.

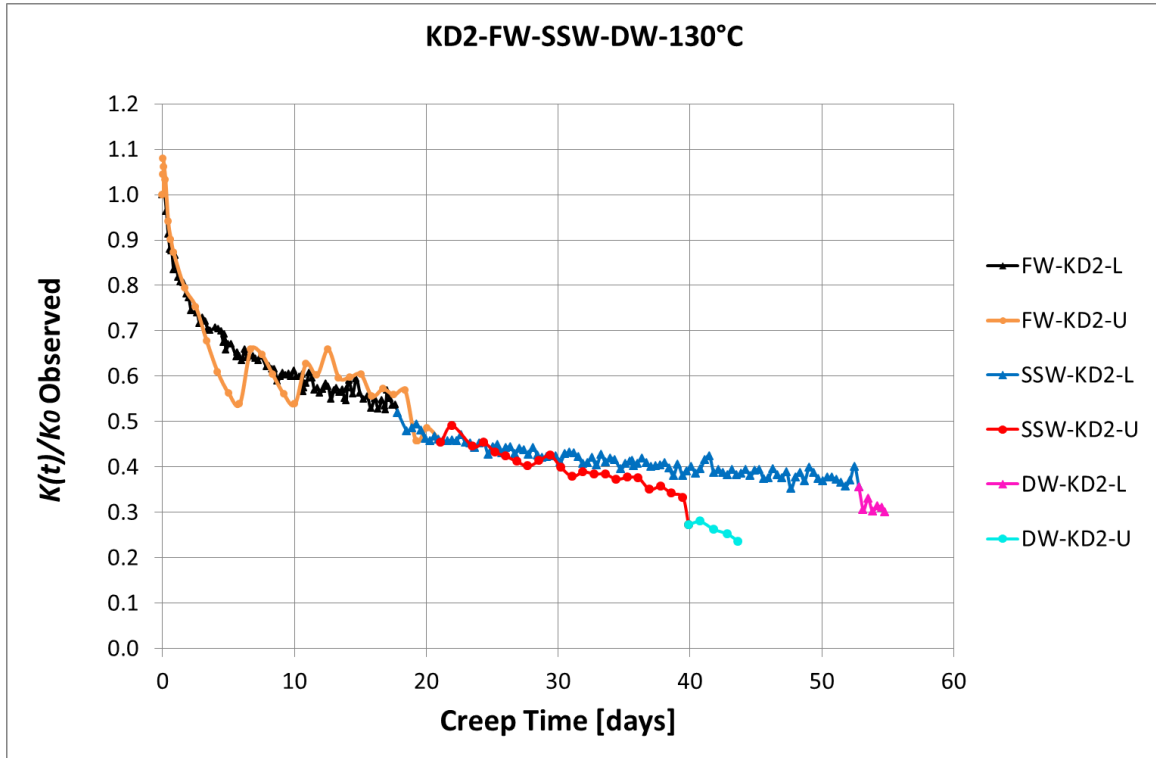


Fig. 4.14. Permeability Evolution ( $K(t)/K_0$ ) versus Time for the test KD2-L and KD-U

### 4.2.8 Permeability Evolution ( $K(t)/K_0$ ) vs. Volumetric Strain ( $\epsilon_v$ )

Permeability evolution observed in our experiment has been plotted versus volumetric strain in Fig. 4.15 and Fig. 4.16 employing Eq. 2.13 and Eq. 2.33. An inverse linear relation can be seen in this term. The slope of the trend line is equal to -0.092 and -0.103 for the test KD2-L and KD2-U respectively.

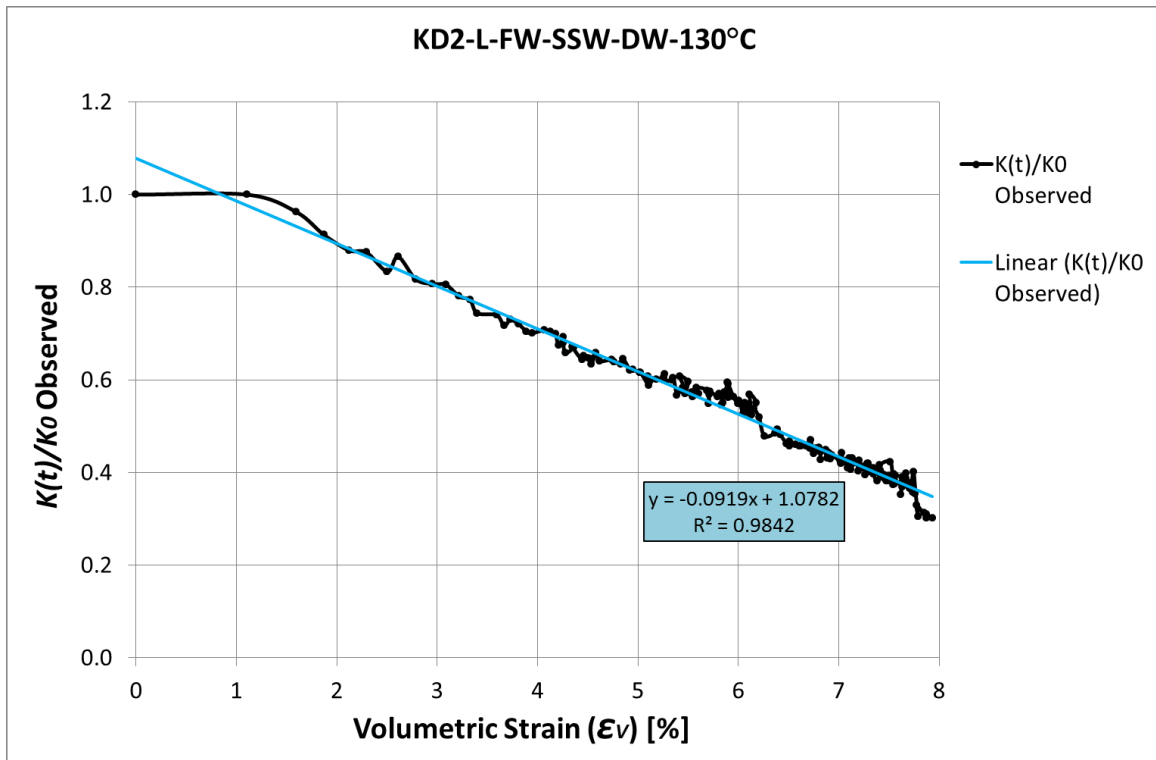


Fig. 4.15. Permeability Evolution ( $K(t)/K_0$ ) versus Volumetric Strain ( $\epsilon_v$ ) for the test KD2-L

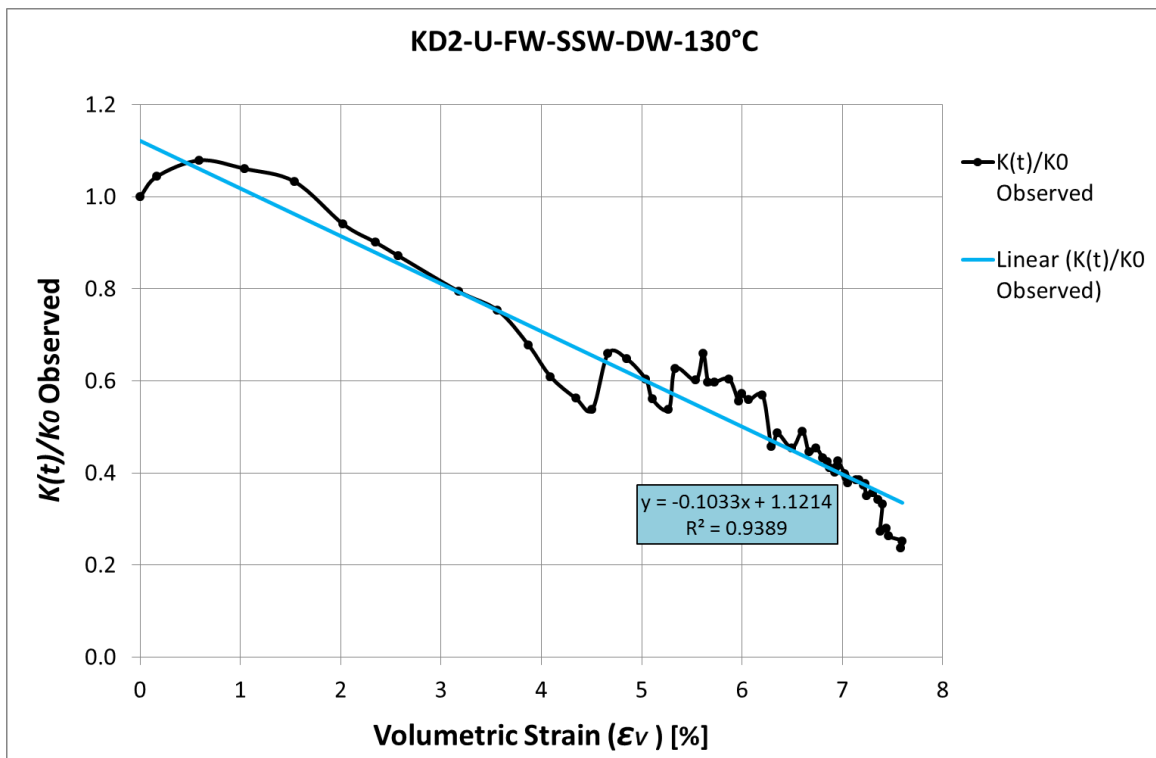


Fig. 4.16. Permeability Evolution ( $K(t)/K_0$ ) versus Volumetric Strain ( $\epsilon_v$ ) for the test KD2-U



## 4.3 Core Analyzing after Test

### 4.3.1 Bulk Volume Measurement

After finishing each test, the triaxial cell was dismantled and the tested core was carefully taken out for core analysis. We have marked the core as shown in the Fig. 3.22 and cut it in to 7 pieces. However, before cutting we have measured the diameter and length three times, in three different directions and the results are summed up in the Table 4.8 and Table 4.9 for the test LD2-L and KD2-U. The arrow next to these tables shows the gradient of average diameter of the tested core. We can see that in the inlet, middle and out let of the core the diameter is higher for both tested core similarly.

We also have taken some images of the cross section surface of each piece; both the inlet and outlet sides of the core. These images illustrate that the inlet sides of the chalk pieces have more or less rough and coarse-grained texture. However, the outlet sides have a smooth and uniform texture. We have included these pictures in the appendix of this thesis.

Using the measurements in table 4.8 and table 4.9, the bulk volume of the cores was calculated based on Eq. 3.1 and the results is presented in the table 4.10 and 4.11 For the tests KD2-L and KD2-U in turn. The total bulk volume for the former is equal to  $69.89 \text{ cm}^3$  and for the latter is equal to  $70.88 \text{ cm}^3$ . We use these measurements later on to calculate the density of the core using Eq.3.2.

KD2-LOWER-FW-SSW-DW-130°C-After Testing					
Line	Diameter Measurement (mm)			Average Diameter (mm)	Average Radial (mm)
	1	2	3		
0	36.58	36.53	36.70	36.60	18.30
1	36.34	36.21	36.23	36.26	18.13
2	36.34	36.36	36.09	36.26	18.13
3	36.36	36.18	36.11	36.22	18.11
4	36.34	36.22	36.32	36.29	18.15
5	36.21	36.05	36.12	36.13	18.06
6	36.26	36.08	36.09	36.14	18.07
7	36.66	36.43	36.55	36.55	18.27
	Length Measurement (mm)			Average Length (mm)	
	1	2	3		
	67.66	67.67	67.64	67.66	

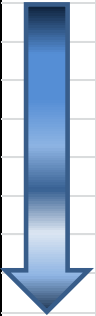


Table 4.8. The length and diameter measurements of the core KD2-L after testing

KD2-UPPER-FW-SSW-DW-130°C-After Testing					
Line	Diameter Measurement (mm)			Average Diameter (mm)	Average Radial (mm)
	1	2	3		
0	36.25	36.52	36.56	36.44	18.22
1	35.97	36.16	36.03	36.05	18.03
2	35.98	36.15	35.97	36.03	18.02
3	36.02	36.15	36.05	36.07	18.04
4	36.03	36.97	36.06	36.35	18.18
5	36.12	35.99	36.00	36.04	18.02
6	36.23	36.08	36.13	36.15	18.07
7	36.75	36.58	36.69	36.67	18.34
	Length Measurement (mm)			Average Length (mm)	
	1	2	3		
	68.99	68.88	68.99	68.95	

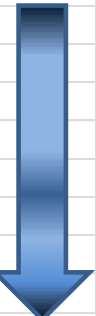


Table 4.9. The length and diameter measurements of the core KD2-U after testing

<b>KD2-LOWER-FW-SSW-DW-130°C</b>		
<b>Number of Pieces</b>	<b>Height H (mm)</b>	<b>Bulk Volume of Pieces VB (cm<sup>3</sup>)</b>
Piece 1	10	10.42
Piece 2	10	10.33
Piece 3	10	10.31
Piece 4	10	10.32
Piece 5	10	10.30
Piece 6	10	10.26
Piece 7	7.66	7.94
<b>Total</b>	<b>67.66</b>	<b>69.89</b>

Table 4.10. The bulk volume calculation of the core KD2-L

<b>KD2-UPPER-FW-SSW-DW-130°C</b>		
<b>Number of Pieces</b>	<b>Height H (mm)</b>	<b>Bulk Volume of Pieces VB (cm<sup>3</sup>)</b>
Piece 1	8.95	9.24
Piece 2	10	10.20
Piece 3	10	10.21
Piece 4	10	10.30
Piece 5	10	10.29
Piece 6	10	10.23
Piece 7	10	10.41
<b>Total</b>	<b>68.95</b>	<b>70.88</b>

Table 4.11. The bulk volume calculation of the core KD2-U

### 4.3.2 Solid Volume Measurement by Pycnometer

Implementing a pycnometer apparatus, we could measure the solid volume of chalk pieces. Each piece was measured twice. On the other hand, the mass of each piece was measured on the scale before using pycnometer. Consequently the solid density was calculated employing Eq. 2.19 and the results are presented in Table 4.12 and Table 4.13 for the test KD2-L and KD2-U sequentially. Once, we measured each piece individually. The average density value of P1-P7 has been calculated using Eq. 3.2 which is equal to 2.7206 gr/cm<sup>3</sup> and 2.7197 gr/cm<sup>3</sup> for tests KD2-L and KD2-U respectively. The other time, all the pieces was measured together in pycnometer which the average volume of that is equal to 2.7125 gr/cm<sup>3</sup> and 2.7190 gr/cm<sup>3</sup> for tests KD2-L and KD2-U in turn. Finally, we took an average value of the both measurements which is equal to 2.7165 gr/cm<sup>3</sup> and 2.7193 gr/cm<sup>3</sup>, the former for KD2-L and the later for KD2-U.

KD2-LOWER-FW-SSW-DW-130°C									
Number of Pieces	Dry Weight (gr)	Solid Volume (cm3)	Standard Deviation (cm3)	Density, $\rho$ (gr/cm3)	Average Dry Weight (gr)	Average Solid Volume (cm3)	Average Standard Deviation (cm3)	Average Dendity, $\rho_{Avg}$ (gr/cm3)	
Piece 1	Measurement.1	18.230	6.7358	0.0082	2.7064	18.234	6.7410	0.0122	2.7049
	Measurement.2	18.238	6.7462	0.0161	2.7034				
Piece 2	Measurement.1	16.312	5.9746	0.0145	2.7302	16.317	5.9671	0.0146	2.7345
	Measurement.2	16.322	5.9596	0.0146	2.7388				
Piece 3	Measurement.1	17.227	6.2959	0.0074	2.7362	17.230	6.2998	0.0095	2.7350
	Measurement.2	17.233	6.3036	0.0116	2.7338				
Piece 4	Measurement.1	16.824	6.1560	0.0153	2.7329	16.829	6.1664	0.0110	2.7291
	Measurement.2	16.833	6.1767	0.0066	2.7252				
Piece 5	Measurement.1	15.638	5.7672	0.0147	2.7115	15.641	5.7693	0.0146	2.7111
	Measurement.2	15.644	5.7714	0.0145	2.7106				
Piece 6	Measurement.1	17.098	6.3237	0.0147	2.7038	17.102	6.3107	0.0149	2.7099
	Measurement.2	17.105	6.2977	0.0151	2.7161				
Piece 7	Measurement.1	12.285	4.5275	0.0062	2.7134	12.291	4.5175	0.0106	2.7208
	Measurement.2	12.297	4.5075	0.0149	2.7281				
All Pieces together	Measurement.1	113.6	41.917	0.0037	2.7106	113.635	41.8935	0.0031	2.7125
	Measurement.2	113.7	41.870	0.0025	2.7144				
Average of P1-P7						113.643	41.7717		2.7206
Total Average of both measurements						113.64	41.8326		2.7165

Table 4.12. The pycnometer and mass measurements; and the density calculation results for KD2-L

KD2-UPPER-FW-SSW-DW-130°C									
Number of Pieces	Dry Weight (gr)		Solid Volume (cm3)	Standard Deviation (cm3)	Density, $\rho$ (gr/cm3)	Average Dry Weight (gr)	Average Solid Volume (cm3)	Average Standard Deviation (cm3)	Average Dendity, $\rho_{Avg}$ (gr/cm3)
Piece 1	Measurement.1	11.150	4.0621	0.0079	2.7449	11.154	4.0543	0.0078	2.7512
	Measurement.2	11.158	4.0464	0.0076	2.7575				
Piece 2	Measurement.1	18.378	6.7795	0.0051	2.7108	18.383	6.7759	0.0050	2.7129
	Measurement.2	18.387	6.7722	0.0049	2.7151				
Piece 3	Measurement.1	14.882	5.4884	0.0027	2.7115	14.887	5.4837	0.0037	2.7148
	Measurement.2	14.892	5.4789	0.0047	2.7181				
Piece 4	Measurement.1	16.376	6.0431	0.0048	2.7099	16.380	6.0472	0.0050	2.7086
	Measurement.2	16.383	6.0512	0.0051	2.7074				
Piece 5	Measurement.1	18.163	6.7202	0.0069	2.7027	18.167	6.6990	0.0076	2.7119
	Measurement.2	18.170	6.6778	0.0082	2.7210				
Piece 6	Measurement.1	16.180	5.9577	0.0056	2.7158	16.184	5.9581	0.0044	2.7162
	Measurement.2	16.187	5.9584	0.0032	2.7167				
Piece 7	Measurement.1	18.680	6.8401	0.0037	2.7310	18.684	6.8380	0.0036	2.7323
	Measurement.2	18.687	6.8359	0.0034	2.7337				
All Pieces together	Measurement.1	113.8	41.8687	0.0051	2.7185	113.830	41.8653	0.0104	2.7190
	Measurement.2	113.8	41.862	0.0156	2.7194				
Average of P1-P7						113.837	41.8560		2.7197
Total Average of both measurements						113.833	41.8606		2.7193

Table 4.13. The pycnometer and mass measurements; and the density calculation results for KD2-U

Before starting the tests, when the drilled core KD2 was cut into two cores KD2-L and KD2-U, we kept the pieces below, above and in between of these cores. The solid volume of these pieces was measured using pycnometer and the dry weight of them also was measured on the scale. Accordingly, the average density was calculated employing Eq. 2.19. Table 4.14 shows these results which varies between 2.71 gr/cm<sup>3</sup> to 2.73 gr/cm<sup>3</sup>.

KD2 Pycnometer Measurements						
Piece Name	Dry Weight (gr)		Solid Volume (cm <sup>3</sup> )	Standard Deviation (cm <sup>3</sup> )	Density, $\rho$ (gr/cm <sup>3</sup> )	Average Density, $\rho_{Avg}$ (gr/cm <sup>3</sup> )
KD2-BELOW	Measurement.1	20.614	7.5866	0.0051	2.7172	2.7204
	Measurement.2	20.626	7.5731	0.0047	2.7236	
KD2-BETWEEN	Measurement.1	24.360	8.9612	0.0072	2.7184	2.7236
	Measurement.2	24.373	8.9317	0.0055	2.7288	
KD2-ABOVE	Measurement.1	24.004	8.8427	0.0094	2.7146	2.7180
	Measurement.2	24.014	8.8238	0.0056	2.7215	

Table 4.14. The solid volume and mass measured and the average density calculated for the pieces KD2-BELOW, KD2-BETWEEN and KD2-ABOVE

The bulk volume, solid volume, porosity and density of the cores KD2-L and KD2-U both before and after the test have been calculated using different measurement methods; and summed up in Table 4.15.

The bulk volume ( $V_B$ ) was calculated according two measurements:

Meas.1; employing Eq. 2.17

Meas.2; employing Eq. 3.1

The solid volume ( $V_S$ ) was calculated according two measurements:

Meas.1; employing Eq. 2.14 and Eq. 2.17

Meas.2; employing Eq. 2.14 and Eq. 3.1

The porosity ( $\phi$ ) was calculated according four measurements:

Meas.1; employing Eq. 2.15 and Eq. 2.17

Meas.2; employing Eq. 2.15 and Eq. 3.1

Meas.3; employing Eq. 2.24

Meas.4; employing Eq. 2.28

The density ( $\rho$ ) was calculated according four measurements:

Meas.1; employing Eq. 2.16 and Eq. 2.17

Meas.2; employing Eq. 2.16 and Eq. 3.1

Meas.3; employing Eq. 3.2

Sample Name	Length L [mm]	Diameter D [mm]	Dry Weight W <sub>D</sub> [gr]	Wet Weight W <sub>w</sub> [gr]	Pore Volume V <sub>p</sub> [cm <sup>3</sup> ]	Bulk Volume V <sub>B</sub> [cm <sup>3</sup> ]		Solid Volume V <sub>s</sub> [cm <sup>3</sup> ]		Porosity Φ [%]				Density ρ [gr/cm <sup>3</sup> ]			
						Meas.1	Meas.2	Meas.1	Meas.2	Meas.1	Meas.2	Meas.3	Meas.4	Meas.1	Meas.2	Meas.3	
KD2-L Before	69.64	36.96	128.97	155.85	26.88	74.68	#	47.80	#	35.99	#	35.99	35.99	2.6982	#	#	#
KD2-L After	67.66	36.31	128.57	#	#	70.03	69.89	#	#	#	#	30.515	31.815	#	#	2.7165	#
KD2-U Before	70.71	36.98	129.44	157.43	27.99	75.91	#	47.92	#	36.87	#	36.87	36.87	2.7013	#	#	#
KD2-U After	68.95	36.23	129.10	152.05	22.96	71.05	70.88	48.09	47.93	32.31	32.38	31.685	32.575	2.6844	2.6935	2.7193	#

Table 4.15. The mechanical properties of the cores KD2-L and KD2-U both before and after the test

## 4.4 Chemical Analysis

### 4.4.1 Ionic Chromatography (IC)

During the test effluent samples were collected in the both tests KD2-L and KD2-U. However, effluent sample was not collected during flooding of distilled water (DW). The effluent samples were used for chemical analysis later on using an ionic chromatography machine. Implementing this method we have plotted several graphs, showing the ionic concentration of different components in the fluid flooded through the core. Fig. 4.17 and Fig. 4.18 shows the concentration on all ions measured in our effluent fluid for both the tests KD2-L and KD2-U respectively. The standard concentration of ions has been determined in these graphs. To be able to see all the lines more clearly, we have plotted ions  $\text{Na}^+$  and  $\text{Cl}^-$  separately from other ions. In Fig. 4.19 and Fig. 4.20 the concentration of  $\text{Na}^+$  and  $\text{Cl}^-$  ions has been presented with the original concentration of each standard. Similarly, Fig. 4.21 and Fig. 4.22 illustrate the ion concentration of other components including  $\text{Mg}^{2+}$ ,  $\text{SO}_4^{2-}$ ,  $\text{Ca}^{2+}$  and  $\text{K}^+$  and their original concentrations of standards.

The figures demonstrate that all of the ions have more or less the same concentration as their originals during flooding of formation water (FW, which is NaCl solution 1.833 mole/l). While flooding synthetic sea water (SSW), the same trend can be seen except for magnesium and calcium. The graphs determine that during SSW injection,  $\text{Ca}^{2+}$  is produced in the effluent and  $\text{Mg}^{2+}$  has been lost. However, the production of  $\text{Ca}^{2+}$  and loss of  $\text{Mg}^{2+}$  decrease over time. Flooding FW continued for 20 days and 22 days for the tests KD2-L and KD2-U respectively while injecting SSW lasted for 35 and 19 days.



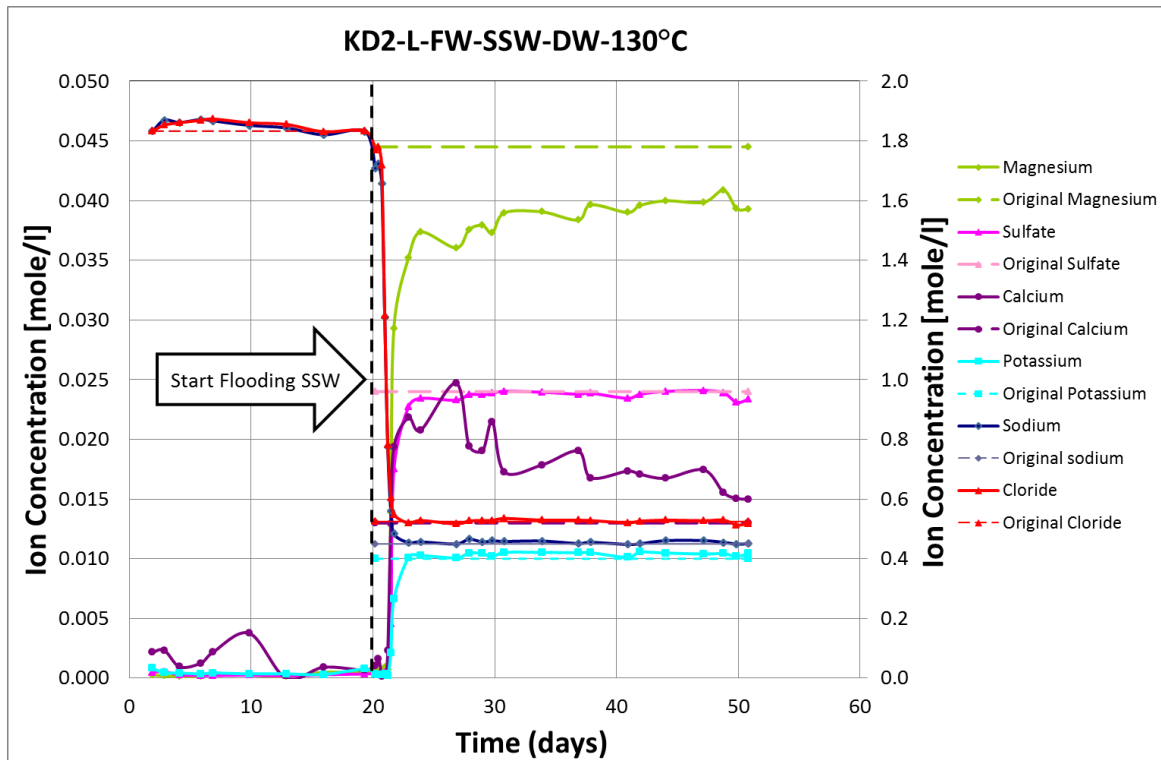


Fig. 4.17. The concentration of containing ions in the effluent samples for the test KD2-L

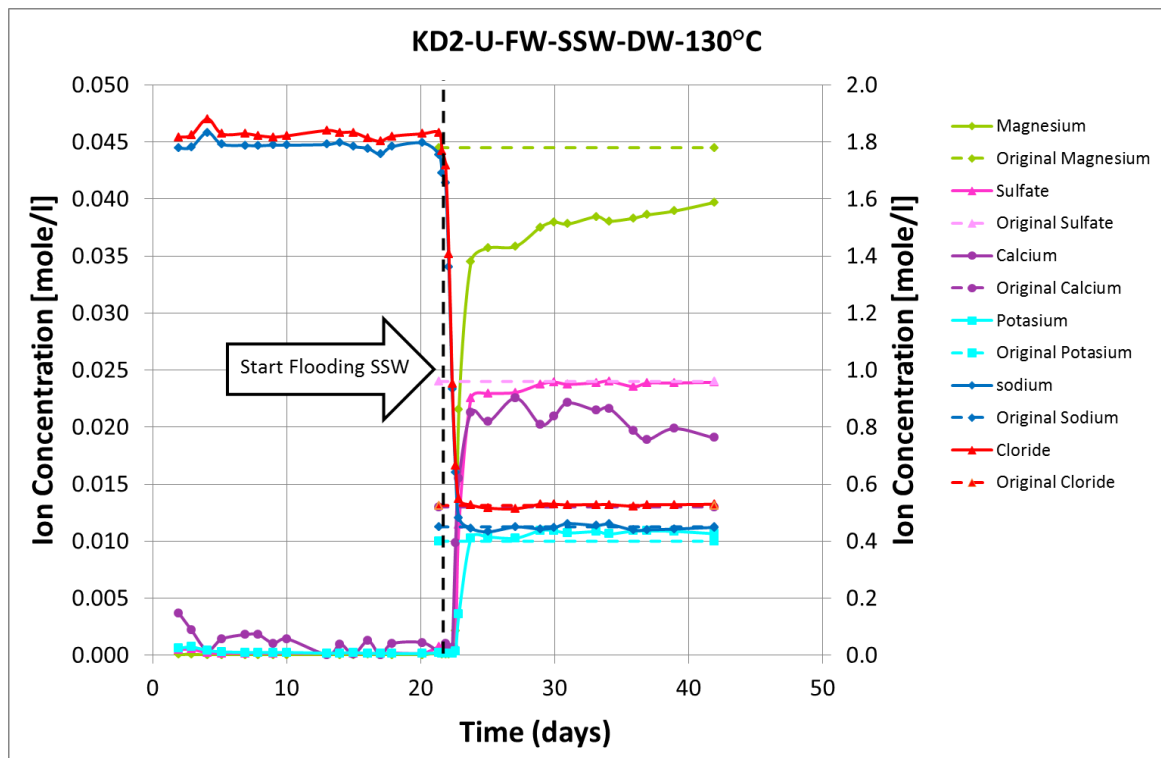


Fig. 4.18. The concentration of containing ions in the effluent samples for the test KD2-U

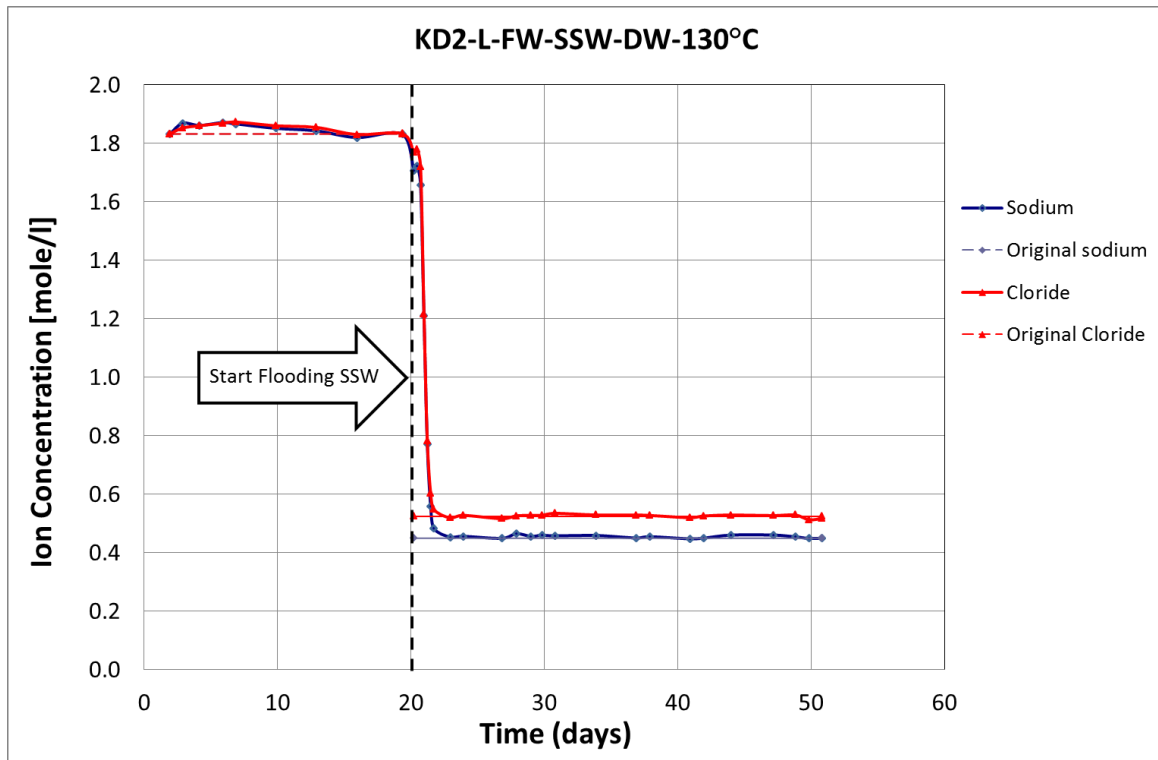


Fig. 4.19. The concentration of  $\text{Na}^+$  and  $\text{Cl}^-$  ions in the effluent samples for the test KD2-L

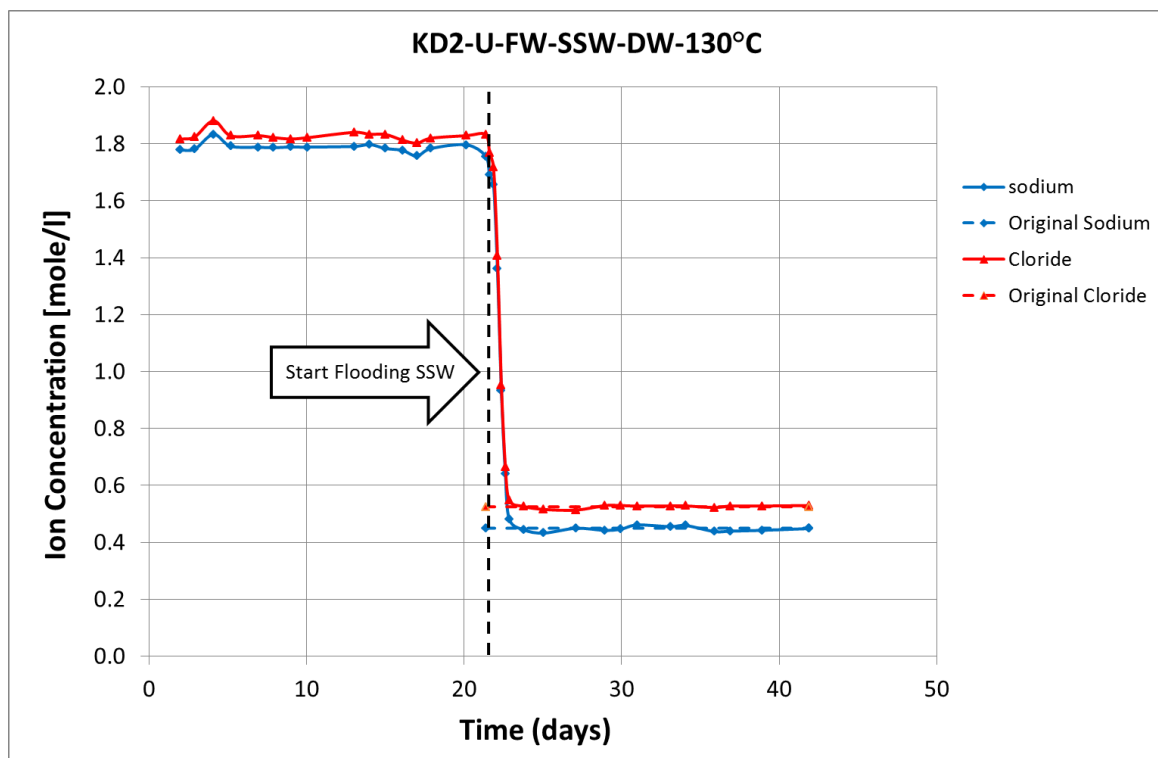


Fig. 4.20. The concentration of  $\text{Na}^+$  and  $\text{Cl}^-$  ions in the effluent samples for the test KD2-U

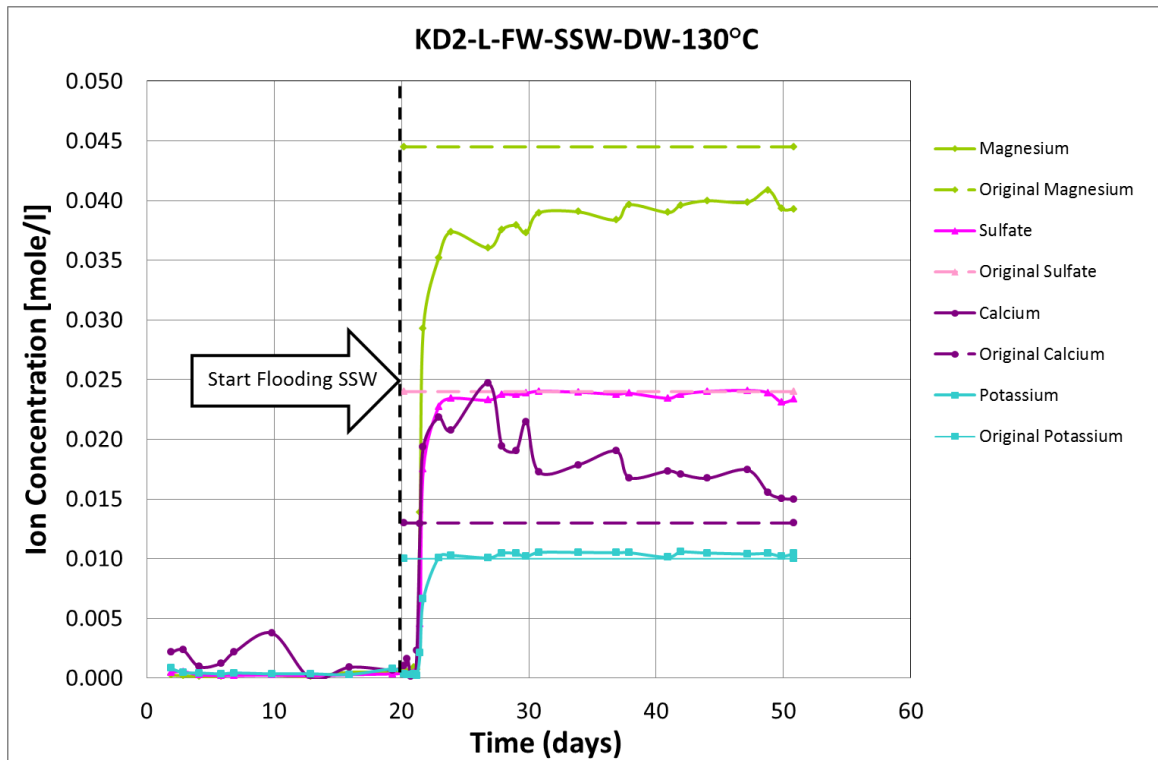


Fig. 4.21. The concentration of  $Mg^{2+}$ ,  $SO_4^{2-}$ ,  $Ca^{2+}$  and  $K^+$  ions in the effluent samples for the test KD2-L

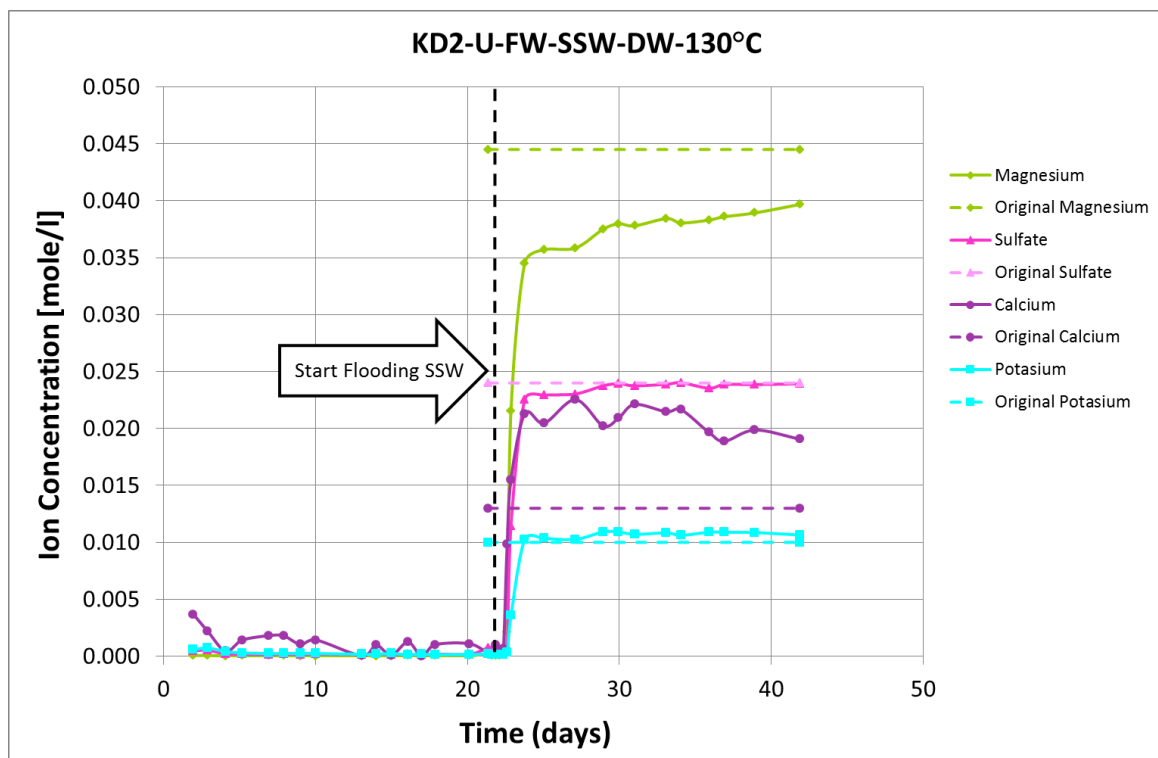


Fig. 4.22. The concentration of  $Mg^{2+}$ ,  $SO_4^{2-}$ ,  $Ca^{2+}$  and  $K^+$  ions in the effluent samples for the test KD2-U

The accumulated production of magnesium and calcium and the total mass change have been plotted in the Fig. 4.23 and Fig. 4.24 for the test KD2-L and KD2-U respectively. The results have been summed up in Table 4.16 which shows the total mass change is equal to 0.036 gr and 0.030 gr for tests KD2-L and KD2-U in order.

Test Name	Chemical Analysis		
	Accumulated Production Mg <sup>2+</sup> [gr]	Accumulated Production Ca <sup>2+</sup> [gr]	Total Mass Change [gr]
KD2-L	-0.155	0.191	0.036
KD2-U	-0.136	0.166	0.030

Table 4.16. Chemical analysis results

The core solid volume change also has been calculated based on the total mass change in the effluent and the density and shown in Fig. 4.25 for both test KD2-L and KD2-L. The solid volume of the core decreased 0.013 and 0.009 cm<sup>3</sup> during flooding FW. Starting injection of SSW has contributed to dramatic increase of 0.020 cm<sup>3</sup> and 0.024 cm<sup>3</sup> of solid volume. Continuing injection of SSW decreased solid volume of the core. In the end of SSW injection the solid volume change is equal to -0.014 and -0.012 cm<sup>3</sup> in the test KD2-L and KD2-U respectively.

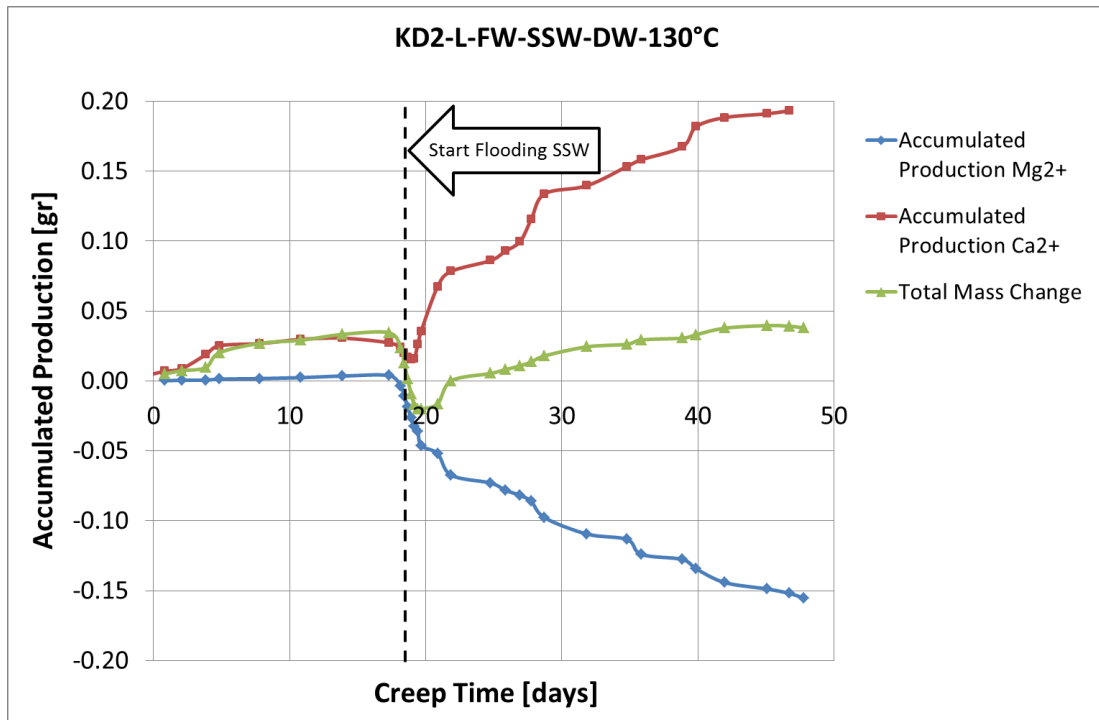


Fig. 4.23. The Effluent Accumulated Production of Mg<sup>2+</sup> and Ca<sup>2+</sup>, and the Effluent Total Mass Change over time for the test KD2-L

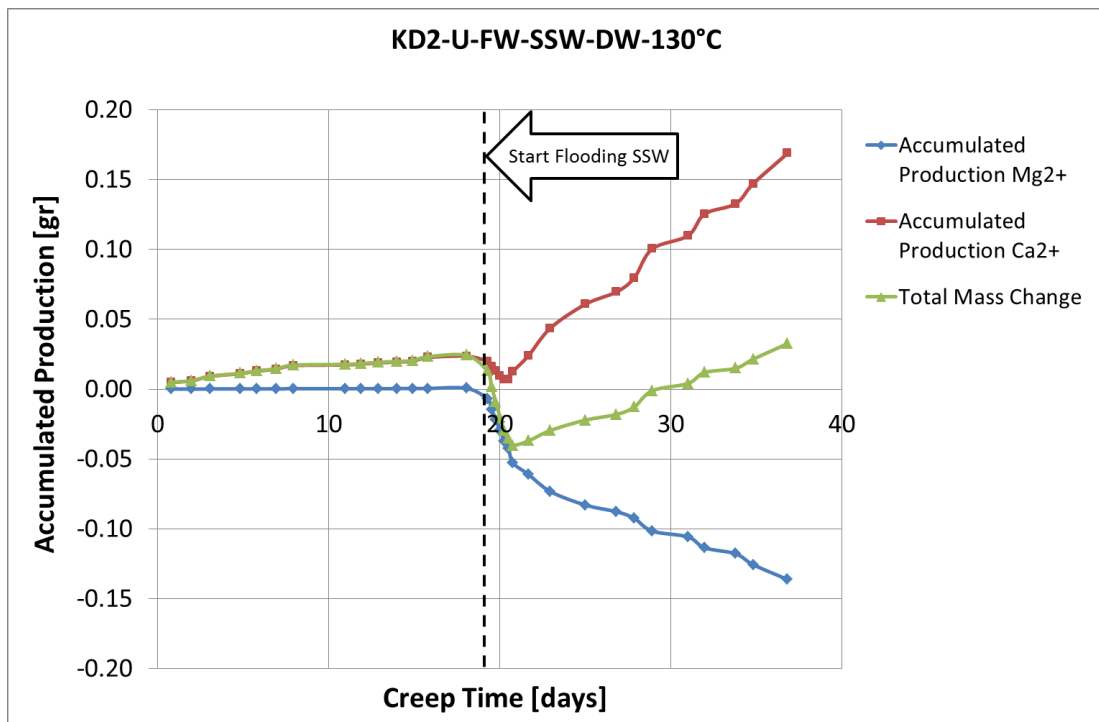


Fig. 4.24. The Effluent Accumulated Production of Mg<sup>2+</sup> and Ca<sup>2+</sup>, and the Effluent Total Mass Change over Creep Time for the test KD2-U

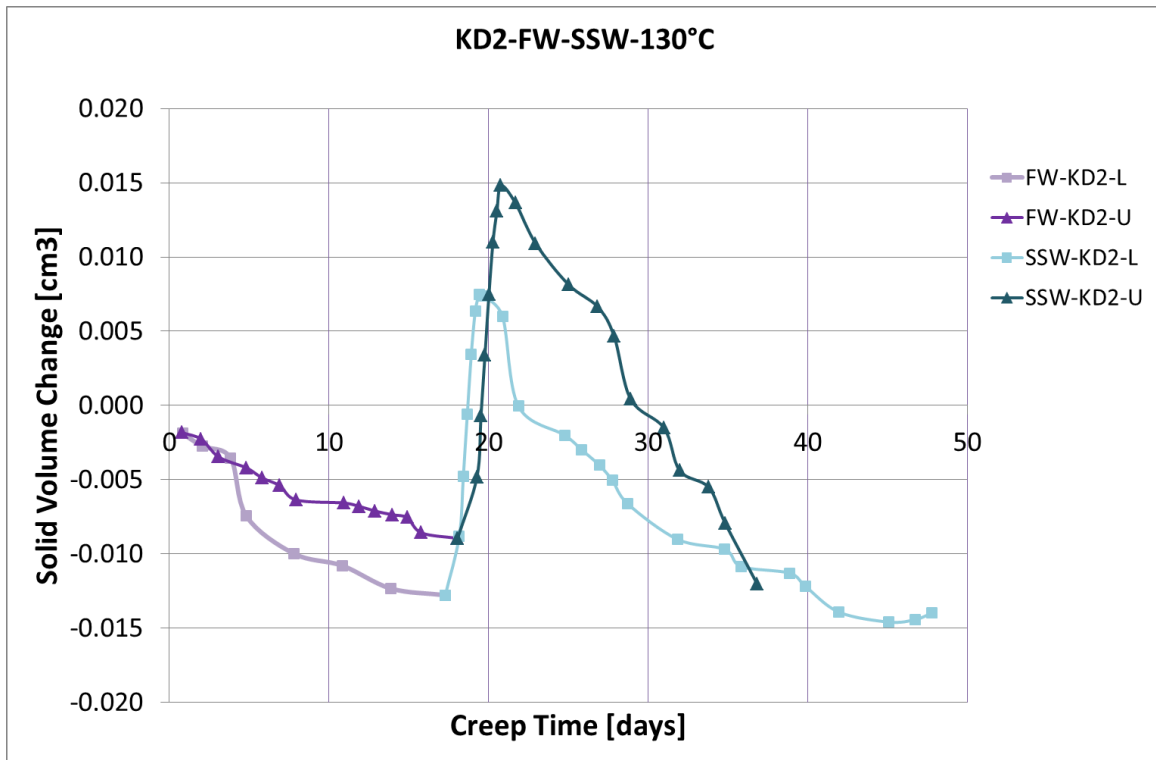


Fig. 4.25. The Core Solid Volume Change over Creep Time for the tests KD2-L and KD2-U

## 5. Discussion

In this study we have flooded formation water (FW) –which is NaCl solution 1.833 mole/l-, synthetic sea water (SSW) and distilled water (DW) continuously through Kansas chalk core for almost 2 mounts for each test. Two hydrostatic tests were completed, one on KD2-L core and the other one on KD2-U. The tests were held in temperature of 130 °C and the maximum confining pressure of 20 MPa in a triaxial cell.

The objective of this survey is to study the mechanical properties of the Kansas chalk and to consider the permeability evolution during our experiments.

### 5.1 Flooding Test

Based on the flooding test results we discuss the following terms.

#### 5.1.1 Stress-Strain

Fig. 4.1 and Fig. 4.2 show the stress strain relation. We can observe the similar relation between these two terms as mentioned in Fig. 2.4 before. And the yield point and K-modulus could be determined easily. Based on the yield point, we can say that the core KD2-U was stronger with the yield equal to 15 MPa than the core KD2-L with the yield equal to 13.5 MPa.

#### 5.1.2 Permeability-Strain

We have expected to see a declining trend in permeability while increasing the strain. Due to compaction of the core, permeability was predicted to decrease. Fig. 4.3 and Fig. 4.4 show this inverse relation between permeability and strain for the both tests similarly.

#### 5.1.3 Creep Strain vs. Creep Time

Fig. 4.5 and Fig. 4.6 show the axial creep strain over time. Change in the strain rate has not been observed significantly when shifting the flooding fluid from FW to SSW in either KD2-L or KD2-U test. However, in a hydrostatic test conducted on the Mons chalk in 130 °C, under 12 MPa confining pressure, a significant increase in the creep -more than 2.5 order of magnitude- had been observed when the flooding of SSW had been started right after flooding NaCl solution with the concentration of 0.657 mole/l (Abubeker 2013, Geitle 2013). In the same study, after some while, they had observed a dramatic increase in  $\Delta P$  which can indicate clogging of the core. Consequently the test had been stopped. The clogging could be rooted in precipitating of minerals –most likely anhydrite in the chalk since a decrease in the concentration of sulfate ions also was observed in the effluent chemical analysis.

In our experiment we have not observed any clogging. On the other hand, almost no change in the concentration of sulfate ions was seen. One of the differences between our experiment and Abubeker (2013) and Geitle (2013) experiment, was the concentration of the formation water (FW). However, we do not consider this as the reason of unlike behavior of the chalk facing SSW after flooding FW because no specific change in the concentration of ions had been observed in the effluent during flooding of FW in either of experiments.

The chalk type can be one of the reasons of this huge difference. The Kansas chalk is a stronger chalk comparing the Mons chalk. The carbonate content or the specific surface area of the chalk could contribute to this unlike behavior.

In a study conducted by Megawati et al. (2012) on the different types of chalk, the specific surface area of the Kansas chalk is reported as 2.95 m<sup>2</sup>/gr and the carbonate content is reported as 97.20 %. In the same study, the effect of sulfate on the chalk mechanics has been established. However, in our experiment we observed fairly minor effect –if any of sulfate ions on the mechanical strength of the chalk which is in not the same as experimental observations in several other studies (Heggheim et al. 2005, Korsnes 2007, Megawati et al. 2012).

Considering the axial creep strain when the distilled water (DW) flooding is started in our tests, demonstrates an increase in the both test KD2-L and KD2-U. The similar upsurge has been observed in an experimental study conducted by Korsnes et al. (2006a) on Stevens Klint chalk and Sutarjana (2008) on Kansas chalk. However, in the study done by Abubeker (2013) and Geitle (2013) on the Mons chalk, we can see that the strain rate has been continued similarly as it had been when flooding the SSW and DW injection did not have particular effect in this matter.

Finally, we compare the total axial strain value calculated based on two different measurements; Meas. 1 using Eq. 2.5 and Meas. 2 employing data from LVDT measurements. This comparison has been summed up in Table 5.1. Table 5.1 confirms that the total axial strain calculated based on Meas. 1 is higher for the both tests KD2-L and KD2-U. It gives the sense that the core was more squeezed when it was inside the triaxial cell than when it was taken out. We debate that the reason can be elastic rebound of the chalk core when it is taken out of the triaxial cell. Meaning that, the axial strain of the core was partially elastic which lead to recover the length change when the pressure is omitted of the core after the test.

Test Name	Total Axial Strain ( $\epsilon_A$ ) [%]	
	Meas.1	Meas.2
KD2-L	2.84	3.78
KD2-U	2.49	3.40

Table 5.1. The total axial strain ( $\epsilon_A$ ) [%] for the tests KD2-L and KD2-U; Meas. 1 is based on the core length value before and after the test and Meas. 2 based on the LVDT measurements.

#### 5.1.4 Permeability vs. Time

The permeability development over time is presented in Fig. 4.5 and Fig. 4.6. We argue the correction which had been done in the permeability calculation as the viscosity used in this calculation for each fluid injected through the core was taken from an online fluid properties calculator (Crewes 2007) in which we could only calculate the viscosity of the sodium chloride solutions (NaCl) with the different concentrations. Thus, using this calculator to obtain the viscosity of SSW including different ions could lead to some errors and the result is not very precise. Since the ion interactions has been ignored by implementing this method.



### 5.1.5 Volumetric Strain vs. Time

The volumetric strain has been calculated according to Eq. 2.15. In this equation volumetric strain is regarded as 3 order of magnitude of the axial strain based on several assumptions. *However, according our observation and measurements of axial creep strain and the bulk volume of the core before and after the test; and also based on the calculations we propose a new factor of 2.5 instead of 3 in the Eq. 2.15.* This new factor gives us the volumetric strain value more close to the practical experiment for the both test KD2-L and KD2-U.

### 5.1.6 Porosity vs. Time

According Eq. 2.13 and Eq. 2.24 the porosity progress has been plotted over time in Fig 4.9 for both tests KD2-L and KD2-U. This way, only the mechanical effects have been taken into account (Meas. 1). However, considering the chemical effect, the mass change and the solid volume change during flooding of the fluids; and employing Eq. 2.27, we have plotted the new graph for the porosity. As follows, both mechanical and chemical effects have been made allowance for (Meas. 2). Fig. 5.1 and Fig. 5.2 illustrate the porosity change over time implementing both mentioned measurements above. As shown in Fig. 5.1 porosity measured implementing both methods is almost 34.4 % in the beginning and after around 48 days of creeping, is almost 31.3 % in test KD2-L. Similarly in Fig. 5.2, porosity measured implementing both methods is around 35.2 % in the beginning and after around 37 days of creeping, is almost 32.1 % in test KD2-U. However, to show the difference between the two porosity values calculated for each test, we have also plotted the “Difference” value ( $\phi_{(mech+chem)} - \phi_{(mech)}$ ) on the secondary axis in Fig. 5.1 and Fig. 5.2. The figures illustrate that the difference value has exactly the inverse trend as the solid volume change had (see Fig. 4.25). This is what we expected. We believe that if we had continued the test for a longer period of time, we could observe a bigger gap between  $\phi_{(mech)}$  and  $\phi_{(mech+chem)}$  over time. The reason is that the strain rate would decrease over time but the dissolution rate of minerals inside the core would be more-or-less constant.

Fig. 5.1 and Fig. 5.2 show that  $\phi_{(mech+chem)}$  is almost 0.020 % and 0.017 % higher than  $\phi_{(mech)}$  for test KD2-L and KD2-U respectively.

Similarly, porosity of the core after the test was calculated for both tests KD2-L and KD2-U employing Eq. 2.24 and Eq. 2.28. The results are given in Table 4.15 called as Meas. 3 and Meas. 4. We can see that porosity is higher considering both chemical and mechanical effects (Meas. 4) comparing Meas. 3 which considers only the mechanical effects. This was completely expected since the tested core was lighter (having less dry weight) after the test comparing before the test (see Table 4.15); meaning that a chemical alteration occurred inside the core.

In addition, for the test KD2-U we have calculated porosity after testing using Eq. 2.15 and Eq. 2.17 which is called Meas.1 in Table 4.15. Also, we have calculated porosity after testing using Eq. 2.15 and Eq. 3.1 which is called Meas.2 in Table 4.15. We got two values: 32.31 % and 32.38 % for each calculation respectively. We can see that porosity calculated considering both the mechanical and chemical effect (Meas. 4) which is 32.57 % is more close to these two values than the porosity calculated considering only the mechanical effect (Meas. 3) which is equal to 31.68 %.

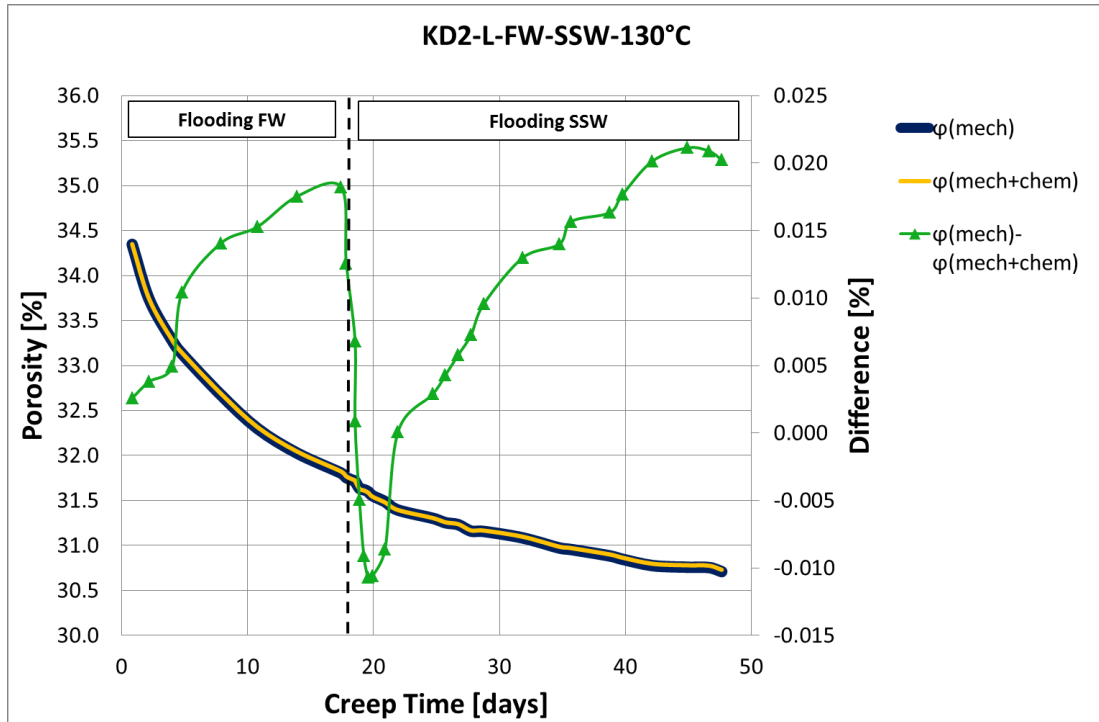


Fig. 5.1. The porosity change over time considering only the mechanical effect ( $\phi_{mech}$ ) in Meas.1 and considering both chemical and mechanical effects ( $\phi_{mech+chem}$ ) in Meas.2 for the test KD2-L

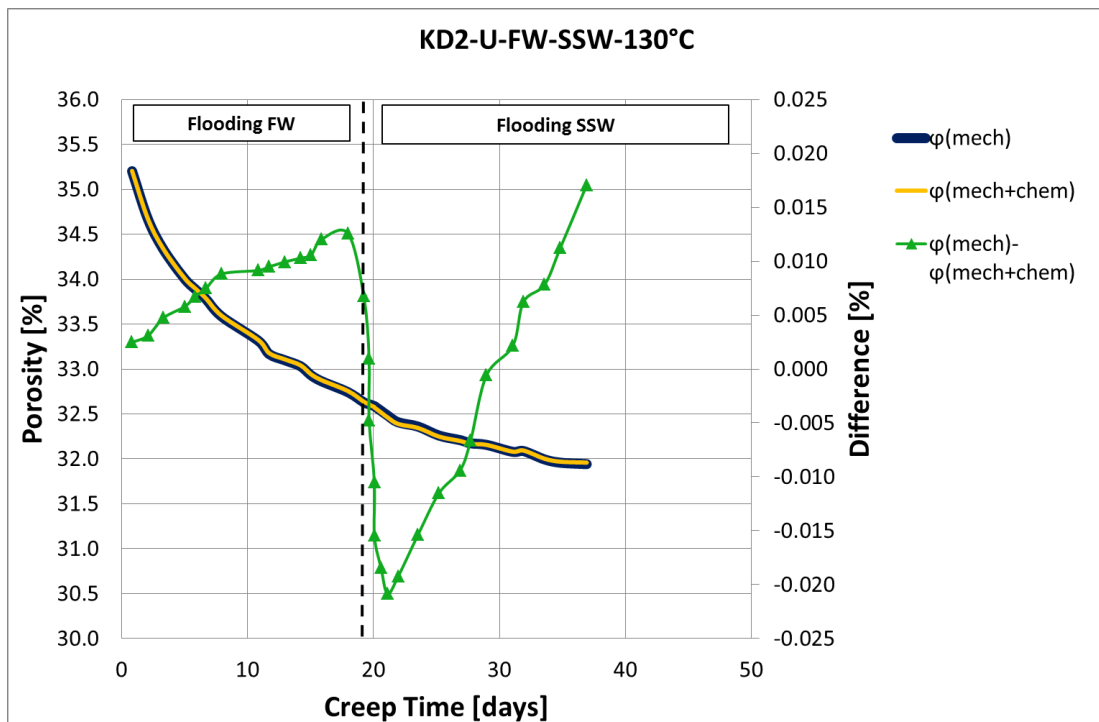


Fig. 5.2. The porosity change over time considering only the mechanical effect ( $\phi_{mech}$ ) in Meas.1 and considering both chemical and mechanical effects ( $\phi_{mech+chem}$ ) in Meas.2 for the test KD2-U

### 5.1.7 Permeability vs. Axial Creep Strain

Fig 4.10 and Fig. 4.11 shows the permeability-axial creep strain relation for the test KD2-L and KD2-U respectively. We can see that there is a linear and inverse relation between these two factors. Furthermore, the equations for the trend lines are quite similar for the test KD2-L and KD2-U. Thus, we argue that we can probably use these equations to predict the permeability of the chalk, having the axial creep strain value. The trend line equation for both tests is given in Table 5.2 probably be used in future studies.

Permeability Vs. Axial creep strain	
Test Name	Trend-Line Equation
KD2-L	$y = -0.3724x + 1.4563$
	$R^2 = 0.9842$
KD2-U	$y = -0.4005x + 1.4485$
	$R^2 = 0.9389$

Table 5.2. The trend line equations of the permeability vs. axial creep strain graph for the Tests KD2-L and KD2-U

### 5.1.8 Permeability Evolution ( $K(t)/K_0$ ) vs. Time

The permeability evolution detected over time has been presented in Fig. 4.14 for both test KD2-L and KD2-U. Applying Eq. 2.33, we have made two predictions for permeability evolution over time.

Prediction-1: Considering  $\varepsilon_V = 2\varepsilon_A$

Prediction-2: Considering  $\varepsilon_V = 3\varepsilon_A$

Fig. 5.3 and Fig. 5.4 show the permeability evolution observed in our study and also the permeability evolution regarding the prediction-1 and prediction-2 for tests KD2-L and KD2-U in sequence. These pictures reveal that the observed  $K(t)/K_0$  over time does not match our predicted models very well and both Prediction-1 and Prediction-2 show over-estimation. However, the prediction-1 has a smaller difference. We discuss this fact that one of the possible reasons could be the assumptions that we made to simplify the *Carman-Kozeny model* (Carman 1956, Dullien 1979) (See Section 2.2.8). We assumed grain diameter ( $D$ ) and toruosity factor ( $t$ ) in Eq. 2.31 to be constant during the flooding. This assumption can be argued based on this difference between our experimental observation and the models. The “Residue” also is plotted in Fig. 5.3 and Fig. 5.4 as defined in Eq. 4.1 to see the gap between the predicted models and the observed permeability evolution over time.

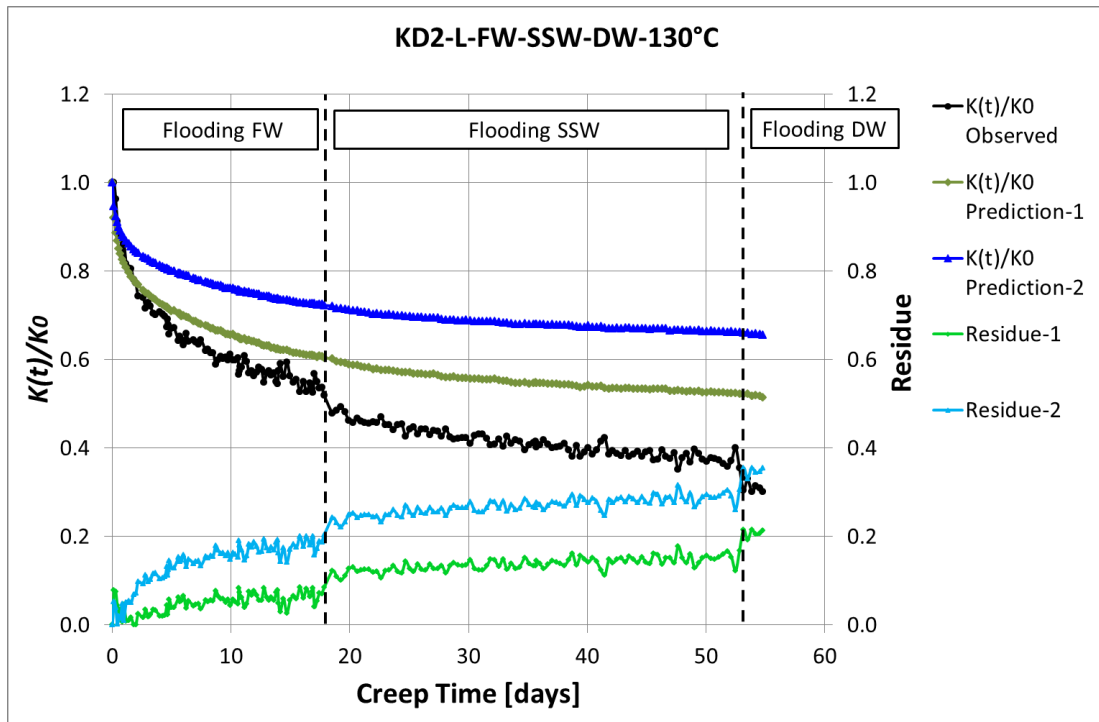


Fig. 5.3. Permeability evolution observed over time and permeability evolution models regarding the prediction-1 and prediction-2 for the test KD2-L

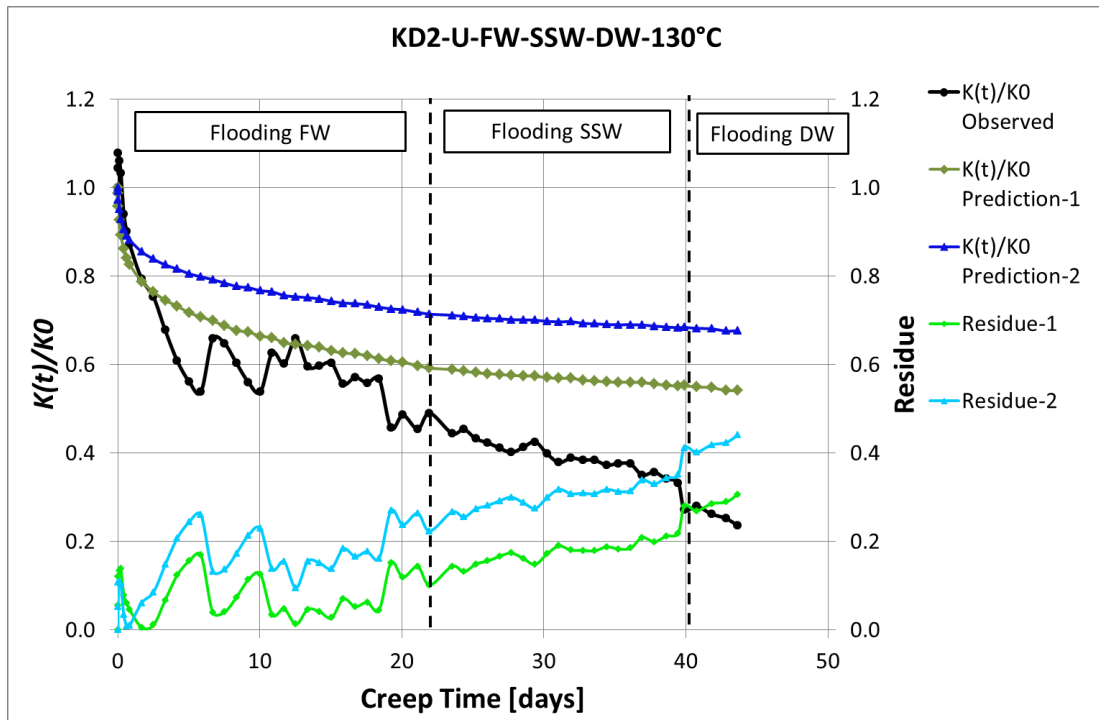


Fig. 5.4. Permeability evolution observed over time and permeability evolution models regarding the prediction-1 and prediction-2 for the test KD2-U

### 5.1.9 Permeability Evolution ( $K(t)/K_0$ ) vs. Volumetric Strain ( $\epsilon_v$ )

Fig. 4.15 and Fig 4.16 show the permeability evolution versus volumetric strain. We have also plotted the permeability evolution based on the prediction-2 vs. volumetric strain in Fig. 5.5 and Fig. 5.6, the former for the test KD2-L and the latter for the test KD2-U. These pictures show under-estimation for prediction-2 in the beginning and over-estimation in the end of the curves. The equations of all the trend lines are given in Table 5.3 probably be useful for future studies.

Permeability evolution observed vs. volumetric strain		
Test Name	Trend-Line Equation	
KD2-L	Observed	$y = -9.1903x + 1.0782$
		$R^2 = 0.9842$
	Prediction-2	$y = -5.7426x + 0.9639$
		$R^2 = 0.9972$
KD2-U	Observed	$y = -10.335x + 1.1214$
		$R^2 = 0.9389$
	Prediction-2	$y = -5.9016x + 0.9824$
		$R^2 = 0.9975$

Table 5.3. The trend line equations for the permeability evolution observed and permeability evolution based on the prediction-2 vs. volumetric strain for the tests KD2-L and KD2-U

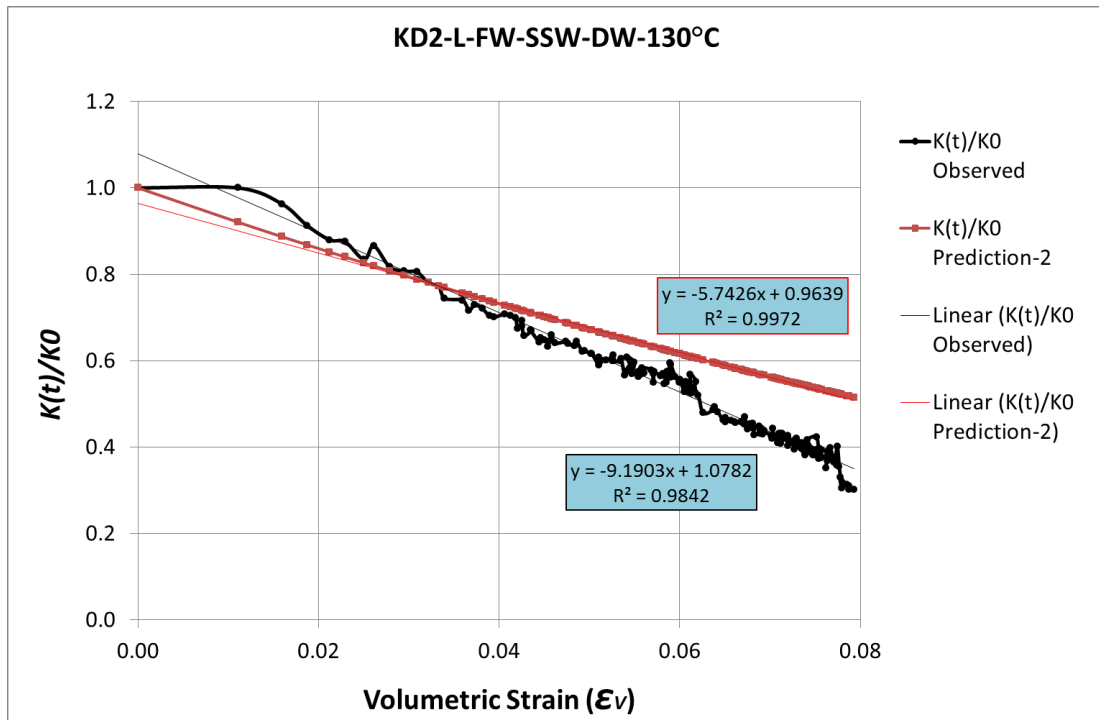


Fig. 5.5. Permeability evolution ( $K(t)/K_0$ ) observed vs. volumetric strain ( $\epsilon_v$ ) and permeability evolution model regarding the prediction-1 for the test KD2-L

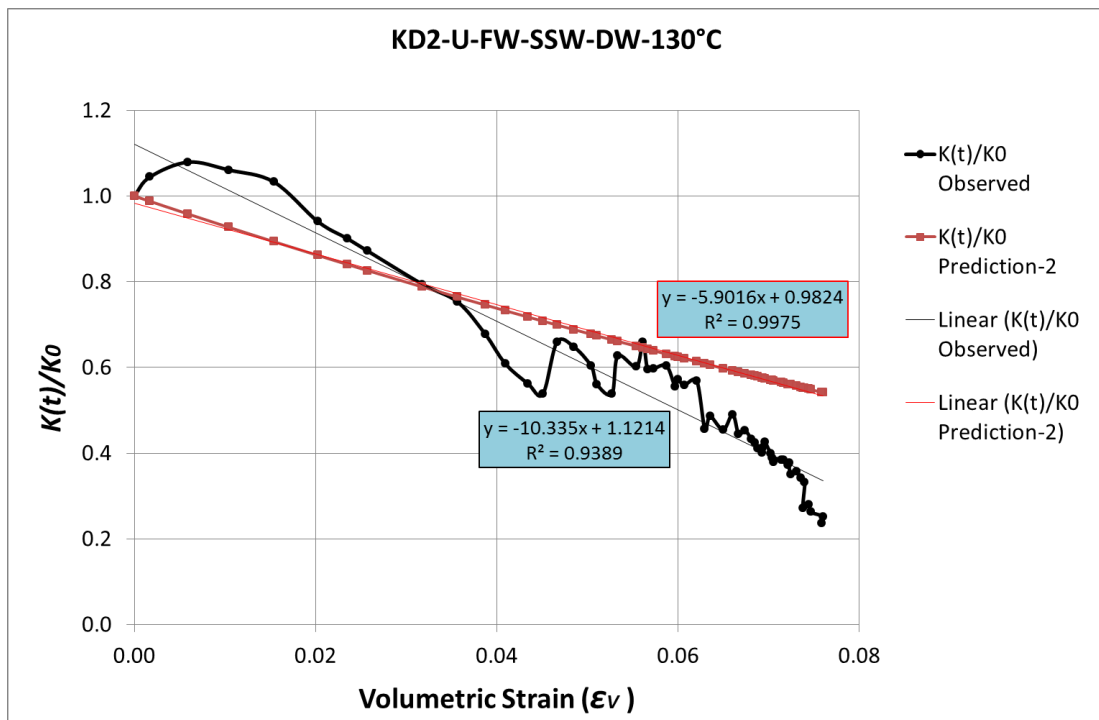


Fig. 5.6. Permeability evolution ( $K(t)/K_0$ ) observed vs. volumetric strain ( $\epsilon_v$ ) and permeability evolution model regarding the prediction-1 for the test KD2-U

## 5.2. Core analyzing after test

### 5.2.1. Solid Volume Measurement by Pycnometer

Considering Table 4.12 and Table 4.13, we have taken an average of so-called “*Total Average of both measurements*” in these two tables which gives us an approx. average density of the whole KD2 core *after testing* which is equal to 2.7179 gr/cm<sup>3</sup>. Considering Table 4.14, we have taken an average of density of all “*KD2-BELOW*”, “*KD2-BETWEEN*” and “*KD2-ABOVE*” pieces which is equal to 2.7207 gr/cm<sup>3</sup> and this is an approx. average density of the whole KD2 core *before testing*. Now we can compare the density ( $\rho$ ) of the KD2 core drilled-out from a Kansas outcrop before and after the test. The results are summed up in Table 5.4. According this table, the density of the core has been decreased after the test. The result can be that the precipitated mineral may have lower density than the dissolved ones which we consider it unlikely. We can also argue that according to the chemical analysis, Mg<sup>2+</sup> ions precipitate in the core and Ca<sup>2+</sup> ions dissolved to the fluid. Thus the question is what mechanism is behind this chemical alteration.

Drilled Core	Density $\rho$ [gr/cm <sup>3</sup> ]
KD2-BEFORE TESTING	2.721
KD2-AFTER TESTING	2.717

Table 5.4. The average density of the drilled core KD2 before and after the test

## 5.3. Chemical Analysis

### 5.3.1. Ionic Chromatography (IC)

The chemical analysis conducted implementing IC method indicates that flooding formation water (FW) containing Na<sup>+</sup> and Cl<sup>-</sup> ions through the core did not have a significant effect on the effluent concentration of ions (see Fig. 4.17 and Fig. 4.18). This is in agreement with the several previous studies (Andersen et al. 2012, Veen 2012, Abubeker 2013, Geitle 2013). Meaning that, no specific chemistry is between this ions and the rock surface. Therefore, it is reasonable to assume that the formation water is in the chemical equilibrium with the chalk under present condition.

However, flooding SSW leads to production of Ca<sup>2+</sup> ions and loss of Mg<sup>2+</sup> ions on one hand, and no significant change in the concentration of Na<sup>+</sup>, Cl<sup>-</sup> and K<sup>+</sup> ions on the other hand which is in agreement with several previous studies (Andersen et al. 2012, Abubeker 2013, Geitle 2013). It can be as a result of precipitating magnesium-bearing minerals and dissolving of calcium-bearing minerals. Generally speaking, subjecting the chalk to fluid not in chemical equilibrium with that; induces dissolution/precipitation which causes mechanical failure.

It should be noted that no substantial change was observed in the concentration of sulfate ions in the effluent, which is in conflict with the results of several previous studies conducted in the similar approach (Heggheim et al. 2005, Tweheyo et al. 2006, Andersen et al. 2012, Abubeker 2013, Geitle 2013). Possibly, it means that no sulfate-bearing mineral was precipitating in our Kansas chalk.

Considering Fig. 4.23 and Fig. 4.24, the accumulated mass of magnesium in the effluent is decreasing and the accumulating mass of calcium is increasing during flooding of SSW. However, the total mass change in the effluent increases over time. Meaning that, the core is losing mass over time. We can see that the overall trend of solid volume change also matches with the total accumulated mass trend (see Fig 4.25).

Regarding the dry weight of the core before and after the test, the core KD2-L and KD2-U have been 0.40 gr and 0.34 gr lighter respectively (see Table 4.15). However, the chemical analysis shows that the total mass change was 0.036 gr and 0.030 gr for the tests KD2-L and KD2-U in turn (see Table 4.16). This difference can be explained by a number of reasons. The first reason is that we did not take any effluent sample when the flooding fluid was shifted from SSW to DW. As a result of this fact, the chemical analysis does not include that period of test time. However, during flooding distilled water (DW) a relatively large amount of minerals may have been dissolved and washed out the core. Specifically because, a significant increase in the axial creep strain was observed while injecting DW. The second reason could be the fact that we have just considered the calcium and the magnesium ions in our IC calculations. Thus other ions (i.e.  $\text{SO}_4^{2-}$ ,  $\text{K}^+$ ,  $\text{CO}_3^{2-}$ ,  $\text{Na}^+$ ,  $\text{Cl}^-$  and etc.) have not been taken into account. Finally, the systematic errors in measurements and IC analysis are absolutely inevitable.



## 6. Conclusion

We performed hydrostatic tests on chalk from quarries of Kansas under in-situ conditions. We studied the link between compaction and permeability evolution both via theoretical modeling and experimental testing.

The testing results show that Kansas chalk is a relatively strong chalk and injecting synthetic sea water did not have a huge effect on its creep strain. In addition, we have not observed a great change in concentration of sulfate ions in effluent comparing the injected fluid. This can be as a result that minor amount –if any–, of sulfate-bearing minerals i.e. anhydrite; have been precipitated inside the core. This possibility can be rooted in the carbonate content or specific surface area of the chalk.

Based on our analysis, we proposed the volumetric strain as 2.5 order of magnitude of the axial strain. In addition, permeability evolution is concluded to be affected by the change in the grains size and minerals density. We have also concluded that chemical alterations impact the porosity evolution linked to compaction. It means that mechanical factors are not the only issues responsible for porosity evolution.

## References

- Aadnøy, B. S. and M. R. Looyeh (2011). Petroleum rock mechanics: drilling operations and well design. Amsterdam, Elsevier.
- Abubeker, E. A. (2013). Water weakening of chalk-comparison of intact and fractured cores. Stavanger, UiS.
- Andersen, M. A. (1995). Petroleum research in North Sea chalk. Stavanger, RF-Rogaland Research.
- Andersen, P. Ø. (2010). Mathematical modeling of water-rock chemistry during water injection and its impact on the composition and porosity of chalk. Stavanger, P.Ø. Andersen.
- Andersen, P. Ø., S. Evje, M. V. Madland and A. Hiorth (2012). "A geochemical model for interpretation of chalk core flooding experiments." Chemical Engineering Science **84**: 218-241.
- Baud, P., W. Zhu and T.-f. Wong (2000). "Failure mode and weakening effect of water on sandstone." Journal of Geophysical Research: Solid Earth **105**(B7): 16371-16389.
- Bernabé, Y., U. Mok and B. Evans (2003). "Permeability-porosity Relationships in Rocks Subjected to Various Evolution Processes." pure and applied geophysics **160**(5-6): 937-960.
- Blanton, T. L. (1981). "Deformation of Chalk Under Confining Pressure and Pore Pressure." Society of Petroleum Engineers Journal **21**(1): 43-50.
- Blatt, H. and R. J. Tracy (1996). Petrology: Igneous, Sedimentary, and Metamorphic.
- Carman, P. C. (1956). Flow of gases through porous media. New York, Academic Press.
- Carman, P. C. (1997). "Fluid flow through granular beds." Process Safety and Environmental Protection: Transactions of the Institution of Chemical Engineers, Part B **75**(Suppl): S32-S48.
- Crewes (2007). Fluid Properties Calculator. [online] Available at <http://www.crewes.org/ResearchLinks/ExplorerPrograms/FlProp/FluidProp.htm> [Last cited: 05 June 2013].
- DaSilva, F., J.P. Sarda and C. Schroeder (1985). Mechanical behavior of chalks 2<sup>nd</sup> North Sea Chalk Symposium, Book 2. Stavanger, Norway.
- David, C., T.-F. Wong, W. Zhu and J. Zhang (1994). "Laboratory measurement of compaction-induced permeability change in porous rocks: Implications for the generation and maintenance of pore pressure excess in the crust." pure and applied geophysics **143**(1-3): 425-456.
- Dullien, F. (1979). Porous Media Fluid Transport and Pore Structure, Elsevier Science.
- Fabricius, I. L. (2010). A Mechanism For Water Weakening of Elastic Moduli And Mechanical Strength of Chalk.

Fjær, E., R. M. Holt, P. Horsrud, A. M. Raaen and R. Risnes (2008). *Petroleum Related Rock Mechanics* (2nd Edition), Elsevier.

Geitle, K. (2013). Chemically induced compaction in fractured and intact chalk cores. Stavanger, UiS.

Ghabezloo, S., J. Sulem and J. Saint-Marc (2009). "Evaluation of a permeability–porosity relationship in a low-permeability creeping material using a single transient test." International Journal of Rock Mechanics and Mining Sciences **46**(4): 761-768.

Hattin, D. E. (1975). "Petrology and origin of fecal pellets in upper Cretaceous strata of Kansas and Saskatchewan." Journal of Sedimentary Research **45**(3): 686-696.

Heggheim, T., M. V. Madland, R. Risnes and T. Austad (2005). "A chemical induced enhanced weakening of chalk by seawater." Journal of Petroleum Science and Engineering **46**(3): 171-184.

Hiorth, A., L. M. Cathles, J. Kolnes, O. Vikane, A. Lohne, R. I. Korsnes and M. V. Madland (2008). A chemical model for the seawater-CO<sub>2</sub>-carbonate system – aqueous and surface chemistry. International Symposium of the Society of Core Analysts, Abu Dhabi, UAE.

Hiorth, A., L. Cathles and M. Madland (2010). "The Impact of Pore Water Chemistry on Carbonate Surface Charge and Oil Wettability." Transport in Porous Media **85**(1): 1-21.

Hedegaard, K. and A. Graue (2011). Does Wettability Affect the Strength of Chalk?, American Rock Mechanics Association.

Korsnes, R. I., M. V. Madland and T. Austad (2006, a). Impact of brine composition on the mechanical strength of chalk at high temperature.

Korsnes, R. I., R. Risnes, I. Faldaas and T. Norland (2006, b). "End effects on stress dependent permeability measurements." Tectonophysics **426**(1–2): 239-251.

Korsnes, R. I., S. Strand, Ø. Hoff, T. Pedersen, M. V. Madland and T. Austad (2006, c). Does the chemical interaction between seawater and chalk affect the mechanical properties of chalk?

Korsnes, R. I. (2007). Chemical induced water weakening of chalk by fluid-rock interactions : a mechanistic study. Stavanger, UiS.

Korsnes, R. I., M. V. Madland, T. Austad, S. Haver and G. Rosland (2008). "The effects of temperature on the water weakening of chalk by seawater." Journal of Petroleum Science and Engineering **60**(3-4): 183-193.

Madland, M. V. (2005). Water weakening of chalk : a mechanistic study. [Stavanger], UiS.

Madland, M. V., A. Finsnes, A. Alkafadgi, R. Risnes and T. Austad (2006). "The influence of CO<sub>2</sub> gas and carbonate water on the mechanical stability of chalk." Journal of Petroleum Science and Engineering **51**(3-4): 149-168.

Madland, M. V., K. Midtgarden, R. Manafov, R. I. Korsnes, T. G. Kristiansen and A. Hiorth (2008). The effect of temperature and brine composition on the mechanical strength of Kansas chalk. the International Symposium of the Society of Core Analysts. Abu Dhabi,.

Madland, M. V., A. Hiorth, R. I. Korsnes, S. Evje and L. Cathles, (2009). Rock Fluid Interactions in Chalk exposed to Injection of Seawater, MgCl<sub>2</sub>, and NaCl Brines with equal Ionic Strength. 15th European Symposium on Improved Oil Recovery Paris, France

Madland, M. V., A. Hiorth, E. Omdal, M. Megawati, T. Hildebrand-Habel, R. I. Korsnes, S. Evje and L. M. Cathles (2011). "Chemical Alterations Induced by Rock-Fluid Interactions When Injecting Brines in High Porosity Chalks." Transport in Porous Media **87**(3): 679-702.

Megawati, M., A. Hiorth and M. V. Madland (2012). "The Impact of Surface Charge on the Mechanical Behavior of High-Porosity Chalk." Rock Mechanics and Rock Engineering: 1-18.

Nelson, P. H. (1994). "Permeability-porosity Relationships In Sedimentary Rocks." The Log Analyst **35**(3).

Newman, G. H. (1983). "The Effect of Water Chemistry on the Laboratory Compression and Permeability Characteristics of Some North Sea Chalks." Journal of Petroleum Technology **35**(5): 976-980.

O.Saar, M. (1998). A relationship between permeability, porosity and microstructure in Vesicular Basalts.

Omdal, E., M. V. Madland, T. G. Kristiansen, R. I. Korsnes, N. B. Nagel and A. Hiorth (under review). "Creep and Water Weakening of Chalk at High Pore Pressure and Temperature."

Pooladi-Darvish, M. and A. Firoozabadi (2000). "Experiments and modelling of water injection in water-wet fractured porous media." Journal of Canadian Petroleum Technology **39**(3): 31-42.

Rhett, D. W. (1990). Compaction behavior of North Sea chalk in contact with seawater, A. A. Balkema, Rotterdam. Permission to Distribute - American Rock Mechanics Association.

Risnes, R. (2001). Deformation and yield in high porosity outcrop chalk. 26 Article.

Risnes, R. and O. Flaageng (1999). "Mechanical properties of chalk with emphasis on chalk-fluid interactions and micromechanical aspects." Oil & Gas Science and Technology-Revue D Ifp Energies Nouvelles **54**(6): 751-758.

Risnes, R., H. Haghghi, R. I. Korsnes and O. Natvik (2003). "Chalk-fluid interactions with glycol and brines." Tectonophysics **370**(1-4): 213-226.

Risnes, R., M. V. Madland, M. Hole and N. K. Kwabiah (2005). "Water weakening of chalk - Mechanical effects of water-glycol mixtures." Journal of Petroleum Science and Engineering **48**(1-2): 21-36.

- Roehl, P. O. and P. W. Choquette (1985). Carbonate petroleum reservoirs. New York, Springer.
- Royne, A., J. Bisschop and D. K. Dysthe (2011). "Experimental investigation of surface energy and subcritical crack growth in calcite." Journal of Geophysical Research-Solid Earth **116**.
- Schlumberger (2013). Market Analysis. [online] Available at [http://www.slb.com/services/industry\\_challenges/carbonates.aspx](http://www.slb.com/services/industry_challenges/carbonates.aspx) [Last cited: 05 June 2013].
- Shouxiang Ma and N. R. Morrow (1996). "Relationships Between Porosity and Permeability for Porous Rocks."
- Sulak, R. M., L. K. Thomas and R. R. Boade (1991). "3D Reservoir Simulation of Ekofisk Compaction Drive (includes associated papers 24317 and 24400 )." Journal of Petroleum Technology **43**(10): 1272-1278.
- Sutarjana, I. K. (2008). Water weakening of lower porosity chalk. Stavanger, I.K. Sutarjana.
- Sylte, J. E., L. K. Thomas, D. W. Rhett, D. D. Bruning and N. B. Nagel (1999). Water induced compaction in the Ekofisk Field.
- Tang, G. Q. and A. Firoozabadi (2001). "Effect of pressure gradient and initial water saturation on water injection in water-wet and mixed-wet fractured porous media." Spe Reservoir Evaluation & Engineering **4**(6): 516-524.
- Tweheyo, M. T., P. Zhang and T. Austad (2006). The Effects of Temperature and Potential Determining Ions Present in Seawater on Oil Recovery From Fractured Carbonates. SPE/DOE Symposium on Improved Oil Recovery. Tulsa, Oklahoma, USA, Society of Petroleum Engineers.
- Veen, S. H. v. d. (2012). Water induced compaction of chalks with varying non-carbonate content : the effect of Mg<sup>2+</sup> and pH of the injected brines, S.H. van der Veen.
- Zangiabadi, B., R. I. Korsnes, T. Hildebrand-Habel, A. Hiorth, I. K. Sutarjana, A. Lian, M. V. Madland (2009). Chemical water weakening of various outcrop chalks at elevated temperature. 4th Biot conference on poromechanics. DEStech Publication Inc. Columbia University, New York: 543-548.
- Zangiabadi, B., P. Kulathilagon and B. Midtun (2011). "Evaluation of rock-fluid interactions in an outcrop chalk: Experimental study with MgCl<sub>2</sub> solution." 45th US Rock Mechanics / Geomechanics Symposium.
- Zangiabadi, B., T. A. Davidian, R. I. Korsnes, K. A. N. Vorland, T. G. Kristiansen and M. V. Madland (2013). The effect of Wetting Conditions on the Mechanical Strength of Chalk. Thermo-Hydrromechanical and Chemical Coupling in Geomaterials and Applications, John Wiley & Sons, Inc.: 179-186.
- Øvstebø, K. A. (2011). A mechanical study of the sulphate effect on chalk. Stavanger, K.A. Øvstebø.

Appendix



KD2\_Lower\_1\_Inlet



KD2\_Lower\_1\_Outlet



KD2\_Lower\_2\_Inlet



KD2\_Lower\_2\_Outlet



KD2\_Lower\_3\_Inlet



KD2\_Lower\_3\_Outlet



KD2\_Lower\_4\_Inlet



KD2\_Lower\_4\_Outlet



KD2\_Lower\_5\_Inlet



KD2\_Lower\_5\_Outlet



KD2\_Lower\_6\_Inlet



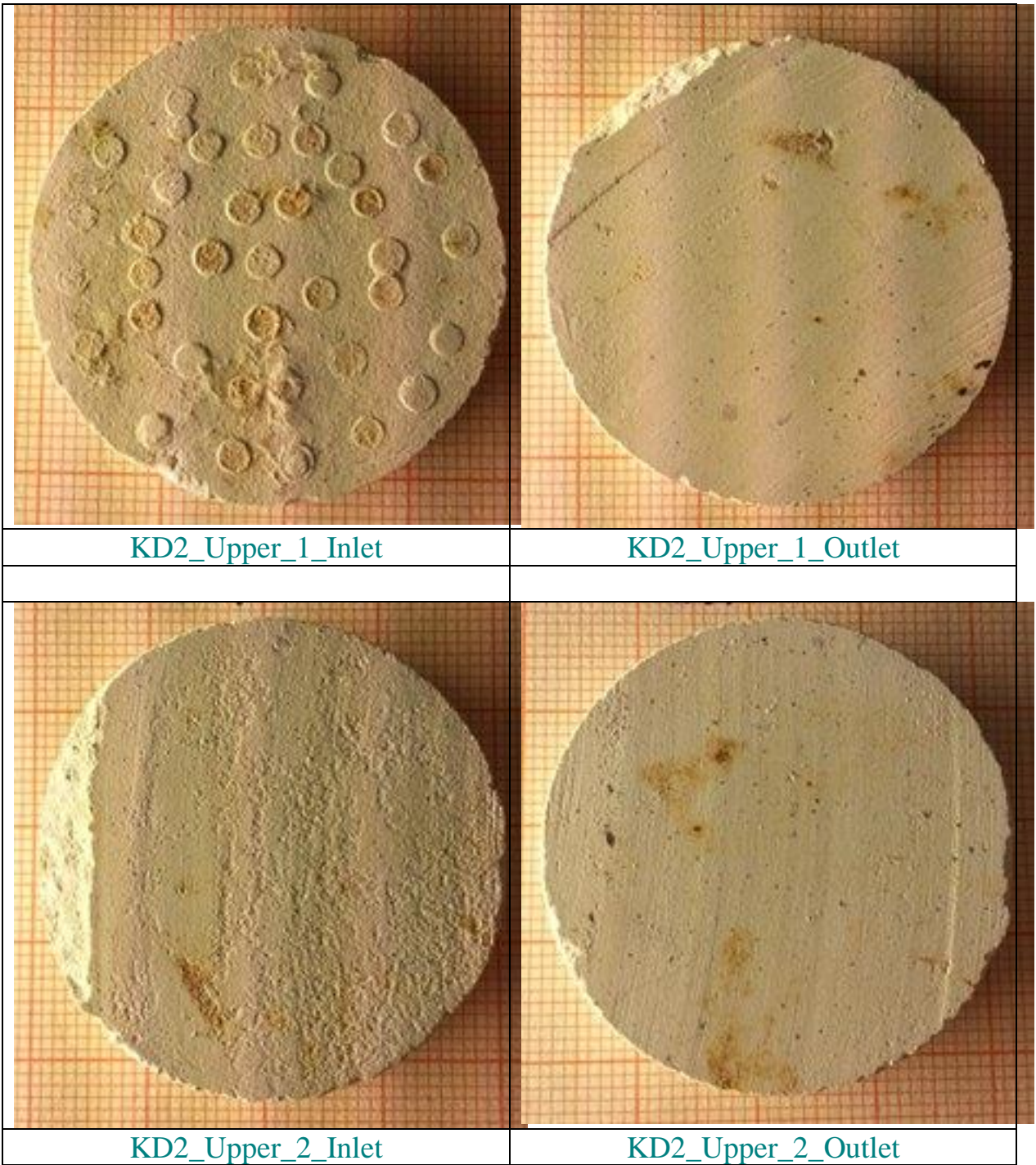
KD2\_Lower\_6\_Outlet





KD2\_Lower\_7\_Inlet

KD2\_Lower\_7\_Outlet





KD2\_Upper\_3\_Inlet

KD2\_Upper\_3\_Outlet



KD2\_Upper\_4\_Inlet

KD2\_Upper\_4\_Outlet



KD2\_Upper\_5\_Inlet



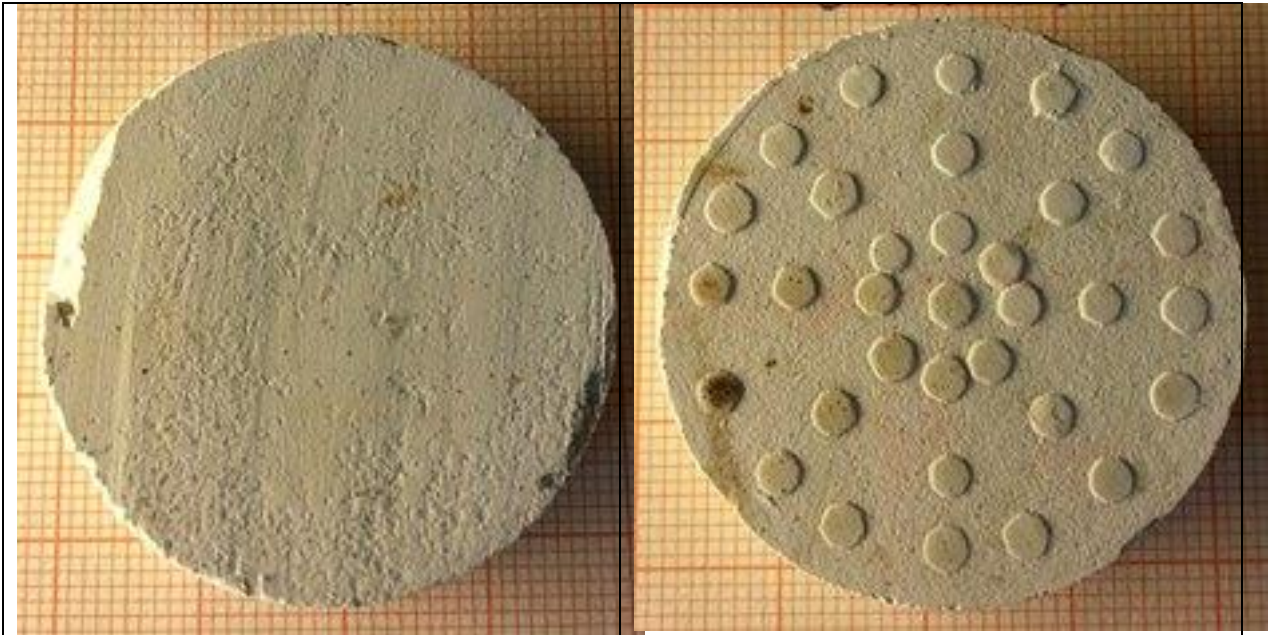
KD2\_Upper\_5\_Outlet



KD2\_Upper\_6\_Inlet



KD2\_Upper\_6\_Outlet



KD2\_Upper\_7\_Inlet

KD2\_Upper\_7\_Outlet